博士論文

Dynamic structure of retinal proteins relevant to the functions as disclosed by solid-state NMR spectroscopy

固体NMRによるレチナールタンパク質の動的構造と機能発現機構の解明

横浜国立大学大学院工学府

機能発現工学専攻

川村 出

Izuru Kawamura

2007年3月

Dynamic structure of retinal proteins relevant to the functions as disclosed by solid-state NMR

固体 NMR によるレチナールタンパク質の動的構造と機能発現機構の解明

2007 March

Izuru Kawamura

Yokohama National University

Abbreviations

Aβ ; Amyloid β peptide

A149S; *p*pR mutant in which Ala149 located EF loop is replaced with Ser

A149V; *p*pR mutant in which Ala149 located EF loop is replaced with Val

bO; Bacterio-opsin

bR; Bacteriorhodopsin

CP-MAS; Cross polarization-magic angle spinning

DD-MAS; Dipolar decoupling-magic angle spinning with single pulse excitation

DM; *n*-dodecyl-β-D-maltoside

D75N; presumed activated state of *p*pR mutant in which Asp75 is replaced with Asn75, neutralization of the Schiff base counterion Asp75

D85N; bR mutant in which Asp85 is replaced with Asn85, neutralization of the Schiff base counterion Asp85

E. coli; *Escherichia coli*

GPCR; G-protein coupled receptor

HAMP domain; Signal transduction domain in **h**istidine kinases, **a**denyl cyclases, **m**ethyl accepting chemotaxis proteins and **p**hosphotases.

hR; Halorhodopsin

H. salinarum; *Halobacterium salinarum*

K_d; Dissociation constants

MAS; Magic angle spinning

MOVS; Magnetically oriented vesicles systems

NMR; Nuclear magnetic resonance

N. pharaonis; *Natronomonas pharaonis*

Ni-NTA; Nickel-nitrilotriacetic acid

PDB; Protein data bank

PM; Purple membrane

*p*pR; *pharaonis* phoborhodopsin

*p*HtrII; *pharaonis* Halobacterial transducer protein II

REDOR; Rotational echo double resonance

SB; Schiff base

sR; Sensory rhodopsin

TPPM; Two pulse phase modulation

Table of contents

List of publications

1. **Izuru Kawamura**, Yoichi Ikeda, Yuki Sudo, Masayuki Iwamoto, Kazumi Shimono, Satoru Yamaguchi, Satoru Tuzi, Hazime Saitô, Naoki Kamo and Akira Naito.
"Participation of the surface structure of *pharaonis* phoborhodopsin, *p*pR and its A149S and A149V mutants, consisting of the C-terminal α-helix and EF loop, in the complex-formation with the cognate transducer *p*HtrII, as revealed by site-directed ^{13}C solid-state NMR"
Photochem. Photobiol. 2007 in press.

2. **Izuru Kawamura**, Yoshiaki Degawa, Satoru Yamaguchi, Katsuyuki Nishimura, Satoru Tuzi, Hazime Saitô and Akira Naito.
"Pressure induced isomerization of retinal on bacteriorhodopsin as disclosed by Fast Magic Angle Spinning NMR"
Photochem. Photobiol. 2007 in press.

3. **Izuru Kawamura**, Naoki Kihara, Masato Ohmine, Katsuyuki Nishimura, Satoru Tuzi, Hazime Saitô and Akira Naito.
"Solid State NMR Studies of Two Backbone Conformations at Tyr185 as a Function of Retinal Configurations in the Dark, Light and Pressure Adapted Bacteriorhodopsins"
J. Am. Chem. Soc. 2007 **129** 1016-1017.

4. **Izuru Kawamura**, Hideaki Yoshida, Yoichi Ikeda, Chisa Hasegawa, Satoru Yamaguchi, Yuki Sudo, Satoru Tuzi, Hazime Saitô, Naoki Kamo and Akira Naito.
"Dynamics changes in the C-terminal and cytoplasmic α-helical regions of *pharaonis* phoborhodopsin and its D75N mutant complexed with *p*HtrII by site-directed solid state ^{13}C NMR"
Biochemistry 2006 submitted.

5. **Izuru Kawamura**, Yoshiaki Degawa, Satoru Yamaguchi, Katsuyuki Nishimura, Satoru Tuzi, Hazime Saitô and Akira Naito.
"Structural changes of bacteriorhodopsin with pressure induced isomerization of retinal as disclosed by Fast Magic Angle Spinning NMR"
in preparation

6. **Izuru Kawamura**, Masato Ohmine, Junko Tanabe, Satoru Tuzi, Hazime Saitô and Akira Naito.
"Dynamics aspects at BC loop in bacteriorhodopsin by relaxation time measurements and the removal of retinal"
in preparation

Reference papers

1. Kazutoshi Yamamoto, Satoru Tuzi, Hazime Saitô, **Izuru Kawamura** and Akira Naito.
"Conformation and dynamics changes of bacteriorhodopsin and its D85N mutant in the absence of 2D crystalline lattice as revealed by site-directed ^{13}C NMR"
Biochim. Biophys. Acta 2006 **1758** 181-189.

2. Akira Naito and **Izuru Kawamura**.
"Solid-state NMR as a method to reveal structures and membrane-interactions of amyloidogenic proteins and peptides" (Review)
Biochim. Biophys. Acta 2007 in press.

Chapter 1
General Introduction

Membrane proteins and cell membrane are important to the life of the cell (**1, 2**). One of the roles of membrane proteins is to transfer ions across the membrane. As a result, electrochemical potential gradient in ion across membranes induced by the activities of ion pump can drive ATP-syntase to synthesis ATP molecules. Membrane proteins, which coupled with the essential role in cell functions, are classified into ion channels, ion pumps, G-protein-coupled receptors (GPCRs) and transporters (**3-7**). The biological importance of dynamic structure of membrane protein for understanding cell function has been recognized by several works of the Nobel laureates in 2003. Those are awarded to R. McKinnon and P. Agre for the works on structural resolution of the potassium channel (**6**) (**Figure 1**) and aquaporin (water channel) (**7**) (**Figure 2**), respectively (**3, 4**). Subsequently odorant receptors (GPCR) and the organization of the olfactory system were discovered by R. Axel and L. Buck in 2004 (**4, 8**).

The function of a bacterial potassium (K^+) channel was mainly revealed based on the structure determined by X-ray diffraction. The channel consists of four identical subunits to form a central pore through the membrane. The structure of selectivity filter explains the exquisite ion selectivity of the channel. When a K^+ ion enters the filter, hydrated waters can be replaced by the carbonyl oxygens in the selectivity filter without losing any energy. This is became the carbonyl oxygens in the filter are located at the appropriate distance to coordinate to K^+ ion (**6**).

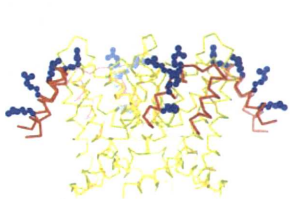

Figure 1 Structure of bacterial K^+ channel

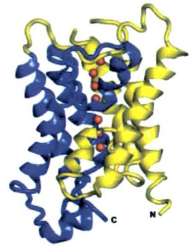

Figure 2 Structure of Aquaporin-1 (AQP-1)

However, it is generally difficult to determine dynamic structures of the membrane proteins in lipid bilayers by X-ray diffractions and solution NMR spectroscopy because they are not easy to grow crystals and have too large molecular weight to measure in solution NMR. Solid-state NMR has been developed to probe the heterogeneous and anisotropic characters of large complexes and to give information on molecular dynamics and orientation in ordered systems such as membranes (**9-11**). High-resolution solid-state NMR can be archived by mechanically averaging the anisotropic interactions by rotating a sample in a rotor. The rotor is set at the 'magic angle', which is making angle of 54.7° with respect to the *z* axis along of the static magnetic field. Therefore, fast spinning of the sample rotor eliminates the chemical shift anisotropy and gives high-resolution NMR spectra with isotropic chemical shifts of membrane proteins and peptides (**12-15**). In contrast, in a static condition, under favorable conditions the plane of lipid bilayers can be mechanically or spontaneously aligned to the static magnetic field (**16-19**). The aligned lipid bilayers have been used to determine the structure and orientation of membrane proteins and peptides in membrane (**20-23**). Using either static or MAS methods, solid-state NMR can now be applied to a number of non-crystalline biological macromolecules. There is no limitation in the sizes of molecules and often heterogeneous systems with other components can be studied; these include GPCR, amyloid fibrils, membrane proteins and peptides etc (**24-30**).

Many organisms contain retinal proteins (rhodopsin) with a retinal as a chromophore to utilize a light (**5, 31**). Halobacteria contains a family of four archaeal retinal proteins. These proteins are heptahelical transmembrane proteins with a retinal *via* Lys in helix G and functionally classified into two distinct classes: First, bacteriorhodopsin (bR) (**Figure 3**) and halorhodopsin (hR) are light-driven ion pumps to transport proton and chloride respectively (**32, 33**). Second, sensory rhodopsin I (sRI) and phoborhodopsin (pR, also called sensory rhodopsin, sRII) are positive and negative phototaxis receptors, respectively (**Figure 4**), by complex-formation with their respective cognate transducer proteins (**34-36**). Although these four retinal proteins have similar structures, these express different functions as pump and sensor types. Some amino acids in bR and *pp*R are known to be important for the functions; in particular, Arg82, Asp85, Asp96, Asp212, etc. (bR) and Asp75, Tyr174, Tyr199, Thr204, etc. (*pp*R) in the vicinity of retinal play important roles in the proton pump and phototaxis activities (**36-40**). The *trans-cis* photoisomerization of retinal triggers a series of photocycle with the changes of retinal-protein interactions, resulting in activating the functions of ion pump and sensor. How retinal configurations activate retinal protein in molecular level?

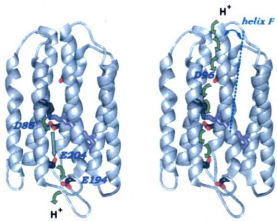

Figure 3. Over all view of bacteriorhodopsin (bR) and the proton transfer pathways are presented with the retinal (purple) and residues directly implicated in proton transport. (**32**)

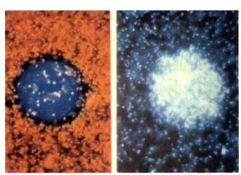

Figure 4. Light trap experiments with *Halobacterium salinarum*. Left: cells escape from a central spot of blue light (Negative phototaxis). Right: cells accumulate in a central spot of orange light (Positive phototaxis). (34)

It is, therefore, important for understanding the functions of these retinal proteins to investigate high-resolution dynamic structures of proteins corresponding to the retinal configurations. Bacteriorhodopsin (bR) and *pharaonis* phoborhodopsin (*p*pR) are known as a membrane protein with proton pump activity and negative phototaxis receptor, respectively. In this study, we have developed powerful methods for the dynamic structural analysis of these retinal proteins with the changes of retinal configurations and have revealed about dynamic structures of bR and *p*pR in view of retinal-protein interactions by solid-state NMR spectroscopy. This thesis is composed of seven chapters including introduction, research reports, and conclusions as follows.

In Chapter 2, noticeable pressure effects on bacteriorhodopsin (bR) in the molecular level were observed at the first time in these experiments. Magic Angle Spinning (MAS) is a standard technique to obtain high-resolution spectra by solid-state NMR and the rotation frequency of 50 kHz is now available. There are a lot of points to be considered such as the efficiency of dipolar decoupling (DD) and cross polarization (CP), sample temperature and pressure for sample etc. in fast MAS experiments. Especially, pressure effects on hydrated fluid sample such as

membrane proteins have not been well considered although it is realized as an important parameter. BR is a membrane protein with retinal in purple membrane. We have detected pressure effects for [ζ-^{15}N]Lys-labeled bR by a fast MAS NMR. In the ^{15}N CP-MAS NMR spectra, both all-*trans* and 13-*cis*, 15-*syn* retinal configurations have been observed at 148.0 and 155.0 ppm, respectively at the MAS frequency of 4 kHz in the dark. The signal intensity of 13-*cis* retinal at 155.0 ppm was increased when the MAS frequency was increased to 12 kHz and subsequently decreased to 4 kHz. It is, therefore, demonstrated that increased pressure induced by fast MAS frequencies generated isomerization from all-*trans* to 13-*cis* retinal in bR. In addition, it is clearly demonstrated that increase of pressure by fast MAS frequencies induced local dynamics change in the vicinity of retinal binding site with pressure induced isomerization.

In Chapter 3, backbone conformations near tyrosine in bacteriorhodopsin (bR) corresponding to all-*trans* and 13-*cis* retinal configurations in the dark, light and pressure adapted states were investigated for Tyr-X peptide bonds by using double amino acid labeling with [1-^{13}C]Tyr,[^{15}N]X-bR by means of rotational echo double resonance (REDOR) technique. The NMR signals obtained from the difference spectra between REDOR and full echo experiments allowed selectively detecting specific tyrosine signals for Tyr185-Pro186, Tyr26-Phe27, and Tyr64-Gly65. Two ^{13}C NMR peaks were observed for REDOR-filtered spectrum of Tyr185 in the dark at ambient temperature. These two signals are attributed to the bR with all-*trans* and 13-*cis* retinals. On the other hand, REDOR-filtered spectra for Tyr26 and 64 show singlet lines because they are located far from the retinal. All-*trans* peak intensity was increased in the light adapted state, while the 13-*cis* state increased for pressure-adapted state. The structure change of protein generated by pressure or light-induced isomerization of retinal occurred in local area in the vicinity of retinal in bR.

In Chapter 4, dynamic modes of extracellular loops in bacteriorhodopsin (bR) have been determined by measuring the relaxation times of resolved signals from Val-Pro consecutive sequences. These signals were reassigned by REDOR (Rotational Echo Double Resonance) filter measurements, in order to assign [1-^{13}C]Val / [^{15}N] Pro signal to the specific sites. The resonance at 172.0 ppm was determined to Val69 by considering significantly dephasing effect. Spin-lattice relaxation times (T_1), spin-spin relaxation times (T_2), cross relaxation times (T_{NH}) and ^{1}H spin-lattice relaxation times in the rotating flame (^{1}H $T_{1\rho}$) on ^{15}N nucleus were measured in [^{15}N]Pro-bR. It turned out that Val69-Pro70 in the extracellular side has rigid β-sheet with large amplitude motions as revealed from ^{13}C and ^{15}N conformation dependent shifts and T_1, T_2 and cross relaxation times. In addition, the BC loop conformation mostly disordered in bacterio-opsin as removal of retinal. Therefore, the motion of BC loop clearly correlates with

the dynamics of retinal binding site.

In Chapter 5, *pharaonis* phoborhodopsin (*p*pR) is a negative phototaxis receptor and forms a complex with its cognate transducer (*p*HtrII) in *Natronobacterium pharaonis*. *p*pR-*p*HtrII interaction at the cytoplasmic surface has been regarded to be important to signal relay. Conformational changes between [3-^{13}C]Ala-labeled *p*pR of the monomer and complex with *p*HtrII were investigated by ^{13}C solid-state NMR spectroscopy. In the ^{13}C DD-MAS NMR spectra, the intensity of the C-terminal signals of *p*pR decreased when it forms complex with *p*pR-*p*HtrII (1-159). This result indicates that *p*HtrII (1-159) interacts with the C-terminal region of *p*pR. It is presumed that the breakdown of salt bridge between C and G helices is a trigger of the phototaxis, and the breakdown occurs in D75N mutant in the dark. In fact, D73N (corresponding to D75N of *N.pharaonis*) mutant of *H.salinarum* is constitutively active. The C-terminal signals of D75N did not decrease by forming complex with *p*HtrII (1-159). These results reveal that the interaction between *p*pR and *p*HtrII (1-159) in transmembrane region becomes weak when *p*pR changes to an activated state. On the other hand, the signals of *p*pR-[3-^{13}C]Ala-labeled *p*HtrII(1-159) decreased when *p*HtrII formed complex with D75N.This result implies that the α–helix of *p*HtrII(1-159) in the cytoplasmic side becomes more rigid as *p*pR changes to an activated state. It is, therefore, clearly demonstrated that interactions of the C-terminus of *p*pR with *p*HtrII (1-159) significantly weakens and *p*HtrII at cytoplasmic surface becomes rigid when *p*pR switches to an activated state.

In Chapter 6, we have recorded ^{13}C solid state NMR spectra of *p*pR mutant [3-^{13}C]Ala-A149S and A149V in EF loop to understand an interaction of EF loop with *p*HtrII(1-159). Because signal at 15.8 ppm was decreased in the CP-MAS NMR spectra, we clearly assigned this signal to Ala149 (α-helix). In addition, the ^{13}C DD-MAS NMR spectral patterns of [3-^{13}C]Ala-*p*pR alone did not change significantly as compared to those of mutants. In contrast, the DD-MAS NMR spectral pattern and signal intensity of [3-^{13}C]Ala-*p*pR, A149S and A149V complexes with *p*HtrII(1-159) were greatly changed because extent of binding with transducer was significantly varied. It turned out that residues in EF loop regulate membrane dynamics of surface area and the intensity of C-terminal regions in *p*pR decreased as a result of binding with *p*HtrII.

In summary, we have revealed the dynamic structure of retinal proteins relevant to the functions for bR and *p*pR, accompanied by retinal isomerization by solid-state NMR under the conditions of fast MAS (pressure effects), *in situ* photo-illumination, REDOR filter and site-directed mutagenesis.

References

1. S. J. Singer and G. L. Nicolson.

The fluid mosaic model of the structure of cell membranes.

Science 1972 **175** 720-731.

2. D. M. Engelman.

Membranes are more mosaic than fluid.

Nature 2005 **438** 579-580.

3. H. R. Bourne.

How receptors talk to trimeric G proteins.

Curr. Opin. Cell Biol. 1997 **9** 134-142.

4. L. B. Buck.

The molecular architecture of odor and pheromone sensing in mammals.

Cell 2000 **100** 611-618.

5. K. Palczwewski, T. Kumasaka, T. Hori, C. A. Behnke, H. Motoshima, B. A. Fox, I. LeTrong, D. C. Teller, T. Okada, R. E. Stenkamp, M. Yamamoto, M. Miyano.

Crystal structure of rhodopsin: A G protein-coupled receptor.

Science 2000 **289** 733-734.

6. E. Gouaux, R. Mackinnon.

Principles of selective ion transport in channels and pumps.

Science 2005 **310** 1461-1465.

7. K. Murata, K. Mitsuoka, T. Hirai, T. Waltz, P. Agre, J. B. Heymann, A. Engel, Y. Fujiyoshi.

Structural determinants of water permeation through aquaporin-1.

Nature 2000 **407** 599-605.

8. J. A. Gogos, J. Osborne, A. Nemes, M. Mendelsohn, R. Axel.

Genetic Ablation and Relation of the Olfactory Topographic Map.

Cell 2000 **103** 609-620.

9. H. Saitô, I. Ando and A. Naito.

Solid state NMR spectroscopy for biopolymers: Principles and applications.

Springer. (2006)

10. H. Saitô, S. Tuzi, M. Tanio and A. Naito.

Dynamic Aspects of Membrane Proteins and Membrane-Associated Peptides as Revealed by ^{13}C NMR: Lessons from Bacteriorhodopsin as an Intact Protein

Annu. Rep. NMR spectrosco. 2002 **47** 39-108.

11. A. Watts.

Solid state NMR in drug design and discovery for membrane embedded targets.

Nature Reviews. Drug Discovery 2005 **4** 555-568.

12. H. Saitô, J. Mikami, S. Yamaguchi, M. Tanio, A. Kira, T. Arakawa, K. Yamamoto, S. Tuzi.

Site-directed ^{13}C solid-state NMR studies on membrane proteins: strategy and goals toward revealing conformation and dynamics as illustrated for bacteriorhodopsin labeled with [1-^{13}C] amino acid residues.

Magn. Reson. Chem. 2004 **42** 218-230.

13. S. Tuzi, N. Uekama, M. Okada, S. Yamaguchi, H. Saitô, H. Yagisawa.

Structure and Dynamics of the Phospholipase C-δ1 Pleckstrin Homology Domain Located at the Lipid Bilayer Surface.

J. Biol. Chem. 2003 **278** 28019-28025.

14. T. Arakawa, K. Shimono, S. Yamaguchi, S. Tuzi, Y. Sudo, N. Kamo, H. Saitô.

Dynamic structure of pharaonis phoborhodopsin (sensory rhodopsin II) and complex with a cognate truncated transducer as revealed by site-directed ^{13}C solid-state NMR.

FEBS Letters 2003 **536** 237-240.

15. M. Kamihira, Y. Oshiro, S. Tuzi, A. Y. Nosaka, H. Saitô, A. Naito.

Effect of Electrostatic Interaction on Fibril Formation of Human Calcitonin as Studied by High Resolution Solid State ^{13}C NMR.

J. Biol. Chem. 2003 **278** 2859-2865.

16. Y. Hori, M. Demura, T. Niidome, H. Aoyagi, T. Asakura.

Orientational behavior of phospholipid membranes with mastoparan studied by ^{31}P solid state NMR.

FEBS Letters 1999 **455** 228-232.

17. R. S. Prosser, F. Evanics, J. L. Kitevski, M. Sameer Al-Abdul-Wahid.

Current Applications of Bicelles in NMR studies of Membrane-Associated Amphiphiles and Proteins.

Biochemistry 2006 **45** 8453-8465.

18. A. Naito, T. Nagao, K. Norisada, T. Mizuno, S. Tuzi, H. Saitô.

Conformation and dynamics of melittin bound to magnetically oriented lipid bilayers by solid-state ^{31}P and ^{13}C NMR spectroscopy.

Biophys. J. 2000 **78** 2405-2417.

19. A. Naito, T. Nagao, M. Obata, Y. Shindo, M. Okamoto, S. Yokoyama, S. Tuzi, H. Saitô.

Dynorphin induced magnetic ordering in lipid bilayers as studied by ^{31}P NMR spectroscopy.

Biochim. Biophys. Acta. 2002 **1588** 34-44.

20. C. M. Franzin, J. Choi, D. Zhai, J. C. Reed F. M. Marrassi.
Structural studies of apoptosis and ion transport regulatory proteins in membranes.
Magn. Reson. Chem. 2004 **42** 171-179.

21. A. A. De Angelis, S. C. Howell, A. A. Nevzorov, S. J. Opella.
Structure Determination of a Membrane Protein with Two Trans-membrane Helices in Aligned Phospholipid Bicelles by Solid-state NMR Spectroscopy.
J. Am. Chem. Soc. 2006 **128** 12256-12267.

22. S. Toraya, K. Nishimura, A. Naito.
Dynamic structure of vesicle-bound melittin in a variety of lipid chain lengths by solid-state NMR.
Biophys. J. 2004 **87** 3323-3335.

23. T. Uezono, S. Toraya, M. Obata, K. Nishimura, S. Tuzi, H. Saitô and A. Naito.
Structure and orientation of dynorphin bound to lipid bilayers by ^{13}C solid-state NMR.
J. Mol. Struct. 2005 **749** 13-19.

24. S. H. Park, S. Prytulla, A. A. De Angelis, J. M. Brown, H. Kiefer, S. J. Opella.
High-Resolution NMR Spectroscopy of a GPCR in Aligned Bicelles.
J. Am. Chem. Soc. 2006 **128** 7402-7403.

25. A. B. Petel, E. Crocker, P. J. Reeves, E. V. Getmamova, M. Eilers, H. G. Khorana, S. O. Smith.
Changes in Interhelical Hydrogen Bonding upon Rhodopsin Activation.
J .Mol. Biol. 2005 **347** 803-812.

26. K. Yamamoto, S. Tuzi, H. Saitô, I. Kawamura, A. Naito.
Conformation and dynamics changes of bacteriorhodopsin and its D85N mutant in the absence of 2D crystalline lattice as revealed by site-directed ^{13}C NMR.
Biochim. Biophys. Acta. 2006 **1758** 181-189.

27. H. Saitô, S. Yamaguchi, K. Ogawa, S. Tuzi, M. Marquez, C. Sanz, E. Padros.
Glutamic acid residues of bacteriorhodopsin at the extracellular surface as determinants for conformation and dynamics as revealed by site-directed solid-state ^{13}C NMR.
Biophys. J. 2004 **86** 1673-1681.

28. A. T. Petkova, W. N. Yau, R. Tycko.
Experimental constraints on quaternary structure in Alzheimer's beta-amyloid fibrils
Biochemistry 2006 **45** 498-512.

29. A. Naito, M. Kamihira, R. Inoue, H. Saitô.

Structural diversity of amyloid fibril formed in human calcitonin as revealed by site-directed ^{13}C solid-state NMR spectroscopy.
Magn. Reson. Chem. 2004 **42** 247-257.

30. A. Naito and I. Kawamura.
Solid-state NMR as a method to reveal structures and membrane-interactions of amyloidogenic proteins and peptide.
Biochim. Biophys. Acta. 2007 in press.

31. J. L. Spudich.
Variations on a molecular switch: transport and sensory signalling by archaeal rhodopsins.
Molecular Microbiology 1998 **28** 1051-0158.

32. J. K. Lanyi.
Mechanism of Ion Transport across Membrans.
J. Biol. Chem. 1997 **272** 31209-31212.

33. G. Varo.
Analogies between halorhodopsin and bacteriorhodopsin.
Biochim. Biophys. Acta **1460** 220-229.

34. W. Stoeckenius, E. K. Wolff, B. Hess.
A Rapid Population Method for Action Spectra Applied to *Halobacteirum halobium.*
J. Bacteriol. 1988 **170** 2790-2795.

35. N. Kamo, K. Shimono, M. Iwamoto and Y. Sudo.
Photochemistry and Photoinduced Proton-Transfer by Pharaonis Phoborhodopsin
Biochemistry (Moscow) 2001 **66** 1580-1587.

36. Y. Sudo, H. Kandori and N. Kamo.
Molecular mechanism of protein-protein interaction of pharaonis phoborhodopsin/transducer and photo-signal transfer reaction by the complex.
Recent Res. Devel. Biophys. 2004 **3** 1-16.

37. H. Luecke, B. Schobert, H.-T., Richter, J.-P. Cartailler, J. K. Lanyi.
Structural Changes in Bacteriorhodopsin During Ion Transport at 2 Angstrom Resolution.
Science 1999 **286** 255-260.

38. M. Shibata and H. Kandori.
FTIR Studies of Internal Water Molecules in the Schiff Base Region of Bacteriorhodopsin.
Biochemistry. 2005 **44** 7406-7413.

39. Y. Sudo, M. Yamabi, S. Kato, C. Hasegawa, M. Iwamoto, K. Shimono and N. Kamo.
Importance of Specific Hydrogen Bonds of Archaeal Rhodopsins for the Binding to the

Transducer Protein.

J. Mol. Biol. 2006 **357** 1274-1282.

40. Y. Sudo and J. L. Spudich.

Three strategically placed hydrogen-bonding residues convert a proton pump into a sensory receptor.

Proc. Natl. Acad. Sci. 2006 **103** 16129-16134.

Chapter 2

Isomerization of retinal and dynamics change of protein in bacteriorhodopsin by fast magic angle spinning NMR

2-1 Pressure induced isomerization of retinal on bacteriorhodopsin as disclosed by Fast Magic Angle Spinning NMR

ABSTRACT

Bacteriorhodopsin (bR) is a retinal protein in purple membrane of *H.salinarum* with functions as a light-driven proton pump. We have detected pressure induced isomerization of retinal in bR by analyzing ^{15}N cross polarization-magic angle spinning (CP-MAS) NMR spectra of [ζ-^{15}N]Lys-labeled bR. In the ^{15}N NMR spectra, both all-*trans* and 13-*cis* retinal configurations have been observed in the Lys N_ζ in protonated Schiff base at 148.0 and 155.0 ppm, respectively, at the MAS frequency of 4 kHz in the dark. When the MAS frequency was increased up to 12 kHz corresponding to the sample pressure of 63 bar, the ^{15}N NMR signals of [ζ-^{15}N]Lys in Schiff base of retinal were broadened. On the other hand, other [ζ-^{15}N]Lys did not show broadening. Subsequently, the increased signal intensity of [ζ-^{15}N]Lys in Schiff base of 13-*cis* retinal at 155.0 ppm was observed when the MAS frequency was decreased from 12 kHz to 4 kHz. These results showed that the equilibrium constant of [all-*trans*–bR] /[13-*cis*-bR] in retinal decreased by the pressure of 63 bar. It was also revealed that the structural changes induced by the pressure occurred in the vicinity of retinal. Therefore, microscopically, hydrogen-bond network around retinal would be disrupted or distorted by a constantly applied pressure. It is, therefore, clearly demonstrated that increased pressure induced by fast MAS frequencies generated isomerization of retinal from all-*trans* to 13-*cis* state in the membrane protein bR.

INTRODUCTION

Bacteriorhodopsin (bR), from *Halobacterium salinarum*, is a 26 kDa seven transmembrane helix protein with a retinal as a chromophore via Lys 216 in helix G and shows proton pump activity starting from proton release in Schiff base initiated by retinal photo isomerization from all-*trans* to 13-*cis*, 15-*anti* state (**1**). The retinal configurations of all-*trans* and 13-*cis*, 15-*syn* states in the dark-adapted bR coexist in the isomeric ratio close to 1 (**2-4**). Primary amino acid residues in the vicinity of Schiff base region of retinal are Arg82, Asp85, Tyr185, and Asp212 forming hydrogen-bond network with strongly hydrogen-bonded water molecules (**5**). BR assembles into naturally occurring 2D crystalline patches known as a purple membrane (PM) in which its trimeric unit is hexagonally packed under the physiological

condition (**6**). 3D structure of bR with 1.55 Å resolutions has been revealed by X-ray diffraction study (**7**). To gain insight into the mechanism of proton pump activity of bR, it is important to understand how retinal configurations influence conformation and dynamics of retinal protein in a molecular level.

The above-mentioned isomeric ratio of retinal ([all-*trans*-bR]/[13-*cis*-bR]) in the dark-adapted state has been shown to decrease from unity when the pressure was increased because of the negative molar volume changes (**8,9**). Namely, pressure for bR in the dark causes the shift of isomer equilibrium from all-*trans* towards 13-*cis* state with two processes accompanied by the molar volume changes of -21 and -7 mL/mol (**10**). Because the molar volume change of the first step is quite large, it is expected that even in the small pressure change would give a large change of the population between 13-*cis* and all-*trans* state. The isomeric ratio in the dark, however, is insensitive to the temperature change (**11, 12**) and bR is thermally very stable (**13**), although it is reported that high temperature intermediate in bR exists at a temperature higher than 60°C (**14**).

We have observed that local conformation and dynamics by ^{13}C NMR study of site specifically isotopic labeled bR (**15-17**). In particular, it turned out that ^{13}C NMR peaks were well-resolved for fully hydrated [3-^{13}C]Ala-, [1-^{13}C]Val-labeled bR, depending upon their local dynamics and conformations of 29 Ala or 21 Val residues, respectively (**18,19**). In this study, pressure effects to isomeric ratio of retinal were observed in the ^{15}N NMR spectra in [ζ-^{15}N]Lys-labeled bR in the dark under the fast magic angle spinning (MAS) conditions. MAS can eliminate the chemical shift anisotropy when the rotation axis of sample is inclined to 54.7° toward the static magnetic field and the rotor frequency is faster than the chemical shift anisotropy (**20,21**). We realized that MAS frequency generates a pressure on the inner wall of the rotor because of the centrifugal forces. Nevertheless solid state NMR experiments on this pressure effects have been reported in a few cases. First, inter lamellar waters of dispersions in multi-lamellar vesicles (DOPC, POPC) decreases with spinning frequency in ^{1}H MAS NMR (**22**). Second, dynorphin (opioid peptide; 17 residues) has partially dissociated from lipid bilayers on ^{13}C MAS NMR condition. In the static condition, the peptide binds to membrane, and consequently forms magnetically oriented vesicle systems (MOVS) (**23,24**).

Here, we will focus attention on pressure effects for bR in PM by solid-state MAS NMR measurements. Retinal configurations in bR were revealed by ^{15}N NMR experiments of [ζ-^{15}N]Lys-labeled bR under the fast MAS conditions. We consider that this experimental system applies constantly low pressure for fully hydrated sample and the pressure of 63 bar was induced at the MAS speed of 12 kHz.

MATERIALS AND METHODS

Halobacterium salinarum S9 was grown in a synthetic medium including [ζ-^{15}N]-L-Lys to yield [ζ-^{15}N]Lys-labeled bR in purple membrane (PM). PM was isolated by the standard method as described (**25**) and suspended in 5 mM HEPES buffer containing 0.02 % NaN_3 and 10 mM NaCl at pH 7. The sample was concentrated by centrifugation and placed in 4.0 mm o.d. ZnO_2 pencil-type rotor for the fast magic angle spinning experiments. Sample rotor was tightly shielded by a piece of optical-fiber cap and glued to the top part of rotor by rapid Alardyte® to prevent dehydration of pelleted samples. *In situ* light-illumination to sample was made through optical fiber. Namely light was delivered from outside to inside of the magnet and illuminated to the top of rotor without any contact, so that the fast MAS condition can be achieved.

^{15}N high-resolution solid-state NMR spectra were recorded on a Chemagnetics CMX-400 infinity FT-NMR spectrometer operating at 100.16 MHz for carbon and 40.3 MHz for nitrogen nuclei. Cross polarization-magic angle spinning (CP-MAS) with a variable amplitude contact pulse of observed nucleus (RAMP-CP) were used (**26**). A double resonance MAS probe equipped with a stator assembly for 4.0 mm o.d. rotor was used throughout the measurements. The spinning frequencies were set to 4-12 kHz and 90° pulse was 5.1 μs. The MAS NMR measurements were performed again at 4 kHz after the measurements at 12 kHz. Ambient conditions of MAS were set at 4 kHz and probe setting temperature at 20 °C. Two pulse phase modulation (TPPM) decoupling (**27**) was employed during the acquisition time. ^{15}N contact time and repetition time were 2 ms, and 4 s, respectively. ^{15}N chemical shifts were externally referenced to 11.59 ppm for the amino nitrogen of glycine from NH_4NO_3.

Pressure on the samples was naturally applied by the centrifugal force induced by MAS frequency. Since the centrifugal force on the inner wall of the cylindrical rotor is proportional to the square of rotor radius and the square of rotor frequency, pressure of inner wall of the rotor with 4mm o.d. can be estimated to be 7 bar and 63 bar for the rotor frequency of 4 and 12 kHz, respectively. Even though pressure distribution will be presented depending on the location of samples, it is expected that most of the samples is located near the inner wall of rotor to show relatively uniform pressure.

RESULTS AND DISCUSSION

Figure 1 (A)-(D) shows ^{15}N CP-MAS NMR spectra of [ζ-^{15}N]Lys-labeled bR at the spinning frequencies of 4, 8, 10 and 12 kHz in the dark. After the NMR spectrum was measured for the spinning sample at the MAS frequency of 12 kHz, CP-MAS spectrum was recorded also at 4 kHz to examine the pressure effects on retinal configurations (Figure 1 (E)). The ^{15}N signals of free [ζ-^{15}N]Lys, backbone amides of naturally abundant amino acid residues and [ζ-^{15}N]Lys of Schiff base were observed at 11.0 ppm, 90-110 ppm and 140-160 ppm, respectively. The signal intensities of the free lysine was largely decreased at the MAS frequencies of 10 and 12 kHz as compared with those of backbone components, because the Hartmann-Hahn matching condition $H_{1H}/\gamma_H=H_{1N}/\gamma_N$ was disturbed by the fast MAS. When the MAS frequency was returned to 4 kHz, the line broadening, intensities and chemical shifts of these signals were recovered.

Figure 2 shows that the ^{15}N CP-MAS spectra of [ζ-^{15}N]Lys-bR in the protonated Schiff base were observed in the spectral range between 140 and 160 ppm. The signals of the protonated Schiff base are shown to be a sensitive probe on the changes of retinal isomerization and environment (Figure 2(A)-(D)) (**10, 28, 29**). Both ^{15}N NMR signals due to all-*trans* and 13-*cis* retinal configurations were observed in the same intensities at 148.0 and 155.0 ppm, respectively, under the MAS frequency of 4 kHz (Figure 2(A)). When the MAS frequency was increased up to 12 kHz, the ^{15}N NMR signals of Schiff base of retinal showed marked broadening (Figure 2(B)). This finding indicates that the hydrogen-bond network around the protonated Schiff base is locally distorted with the induced pressure under the fast MAS condition (Figure 3). The increased signal intensity of the 13-*cis* retinal at 155.0 ppm was appeared increased as the MAS frequency was decreased from 12 kHz to 4 kHz (Figure 1 (E) and 2 (C)). This observation was made possible when the line narrowing in the MAS frequency of 4 kHz recovered to be able to distinguish all-*trans* from 13-*cis* signals. It was also noticed that the retinal configurations showed hysteresis by the fast MAS experiments. Namely the exchange rate from 13-*cis* to all-*trans* retinal is very slow. To assign the ^{15}N NMR signals to either 13-*cis* or all-*trans* configuration, white light was irradiated continuously to bR and significant increase of the signal of all-*trans* was observed (Figure 2(D)). It was clearly shown that the all-*trans* retinal configuration appeared at 148 ppm in the ^{15}N peak-position by illumination of the white light. Therefore, it turned out that retinal configurations of bR was changed from the all-*trans* to 13-*cis* retinal of [ζ-^{15}N]Lys-labeled bR by the fast MAS experiments. Obviously, the present observation suggests that the pressure induced isomerization of retinal also causes distortion of such hydrogen-bond networks in the vicinity of retinal (Figure 3) (7), together with a possible dehydration effect of surrounding water molecules by centrifuging effect of the fast MAS. It is noticed that the isomerization from

all-*trans* to 13-*cis* state occurred at the pressure of 63 bar in the solid state NMR experiment. This pressure is much lower than the reported case where the populations of isomers were estimated from the absorption spectra (**8, 9**). ^{15}N NMR spectra have been observed previously under the condition of the MAS frequency of 3 kHz and -75 °C to show two signals due to all-*trans* and 13-*cis* states of bR. However, the increase of *13*-cis state was not observed because of the experimental conditions where the pressure was very low (**4**).

It is important to point out that the fast MAS also generate the increased sample temperature because of the heating by friction. Therefore, we have measured the sample temperature within the rotor under the fast MAS condition by monitoring ^{207}Pb chemical shifts of lead nitrate (**30**). It turned out that the temperature of the sample was increased by 20 °C at the MAS frequency of 12 kHz. We, therefore, raised the temperature to 40 °C by keeping the MAS frequency at 4 kHz. The increased intensity of 13-*cis* peak was not observed although the some line broadening was noted. These experiments indicate that isomerization from all-*trans* to 13-*cis* is mainly caused by the pressure increase, although the line broadening in the fast MAS condition can be caused by both temperature and pressure effects.

Isomerization from all-*trans* to 13-*cis* has been studied by extraction techniques and absorption spectroscopy of the range from low to high pressure (1-3000 bar) in which the isomer equilibrium shifts from all-*trans* to 13-*cis* state at two processes with the molar volume changes in the dark (**10**). Thermodynamically, this change of equilibrium constant of [all-*trans*-bR]/[13-*cis*-bR] can be attributed to the large molar volume change from all-*trans* to 13-*cis* state. Microscopically, locations of water molecules in the vicinity of retinal (**7**) and hydrogen-bond networks via water molecules that correlate with proton pump activity may be distorted by the increased pressure. In solution high-pressure $^{15}N/^{1}H$ NMR techniques utilizing pressure cell, fluctuations of hen lysozyme are found to be localized near the cavities containing water molecules (**31,32**). In general, hydrogen bonding H···O or H···N distances in protein are changed by pressure accompanied by a molar volume change (**32**). Therefore, the pressure induced isomerization of retinal and modulation of the hydrogen-bond network can cause the change in structure and motion of residues in proteins located in the vicinity of retinal.

Noticeable pressure effects on bR in purple membrane in the molecular level were observed at the first time in these experiments. Increased pressure by the fast MAS frequencies induces isomerization from the all-*trans* to 13-*cis* retinal. It is possible to increase 13-*cis* state by applying pressure and the all-*trans* state by irradiation of light. It is stressed that the MAS experiment is a good source of pressure since the induced pressure will be proportional to the square of MAS frequency. This kind of pressure effect in membrane protein has not yet been studied because it was thought that the application of pressure in the solid state NMR

spectroscopy was difficult. This experiment, therefore, clearly showed that pressure induced experiment can be successfully applied by the fast MAS experiment. It is also important to point out that it is possible to change the protein equilibrium by applying the pressure because a large molar volume change in a large heterogeneous system such as membrane protein can be altered the equilibrium constant by relatively small change of pressure.

References

1. J. K. Lanyi, and B. Schobert.
Local-global conformational coupling in a heptahelical membrane protein: Transport mechanism from crystal structure of the nine states in the bacteriorhodopsin photocycle.
Biochemistry 2004 **43** 3-8.

2. A. Maeda, T. Iwasa, and T. Yoshizawa.
Isomeric composition of retinal chromophore in dark-adapted bacteriorhodopsin.
J. Biochem. 1977 **82** 1599-1604.

3. H-W. Trissl, and W. Gartner
Rapid charge separation and batochromic absorption shift of flash-excited bacteriorhodopsin containing 13-*cis* or all-*trans* forms of substituted retinals.
Biochemistry 1987 **26** 751-758.

4. H. J. M. De Groot, G. S. Harbison, J. Herzfeld, and R. G. Griffin
Nuclear magnetic resonance study of the Schiff base in bacteriorhodopsin: Counterion effects on the ^{15}N shift anisotropy.
Biochemistry 1989 **28** 3346-3353.

5. M. Shibata and H. Kandori
FTIR studies of internal water molecules in the Schiff base region of bacteriorhodopsin.
Biochemistry 2005 **44** 7406-7413.

6. N. Grigorieff, T. A. Ceska, K. H. Downing, J. M. Baldwin, R. Henderson
Electron-crystallographic refinement of the structure of bacteriorhodopsin.
J. Mol. Biol. 1996 **259** 393-421.

7. H. Luecke, B. Schobert, H-T. Richter, J-P. Cartailler and J. K. Lanyi

Structure of bacteriorhodopsin at 1.55Å resolution.
J. Mol. Biol. 1999 **291** 899-911.

8. M. Tsuda and T. G. Ebrey
Effect of high pressure on the absorption spectrum and isomeric composition of bacteriorhodopsin. *Biophys. J.* 1980 **30** 149-158.

9. M. Tsuda, R. Govindjee, T. G. Ebrey.
Effects of pressure and temperature on the M412 intermediate of the bacteriorhodopsin photocycle. Implications for the phase transition of the purple membrane.
Biophys. J. 1983 **44** 249-254.

10. K. Bryl and K. Yoshihara.
Two processes lead to a stable all-*trans* and 13-*cis* isomer equilibrium in dark-adapted bacteriorhodopsin; effect of high pressure on bacteriorhodopsin, bacteriorhodopsin mutant D96N and fluoro-bacteriorhodopsin analogues.
Eur. Biophys. J. 2002 **31** 539-548.

11. N. A. Dencher, Ch. N. Rafferty and W. Sperling
13-cis and trans bacteriorhodopsin: photochemistry and dark equilibrium.
Biophys. Struct. Mechan. 1977 **3** 79-94.

12. K. Ohno, Y. Takeuchi, M. Yoshida.
Light-induced formation of the 410 nm intermediate from reconstitued bacteriorhodopsin.
J. Biochem. (Tokyo) 1977 **82** 1177-1180.

13. Y. Mukai, N. Kamo, and S. Mitaku.
Light-induced denaturation of bacteriorhodopsin solubilized by octyl-β-glucoside.
Protein Eng. 1999 **12** 755-759.

14. Y. Yokoyama, M. Sonoyama, and S. Mitaku.
Irreversible photobleaching of bacteriorhodopsin in a high-temperature intermediate state.
J. Biochem. 2002 **131** 785-90.

15. H. Saitô, S. Tuzi, S. Yamaguchi, M. Tanio and A. Naito.
Conformation and backbone dynamics of bacteriorhodopsin revealed by ^{13}C-NMR.
Biochim. Biophys. Acta. 2000 **1460** 39-48.

16. H. Saitô, J. Mikami, S. Yamaguchi, M. Tanio, A. Kira, T. Arakawa, K. Yamamoto, and S. Tuzi. Site-directed ^{13}C solid-state NMR studies on membrane proteins: strategy and goals toward revealing conformation and dynamics as illustrated for bacteriorhodopsin labeled with [1-^{13}C]amino acid residues.
Magn. Reson. Chem. 2004 **42** 218-230.

17. H. Saitô, S. Yamaguchi, H. Okuda, A. Shiraishi and S. Tuzi.

Dynamic aspect of bacteriorhodopsin as a typical membrane protein as revealed by site-directed solid-state ^{13}C NMR.
Solid State Nucl. Magn. Reson. 2004 **25** 5-14.

18. H. Saitô, S. Tuzi and A. Naito.
Empirical versus nonempirical evaluation of secondary structure of fibrous and membrane proteins by solid-state NMR: a practical approach, *Annu. Rep. NMR Spectrosc.* 1998 **36** 79-121.

19. H. Saitô, S. Tuzi, M. Tanio, A. Naito.
Dynamic aspects of membrane proteins and membrane-associated peptides as revealed by ^{13}C NMR: Lessons from bacteriorhodopsin as an *intact* protein.
Annu. Rep. NMR Spectrosc. 2002 **47** 39-108.

20. E. R. Andrew, A. Bradbury, R.G. Eades
Nuclear magnetic resonance spectra from a crystal rotated at high speed.
Nature 1958 **182** 1659.

21. I. J. Lowe.
Free induction decays of rotating solids
Phys. Rev. Lett. 1959 **2** 285-287.

22. Z. Zhou, R.G. Sayer, D.W. Hughes, R.E. Stark, R.M. Epand
Studies of phospholipid hydration by high-resolution magic-angle spinning nuclear magnetic resonance.
Biophys. J. 1999 **76** 387-399.

23. A. Naito, T. Nagao, M. Obata, Y. Shindo, M. Okamoto, S. Yokoyama, S. Tuzi, and H. Saitô.
Dynorphin induced magnetic ordering in lipid bilayers as studied by ^{31}P NMR spectroscopy.
Biochim. Biophys. Acta. 2002 **1558** 34-44.

24. T. Uezono, S. Toraya, M. Obata, K. Nishimura, S. Tuzi, H. Saitô and A. Naito.
Structure and orientation of dynorphin bound to lipid bilayers by ^{13}C solid-state NMR.
J. Mol. Struct. 2005 **749** 13-19.

25. D. Oesterhelt, and W. Stoeckenius.
Isolation of the cell membrane of *Halobacterium halobium* and its fractionation into red and purple membrane.
Methods Enzymol. 1974 **31** 667-678.

26. G. Metz, X. Wu and S. O. Smith.
Ramped amplitude cross polarization in magic angle spinning NMR.
J. Magn. Reson. ser. A 1994 **110** 219-227.

27. A. W. Bennet, C.M. Rienstra, M. Augar, K.V. Lakshmi, and R.G. Griffin.

Heteronuclear decoupling in rotating solids.
J. Chem. Phys. 1995 **103** 6951-6958.

28. S. O. Smith, H. J. M. De Groot, R. Gebhard, J. M. L. Courtin, I. Lugtenburg, J. Herzfeld and R. G. Griffin.
Structure and protein environment of the retinal chromophore in light- and dark-adapted bR studied by solid state NMR.
Biochemistry 1989 **28** 8897-8904.

29. M. E. Hatcher, J. G. Hu, M. Belenky, P. Verdegem, J. Lugtenburg, R. G. Griffin, and J. Herzfeld Control of the pump cycle in bacteriorhodopsin: Mechanisms elucidated by solid-state NMR of the D85N mutant.
Biophys. J. 2002 **82** 1017–1029.

30. A. Bielecki and D.P. Burum.
Temperature dependence of ^{207}Pb MAS spectra of solid lead nitrate. An accurate, sensitive thermometer for variable-temperature MAS.
J. Magn. Reson. Ser.A 1995 **116** 215-220.

31. Y. O. Kamatari, H. Yamada, K. Akasaka, J.A. Jones, C.M. Dobson, and L.J. Smith.
Response of native and denatured hen lysozyme to high pressure studied by $^{15}N/^{1}H$ NMR spectroscopy.
Eur. J. Biochem. 2001 **268** 1782-1793.

32. K. Akasaka.
Highly fluctuating protein structures revealed by variable-pressure nuclear magnetic resonance. *Biochemistry* 2003 **42** 10875-10885.

33. H. Michael, H. Patzelt, A. Ocenfels, W. Gartner, D. Oesterhelt, and B. Bechinger.
Refinement of the Geometry of the Retinal Binding Pocket in Dark-Adapted Bacteriorhodopsin by Heteronuclear Solid-State NMR Distance Measurements.
Biochemistry 2000 **39** 10066-10071.

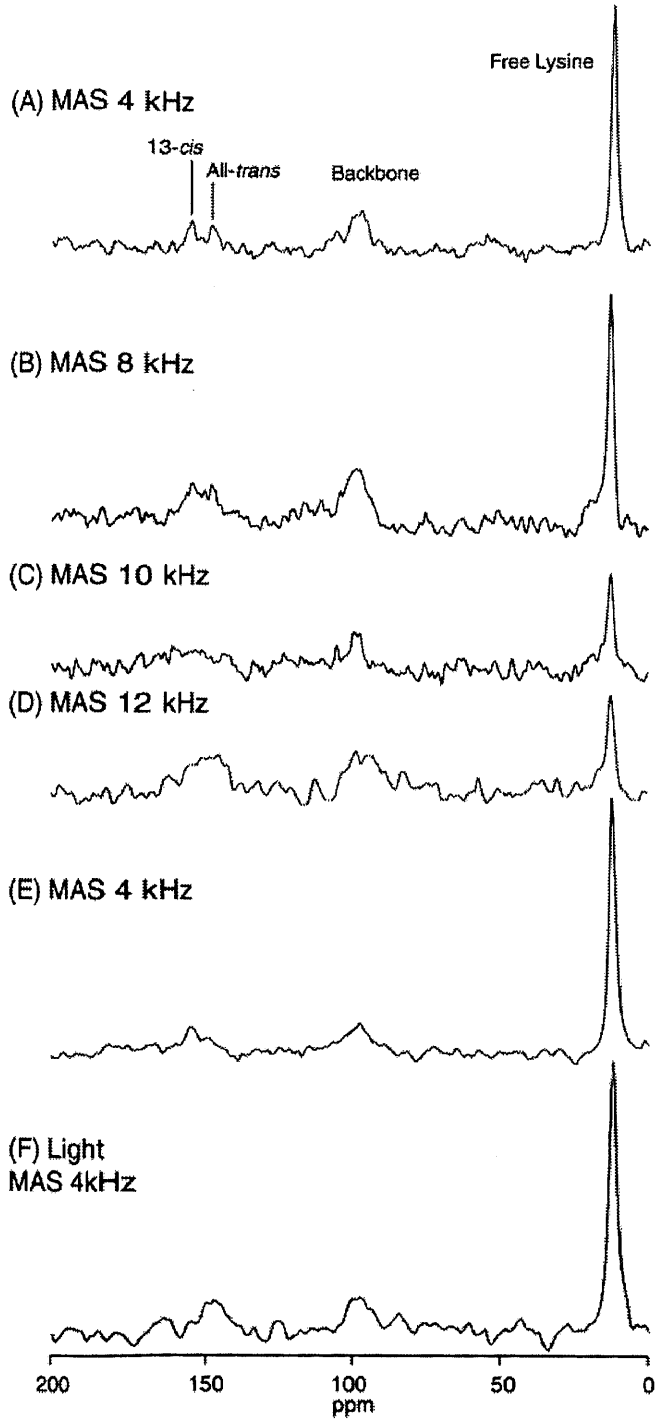

Figure 1. ^{15}N CP-MAS NMR spectra of [ζ-^{15}N]Lys-labeled bR at various magic angle spinning frequencies up to 12 kHz ((A)-(D)). After spinning sample at 12 kHz, ^{15}N CP-MAS NMR spectrum was recorded at 4 kHz (E). *In situ* light-irradiation spectrum of bR (F).

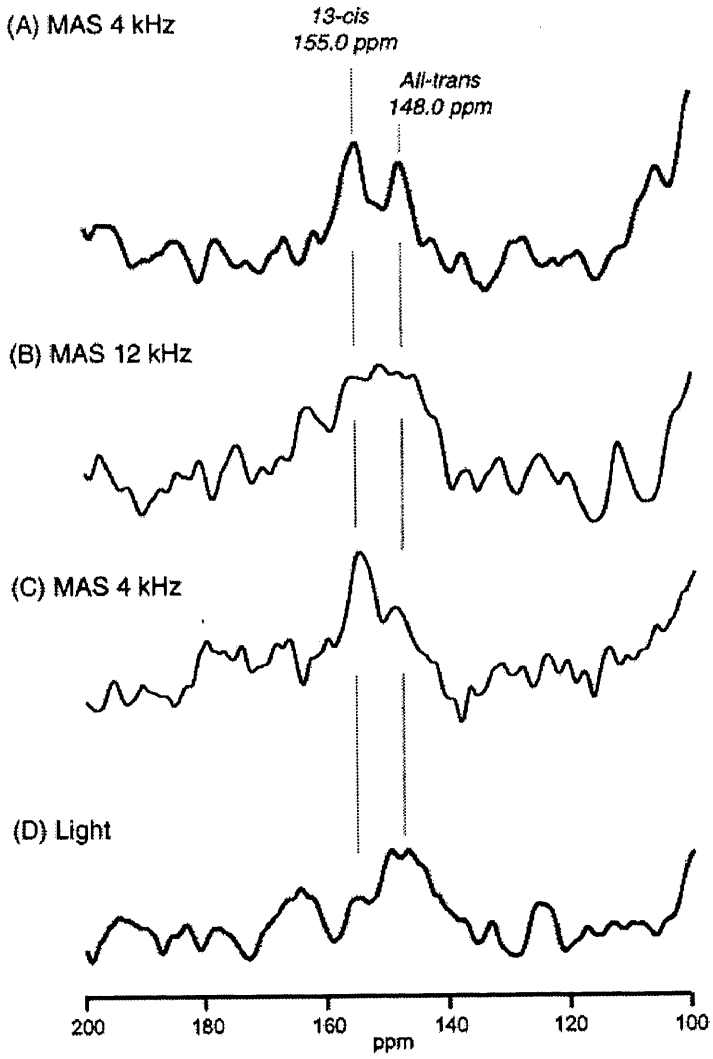

Figure 2. ^{15}N CP-MAS NMR spectra of [ζ-^{15}N]Lys of Schiff base in bR at MAS frequency of 4 and 12 kHz, respectively ((A) and (B)). After spinning sample at 12 kHz, CP-MAS NMR spectrum was observed at 4 kHz (C). *In situ* light-irradiation spectrum of bR (D).

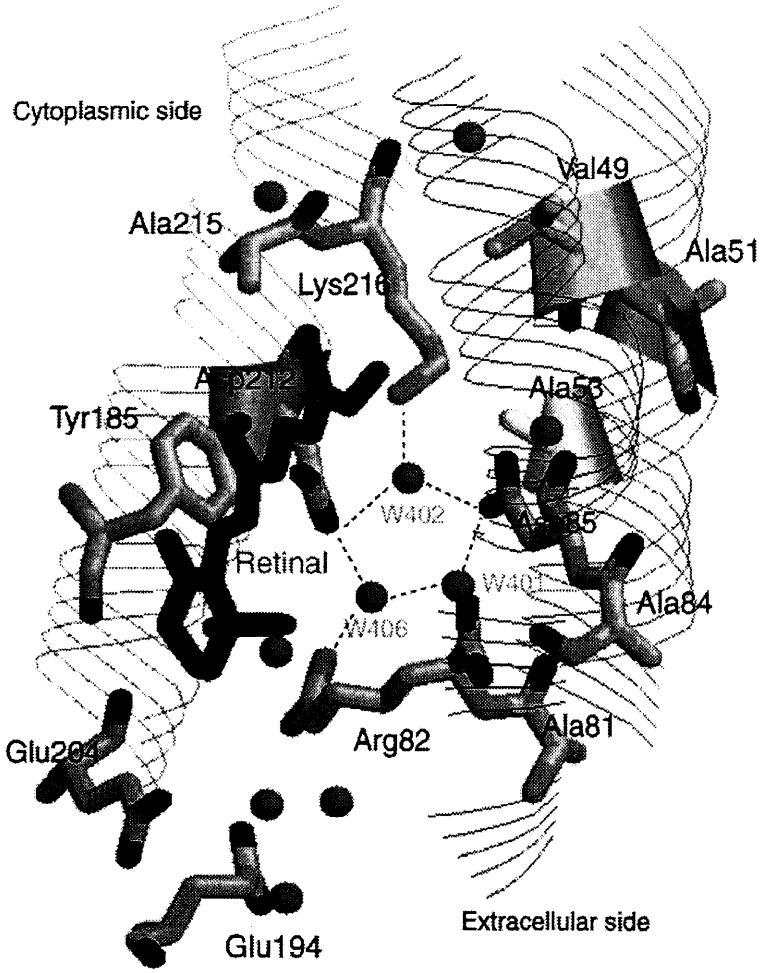

Figure 3. Schematic representation of primary amino acid residues and water in the vicinity of retinal in bR. (7) (PDB Code: 1C3W).

2-2 Structural changes of bacteriorhodopsin with pressure induced isomerization of retinal as disclosed by Fast Magic Angle Spinning NMR

Abstract

Bacteriorhodopsin (bR), a retinal protein in purple membrane of *H. salinarum*, shows function as a light-driven proton pump. We have detected pressure effects upon fast MAS NMR spectra of [ζ-^{15}N]Lys-, [3-^{13}C]Ala- and [1-^{13}C]Val-labeled bR. ^{15}N CP-MAS (Cross Polarization-Magic Angle Spinning) spectra of [ζ-^{15}N]Lys-bR were measured, as a sensitive probe on retinal isomerization. In the ^{15}N NMR signals, both all-*trans* and 13-*cis* retinal configurations have been observed at 148.0 and 155.0 ppm under the condition of MAS 4 kHz, respectively. When the MAS frequency was increased up to 12 kHz, the ^{15}N NMR signals of Schiff Base of retinal showed broadening at a spinning frequency higher than 10 kHz. The signal intensity of 13-*cis* retinal at 155.0 ppm increased when the MAS frequency was decreased from 12 kHz to 4 kHz. In the DD-MAS (Dipolar Decoupling-Magic Angle Spinning) ^{13}C NMR spectra, the signal of [3-^{13}C]Ala-labeled bR appeared at 16.6 ppm at a spinning frequency higher than 10 kHz and deduced from Ala84 in the vicinity of retinal. In addition, this component at 16.6 ppm did not disappear after the MAS frequency was decreased to 4 kHz. It is, therefore, clearly demonstrated that increase of pressure by fast MAS frequencies induced 13-*cis* isomerization of retinal and dynamics change in the vicinity of retinal binding site.

Introduction

Bacteriorhodopsin (bR), in *Halobacterium salinarum*, is a 26 kDa seven transmembrane helix protein with a retinal via Lys 216 in helix G and utilizes light to release proton by retinal photo-isomerization from cytoplasmic side to extracellular side (**1**). BR assembles into naturally occurring 2D crystalline patches known as purple membrane (PM) in which its trimeric unit is hexagonally packed under physiological condition (**2**). 3D structure of bR with 1.55 Å resolutions has been revealed by X-ray diffraction (**3**). And crystal structure of 13-*cis* bacteriorhodopsin in the dark-adapted state (**4**). Strongly hydrogen-bonded water molecules with Asp85 to Asp212 in the vicinity of retinal play an important role in the proton transfer of bR (**5**). BR is also important as a model protein such as a G-protein coupled receptor (GPCR),

including rhodopsin (**6, 7**).

The retinal configurations in the dark adapted state bR are all-*trans* and 13-*cis* state as the isomeric ratio close to 1 (**8-10**). The isomeric ratio in the dark is insensitive to temperature (**11, 12**). Pressure dependencies have been revealed for photocycle of bR and isomeric retinal components of the dark-adapted state with the molar volume changes (**13-15**). In addition, pressure effects for bR in the dark have been suggested that the isomer equilibrium shifts from all-*trans* towards 13-*cis* state at two processes with the molar volume changes (**16**). The first process on few MPa may be contributed to changes conformation of functionally important residues Tyr185 and Asp212 in the vicinity of retinal. Further, bR is very stable as thermal (**17**) and high temperature intermediate in bR exists > 60°C (**18**).

We have revealed that local conformation and dynamics for amino acid selective isotope labeled bR (**19-21**). In particular, it turned out that ^{13}C NMR peaks were well-resolved for fully hydrated [3-^{13}C]Ala-, [1-^{13}C]Val-labeled bR, depending upon their locations with specific local dynamics and conformations of 29 Ala or 21 Val residues, respectively (Figure 1) (**22, 23**). For example, dynamics of surface residues at various environmental factors as temperature, pH and ionic strength, and conformational changes of key residues for proton transfer on the extracellular side in bR by Mn^{2+} ion and site-directed or multiple mutations (**24-29**). In this study, pressure effects as isomeric ratio of retinal, conformational changes and dynamics for [ζ-^{15}N]Lys-, [3-^{13}C]Ala- and [1-^{13}C]Val-labeled bR in the dark were detected on MAS (Magic Angle Spinning) condition at high spinning frequency. MAS can eliminate the chemical shift anisotropy when the rotation axis of the sample is inclined to 54.7° to the static magnetic field (so called Magic Angle) and the sample rotor is fast spinning (**30, 31**). Centrifugal force generates constantly pressure for fully hydrated sample as a function of square rotor frequency and square of radius. For example, the changes of cell volume of multi-lamellar vesicles (DOPC, POPC) or red-blood cells were induced by ^{1}H or ^{31}P fast MAS NMR (**32, 33**). Increased pressure by the fast MAS frequencies induces isomerization from the all-*trans* to 13-*cis* retinal. (**34**)

Therefore, we will focus on pressure effects for bR in PM by solid state MAS NMR measurements. Retinal configurations in bR were revealed by ^{15}N NMR spectra of [ζ-^{15}N]Lys-labeled bR on fast MAS conditions. Moreover, local dynamics changes of protein with isomerization of 13-*cis* retinal by pressure were also found by ^{13}C NMR spectra of [3-^{13}C]Ala- and [1-^{13}C]Val-labeled bR on fast MAS conditions. It turned out that increased of pressure by fast MAS frequencies induced the change of molecular motions of site-directed residues in the vicinity of retinal.

Materials and Methods

Halobacterium salinarum S9 was grown in temporary synthetic medium including [ζ-^{15}N]-L-Lys, [3-^{13}C]-L-Ala and [1-^{13}C]-L-Val to yield [ζ-^{15}N]Lys-, [3-^{13}C]Ala-, [1-^{13}C]Val-labeled bR in purple membrane (PM). Ala (*circles*), Val (*boxes*) and other residues (*triangles*) in the vicinity of retinal were showed in Figure 1 based on X-ray diffraction of bR. PM was isolated by the standard method as described (**35**) and suspended in 5 mM HEPES buffer containing 0.02 % NaN_3 and 10 mM NaCl at pH 7. The sample was concentrated by centrifugation and placed in 4.0 mm o.d. ZnO_2 pencil-type rotor for fast magic angle spinning (MAS). Sample rotors were tightly shielded by Teflon caps and glued to the rotor by rapid Alardyte to prevent dehydration of pelleted samples.

^{13}C and ^{15}N high-resolution solid-state NMR spectra in this study were recorded on Chemagnetics CMX-400 infinity FT-NMR Spectrometer at 100.16 MHz carbon and 40.3 MHz nitrogen frequencies. Cross Polarization-Magic Angle Spinning (CP-MAS) on variable amplitude contact pulse of observed nucleus (**36**) and single pulse excitation with Dipolar Decoupling-Magic Angle Spinning (DD-MAS). A double resonance MAS probe with 4.0 mm o.d. rotor was used at all measurements. The spinning frequencies were set to 4-12 kHz and 90° pulse for proton and carbon nucleus was 5.1 μs. All the measurements at the second 4 kHz were performed after 12 kHz. Ambient conditions are used for MAS experiment at 4 kHz and probe temperature was set at 20°C. Sample temperature on MAS frequencies was calibrated using $PbNO_3$ prior to the series of experiments (**37**). Since the pressure induced by the centrifugal force is proportional to the rotor radius and the square of rotor frequency, pressure of inner wall of the ZrO_2 rotor can be estimated 63 bar for the frequency of 12 kHz. In variable amplitude CP-MAS with TPPM (Two Pulse Phase Modulation) decoupling (**38**) was 10.0 μs to proton decoupling, ^{13}C and ^{15}N contact time, and repetition time were 1 and 2 ms, and 4 s. ^{13}C chemical shifts and ^{15}N chemical shifts were externally referred to 176.03 ppm and 11.59 ppm for the carbonyl carbon and amine nitrogen of glycine from TMS and NH_4NO_3, respectively.

Results

NMR spectrum of $Pb(NO_3)$ has only one sharp resonance and chemical shifts of this peak are very sensitive to temperature change (**37**). Figure 2 (A) is a plot of ^{207}Pb chemical shift versus temperature. ^{207}Pb chemical shifts were internally referred to 0 ppm at 20°C, MAS 2 kHz. Temperature-Chemical shifts relation is linear in this temperature range. The relationship of ^{207}Pb chemical shifts against temperatures is 0.656 ppm/°C. MAS heating effects to 12 kHz are

presented in Figure 2 (B). It was observed that temperature of the sample using the relation of ^{207}Pb chemical shifts against temperatures increased by 20°C as the spinning frequency increases to 12 kHz by 10 kHz.

Figure 3 (A)-(D) show the ^{15}N CP-MAS NMR spectra of [ζ-^{15}N]Lys-bR in the spectral range between 100 and 200 ppm. Both ^{15}N NMR signals due to all-*trans* and 13-*cis* retinal configurations in the dark were observed at 148.0 and 155.0 ppm under the MAS frequency of 4 kHz (Figure 3(A)). When the MAS frequency was increased up to 12 kHz, the ^{15}N NMR signals of Schiff base of retinal showed broadening (Figure 3 (B)). The signal intensity of the 13-*cis* retinal at 155.0 ppm increased as the MAS frequency was decreased from 12 to 4 kHz (Figure 3(C)). Retinal configurations caused hysteresis by the fast MAS experiments. When temperature was increased to 40°C corresponding to the temperature at 12 kHz and subsequently decreased to 20°C by keeping the rotor speed of 4 kHz, the signal of 13-*cis* was not increased. These results clearly indicate that isomerization from all-*trans* to 13-*cis* occur in the presence of pressure about 63 bar. We refer to this 13-*cis* populated state as a pressure adapted state. A white light was irradiated continuously to bR and significant increase of the signal of all-*trans* was observed (Figure 3(D)). The proportions of retinal isomers are the same as the dark-adapted state bR, which is shifted from all-*trans* to 13-*cis* rich state by the application of pressure and from 13-*cis* to all-*trans* rich state by the photo-illumination.

Figure 4 (A)-(E) show the ^{15}N CP-MAS NMR spectra of [ζ-^{15}N]Lys-bR at various temperature by keeping the rotor speed of 4 kHz. The signals of protonated Schiff base in bR was broadening at 40°C corresponding to the MAS frequency of 12 kHz (Figure 3(B) and Figure 4 (C)). However, retinal configurations in bR did not caused hysteresis by temperature change. The retinal isomeric ratio in the dark is insensitive to the temperature change. Therefore, the change of retinal isomeric ratio was caused by pressure effect induced by fast MAS.

Figure 5 shows ^{13}C DD-MAS NMR spectra of [3-^{13}C]Ala-labeled bR at 4, 6, 8, 10 and 12 kHz spinning in the dark. After measured at 12 kHz, DD-MAS NMR spectrum was observed at 4 kHz again. So far, observed NMR signals of [3-^{13}C]Ala-labeled bR were sufficiently assigned to ^{13}C chemical shifts, for instance, NMR signals of C-terminal random coil (Ala240, 244-246) and C-terminal α-helix (Ala228, 233) at 16.88 and 15.91 ppm as ^{13}C conformation-dependent chemical shifts (**19, 23, 26, 41, 42**). In addition, we supposed that a fluctuated α-helix conformation could be recognized as an α_{II}-helix from ^{13}C NMR data on bR (**19**), instead of IR spectra (**43**). As MAS spinning frequency increased, two changes could be obviously found. First, NMR signal of C-terminal α-helix at 15.9 ppm shifts to low-field. As is mentioned in Figure 2, sample temperature at 12 kHz is about 40°C, which is the temperature effect caused

by fast MAS. After fast sample spinning, the signal at 4 kHz returned to former position at 15.9 ppm. C-terminal α-helix is very sensitive to temperature change (**26**). Second, interestingly, in the spectra under fast spinning at 10, 12 kHz, ^{13}C NMR signal at 16.6 ppm pronouncedly appeared as a sharp peak (As shown in Figure 4). The sample in the rotor constantly pressurize by the MAS frequency during the measurements. This signal is irreversible component because it was sufficiently remained the signal at 4 kHz after the fast spinning. This peak observed in DD-MAS indicated to fast molecular motions because of decreasing of interference of ^{1}H decoupling field with the increase of molecular fluctuation (**44**). Only this signal at 16.6 ppm caused hysteresis by fast MAS experiments and it is therefore attributed to the pressure effects for bacteriorhodopsin by fast MAS.

Figure 6 shows ^{13}C CP-MAS NMR spectra of [3-^{13}C]Ala-labeled bR at 4, 8, 10, 12, 4 kHz. At 10, 12 kHz, changes of spectral pattern may be for increased temperature, and in fact, are similar with NMR spectra at elevated temperature (**26**). After a fast spinning, ^{13}C CP-MAS NMR spectrum at secondary 4 kHz was almost unchanged as compared with that at 4 kHz. Only change is the reduction of peak intensity at 16.6-8 ppm. This peak is assigned to Ala 81, 84 near Asp85 as a counteranion of protonated Schiff Base (**23, 24, 27**). In addition, this peak displacement consists of that of the pressure effects in DD-MAS under fast MAS conditions.

Figure 7 (A)-(F) show ^{13}C CP-MAS NMR spectra of [1-^{13}C]Val-labeled bR at 4, 6, 8, 10, 12 kHz. In order to detect pressure effects on global protein backbone conformations in bR from ^{13}C CP-MAS NMR narrow signals of [1-^{13}C]Val-labeled bR, ^{13}C NMR spectral pattern at the MAS frequency of 4 kHz was compared to that at secondary MAS frequency of 4 kHz. These spectral patterns were almost no change by fast MAS experiments. It turned out to be caused by the pressure effect on local site in the vicinity of retinal of bR.

Discussion

The pressure effects induced by Fast MAS for bacteriorhodopsin as dynamics change in the vicinity of retinal

Retinal configurations in bR changed from all-*trans* to 13-*cis* retinal by fast MAS experiments of [ζ-^{15}N]Lys-labeled bR (Figure 3). The MAS frequency of 12 kHz raised the temperature about 20°C compared to that of 2 kHz (See Figure 2). The signal at 16.6 ppm in the DD-MAS NMR spectra of [3-^{13}C]Ala-labeled bR did not appear at the temperature corresponding to the MAS frequency of 12 kHz (See Figure 5, 6) (**26**). Further this peak is irreversible because of appearance at 4 kHz. Following possibilities are discussed for the appearance of the signal at 16.6 ppm. We considered that this ^{13}C NMR peak clearly appears at 16.6 ppm and this dynamics dramatically changes with isomerization to 13-*cis* retinal by the fast MAS pressure to bR in PM. As a result, retinal isomer's components almost equaled in the dark-adapted state of bR have shifted from all-*trans* to 13-*cis* state (**13,14**). Besides, it was confirmed by extraction techniques and absorption spectroscopy of the range from low to high pressure that the isomer equilibrium shifts from all-*trans* to 13-*cis* state at two processes with the molar volume changes in the dark (**16**). As population of 13-*cis* increases by pressure (Figure 3), dynamics of Ala residues in the vicinity of retinal is increased to lead the signal intensity at 16.6 ppm. Therefore, it is considered that the signal at 16.6 ppm in the DD-MAS spectra was deduced from 13-*cis* retinal induced by pressure. It is important to point out the influences of pressure by fast MAS condition upon Ala residues Ala81, 84 and 215 in the vicinity of retinal. Therefore, the Ala81, 84 and 215 NMR signals may be observed at 16.6 ppm in solid-state ^{13}C CP-MAS and DD-MAS NMR spectra under fast MAS condition. Locations of water molecules in the vicinity of retinal were confirmed (**3**) and hydrogen-bond network via water molecules that correlate with proton pump activity exist in bR (**5, 45**). In High-Pressure ^{15}N/^{1}H NMR techniques, fluctuations of hen lysozyme are found to be localized near the cavities containing water molecules (**46, 47**). In general, hydrogen bonds of protein structure changed H···O distance to pressure with molar volume change (**47**). Therefore, the pressure induced isomerization of retinal and modulation of the hydrogen-bond network, as a result, the change in motion of residues located in the vicinity of retinal. In addition, it is considered that the Ala81 and 84 signal near Arg82 increase the intensity in the case where the side chain of Arg82 may move from up or down by the pressure (**24**). Moreover, ^{13}C CP-MAS signals of bR also vary with the change of pH and ionic strengths, and were observed to be similar to NMR spectra under fast MAS condition (**26, 28**). In the fast MAS condition, it was considered that increase of pressure by fast MAS frequencies induced the change of molecular motions of site-directed residues as Ala81, 84 belonging to α_{II}-helix in the vicinity of retinal.

Conclusions

Noticeable pressure effects on bR in purple membrane were observed. Increased pressure (63 bar) by the fast MAS frequencies induced isomerization from all-*trans* to 13-*cis* retinal and dynamical change of site-directed residues belonging to α_{II}-helix in the vicinity of retinal as assigned by conformation-dependent chemical shifts. It turned out that the conformational change was caused by the pressure effect on the local site in the vicinity of retinal in bR.

Reference

1. J. K. Lanyi, and B. Schobert

Local-Global Conformational Coupling in a Heptahelical Membrane Protein: Transport Mechanism from Crystal Structure of the Nine States in the Bacteriorhodopsin Photocycle.

Biochemistry 2004 **43** 3-8.

2. N. Grigorieff, T. A. Ceska, K. H. Dowing, J. M. Baldwin, R. Henderson

Electron-crystallographic refinement of the structure of bacteriorhodopsin.

J. Mol. Biol. 1996 **259** 393-421.

3. H. Luecke, B. Schobert, H-T. Richter, J-P. Cartailler and J. K. Lanyi.

Structure of bacteriorhodopsin at 1.55Å resolution.

J. Mol. Biol. 1999 **291** 899-911.

4. T. Nishikawa, M. Murakami, T. Kouyama

Crystal structure of the 13-cis isomer of bacteriorhodopsin in the dark-adapted state.

J. Mol. Biol. 2005 **352** 319-328.

5. M. Shibata and H. Kandori

FTIR studies of internal water molecules in the Schiff base region of bacteriorhodopsin

Biochemistry 2005 **44** 7406-7413.

6. E. Crocker, M. Eilers, S. Ahuja, V. Hornak, A. Hirshfeld, M. Sheves, and S. O. Smith

Location of Trp265 in Metarhodopsin II: Implications for the Activation Mechanism of the Visual Receptor Rhodopsin

J. Mol. Biol. 2006 **357** 163-172.

7. T. Okada, Y. Fujiyoshi, M. Silow, J. Navarro, E. M. Landau and Y. Shichida

Functional role of internal water molecules in rhodopsin revealed by X-ray crystallography

Proc. Natl. Acad. Sci. U.S.A. 2002 **99** 5982-5987.

8. A. Maeda, T. Iwasa, and T. Yoshizawa.

Isomeric composition of retinal chromophore in dark-adapted bacteriorhodopsin.

J. Biochem. 1977 **82** 1599-1604.

9. H-W. Trissl, and W. Gartner.

Rapid charge separation and batochromic absorption shift of flash-excited bacteriorhodopsin containing 13-*cis* or all-*trans* forms of substituted retinals.

*Biochemistry*1987 **26** 751-758.

10. H. J. M. De Groot, G. S. Harbison, J. Herzfeld, and R. G. Griffin.

Nuclear Magnetic Resonance Study of the Schiff Base in Bacteriorhodopsin: Counterion Effects on the ^{15}N Shift Anisotropy.

Biochemistry 1989 **28** 3346-3353.

11. N. A. Dencher, Ch. N. Rafferty and W. Sperling.

13-cis and trans bacteriorhodopsin: photochemistry and dark equilibrium.

Biophys. Struct. Mechan. 1977 **3** 79-94

12. K. Ohno, Y. Takeuchi, M. Yoshida.

Light-Induced Formation of the 410 nm Intermediate from Reconstitued Bacteriorhodopsin

J. Biochem. (Tokyo) 1977 **82** 1177-1180.

13. M. Tsuda, and T. G. Ebrey.

Effect of high pressure on the absorption spectrum and isomeric composition of bacteriorhodopsin.

Biophys. J. 1980 **30** 149-158.

14. M. Tsuda, R. Govindjee, T. G. Ebrey.

Effects of pressure and temperature on the M412 intermediate of the bacteriorhodopsin photocycle. Implications for the phase transition of the purple membrane.

Biophys. J. 1983 **44** 249-254.

15. B. U. Klink, R. Winter, M. Engelhard, and I. Chizhov,

Pressure Dependence of the Photocycle Kinetics of Bacteriorhodopsin.

Biophys. J. 2002 **83** 3490-3498.

16. K. Bryl, and K. Yoshihara,

Two processes lead to a stable all-*trans* and 13-*cis* isomer equilibrium in dark-adapted bacteriorhodopsin; effect of high pressure on bacteriorhodopsin, bacteriorhodopsin mutant D96N and fluoro-bacteriorhodopsin analogues

Eur. Biophys. J. 2002 **31** 539-548.

17. Y. Mukai, N. Kamo, and S. Mitaku,

Light-induced denaturation of bacteriorhodopsin solubilized by octyl-β-glucoside.

Protein Eng. 1999 **12** 755-759.

18. Y. Yokoyama, M. Sonoyama, and S. Mitaku.

Irreversible Photobleaching of Bacteriorhodopsin in a High-Temperature Intermediate State.

J. Biochem. 2002 **131** 785-90.

19. H. Saitô, S. Tuzi, S. Yamaguchi, M. Tanio and A. Naito.

Conformation and backbone dynamics of bacteriorhodopsin revealed by ^{13}C-NMR

Biochem. Biophys. Acta. 2000 **1460** 39-48.

20. H. Saitô, J. Mikami, S. Yamaguchi, M. Tanio, A. Kira, T. Arakawa, K. Yamamoto, and S. Tuzi.

Site-directed ^{13}C solid-state NMR studies on membrane proteins: strategy and goals toward revealing conformation and dynamics as illustrated for bacteriorhodopsin labeled with

[1-^{13}C]amino acid residues.

Magn. Reson. Chem. 2004 **42** 218-230.

21. H. Saitô, S. Yamaguchi, H. Okuda, A. Shiraishi and S. Tuzi.

Dynamic aspect of bacteriorhodopsin as a typical membrane protein as revealed by site-directed solid-state ^{13}C NMR.

Solid State Nucl. Magn. Reson. 2004 **25** 5-14.

22. H. Saitô, S. Tuzi and A. Naito.

Empirical versus nonempirical evaluation of secondary structure of fibrous and membrane proteins by solid-state NMR: a practical approach.

Annu. Rep. NMR Spectrosco. 1998 **36** 79-121.

23. H. Saitô, S. Tuzi, M. Tanio, A. Naito.

Dynamic Aspects of Membrane Proteins and Membrane-Associated Peptides as Revealed by ^{13}C NMR: Lessons from Bacteriorhodopsin as an *Intact* Protein.

Annu. Rep. NMR Spectrosco. 2002 **47** 39-108.

24. M. Tanio, S. Tuzi, S. Yamaguchi, R. Kawaminami, A. Naito, R. Needleman, J. K. Lanyi, and H. Saitô.

Conformational Changes of Bacteriorhodopsin along the Proton-Conduction Chain as Studied with ^{13}C NMR of [3-^{13}C]Ala-labeled Protein: Arg^{82} May Function as an Information Mediator

Biophys. J. 1999 **77** 1577-1584

25. S. Yamaguchi, S. Tuzi, M. Tanio, A. Naito, J. K. Lanyi, R. Needleman, and H. Saitô.

Irreversible Conformational Change of Bacterio-opsin Induced by Binding of Retinal during Its Reconstitution to Bacteriorhodopsin, as Studied by ^{13}C NMR.

J. Biochem. 2000**127** 861-869.

26. S. Yamaguchi, K. Yonebayashi, H. Konishi, S. Tuzi, A. Naito, J. K. Lanyi, R. Needleman, and H. Saitô.

Cytoplasmic surface structure of bacteriorhodopsin consisting of interhelical loops and C-terminal α helix, modified by a variety of environmental factors as studied by ^{13}C NMR

Eur. J. Biochem. 2001 **268** 2218-2228.

27. S. Tuzi, J. Hasegawa, R. Kawaminami, A. Naito, H. Saitô

Regio-selective detection of dynamic structure of transmembrane a-helices as revealed from ^{13}C NMR spectra of [3-^{13}C]Ala-labeled bacteriorhodopsin in the presence of Mn^{2+} ion.

Biophys. J. 2001 **81** 425-434.

28. K. Yonebayashi, S. Yamaguchi, S. Tuzi and H. Saitô.

Cytoplasmic surface structures of bacteriorhodopsin modified by site-directed mutations and cation binding as revealed by ^{13}C NMR

Eur. Biophys. J. 2003 **32** 1-11.

29. H. Saitô, S. Yamaguchi, K. Ogawa, S. Tuzi, M. Marquez, C. Sanz and E. Padros
Glutamic Acid Residues of Bacteriorhodopsin at the Extracellular Surface as Determinants for Conformation and Dynamics as Revealed by Site-Directed Solid-State ^{13}C NMR
Biophys. J. 2004 **86** 1673-1681.

30. E. R. Andrew, A. Bradbury and R. G.. Eades.
Nuclear Magnetic Resonance Spectra from a Crystal rotated at High Speed.
Nature 1958 **182** 1659.

31. I. J. Lowe.
Free Induction Decays of Rotating Solids
Phys. Rev. Lett. 1959 **2** 285-287.

32. Z. Zhou, R. G. Sayer, D. W. Hughes, R. E. Stark, and R. M. Epand.
Studies of Phospholipid Hydration by High-Resolution Magic-Angle Spinning Nuclear Magnetic Resonance
Biophys. J. 1999 **76** 387-399.

33. P. W. Kuchel, W. A. Bubb, S. Ramadan, B. E. Chapman, D. J. Philp, M. Coen, J. E. Gready, P. J. Harvey, A. J. McLean and J. Hook.
^{31}P MAS-NMR of Human Erythrocytes: Independence of Cell Volume from Angular Velocity.
Magn. Reson. Med. 2004 **52** 663-668.

34. I. Kawamura, Y. Degawa, S. Yamaguchi, K. Nishimura, S. Tuzi, H. Saitô and A. Naito.
Pressure Induced Isomerization Retinal on Bacteriorhodopsin as Disclosed by Fast Magic Angle Spinning NMR.
Photochem. Photobiol. 2007 in press.

35. D. Oesterhelt and W. Stoeckenius 1974.
Isolation of the cell membrane of *Halobacterium halobium* and its fractionation into red and purple membrane.
Methods Enzymol. **31** 667-678.

36. G. Metz, X. Wu and S. O. Smith 1994.
Ramped amplitude cross polarization in magic angle spinning NMR.
J. Magn. Reson. ser. A **110** 219-227.

37. A. Bielecki, A. and Burum, D. P. 1995.
Temperature Dependence of ^{207}Pb MAS spectra of Solid Lead Nitrarte. An Accurate, Sensitive Thermometer for Variable-Temperature MAS.
J. Magn. Reson. ser. A **116** 215-220.

38. A. W. Bennet, Rienstra, C. M., Augar, M., Lakshmi, K. V., and Griffin, R. G. 1995.

Heteronuclear decoupling in rotating solids.

J. Chem. Phys. **103** 6951-6958.

39. S. O. Smith, H. J. M. De Groot, R. Gebhard, J. M. L. Courtin, I. Lugtenburg, J. Herzfeld and R. G. Griffin 1989.

Structure and Protein Environment of the Retinal Chromophore in Light- and Dark-Adapted BR Studied by Solid State NMR

Biochemistry **28** 8897-8904.

40. M. E. Hatcher, J. G. Hu, M. Belenky, P. Verdegem, J. Lugtenburg, R. G. Griffin, and J. Herzfeld 2002

Control of the Pump Cycle in Bacteriorhodopsin: Mechanisms Elucidated by Solid-State NMR of the D85N Mutant

Biophys. J. **82** 1017–1029.

41. H. Saitô 1986

Conformational-dependent ^{13}C chemical shifts: a new means of conformational characterization as obtained by high resolution solid-state ^{13}C NMR

Magn. Reson. Chem. **24** 835-852.

42. H. Saitô and I. Ando 1989.

High-resolution solid-state NMR studies of synthetic and biological macromolecules.

Annu. Rep. NMR Spectrosco. **21** 209-290.

43. S. Krimm and A. M. Dwivedi 1982.

Infrared spectrum of the purple membrane: clue to a proton conduction mechanism?

Science **216** 407-408.

44. W. P. Rothwell, and Waugh J. S. 1981.

Transverse relaxation of dipolar coupled spin systems under rf irradiation: detection motions in solid.

J. Chem. Phys. 75: 2721-2732.

45. H. Kandori 2000.

Role of internal water molecules in bacteriorhodopsin

Biochim. Biophys. Acta. 1460:177-191.

46. Y. O. Kamatari, Yamada, H., Akasaka, K., Jones, J. A., Dobson, C. M. and Smith, L. J. 2001.

Response of native and denatured hen lysozyme to high pressure studied by $^{15}N/^{1}H$ NMR spectroscopy.

Eur. J. Biochem. 268:1782-1793.

47. K. Akasaka, 2003

Highly Fluctuating Protein Structures Revealed by Variable-Pressure Nuclear Magnetic

Resonance
Biochemistry 42:10875-10885.

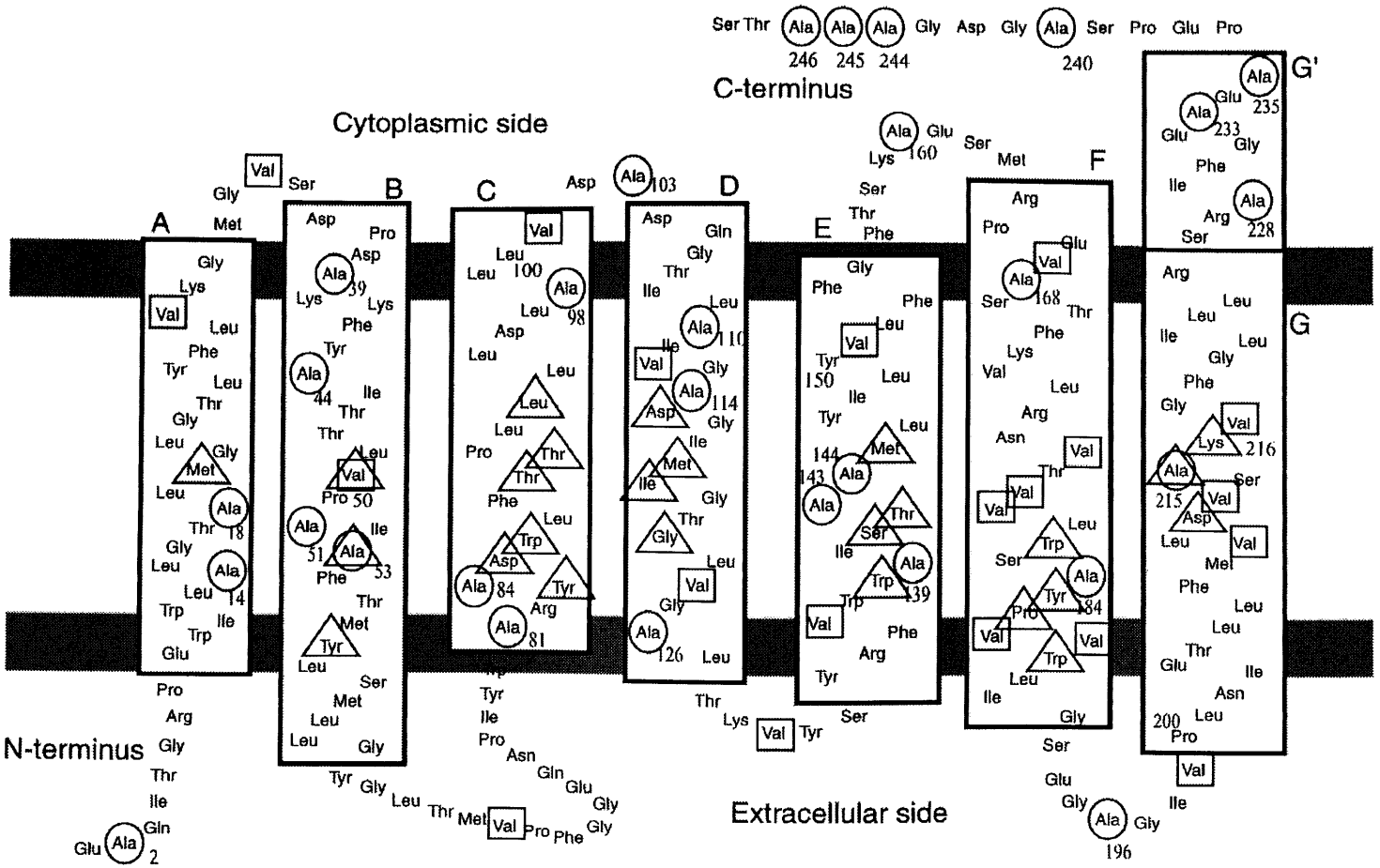

Figure 1. A schematic representation of the secondary structure of bR based on X-ray diffraction report (PDB code 1C3W). Shown as Ala (circles), Val (boxes) and residues in the vicinity of retinal (triangles). The surface areas of lipid bilayer are represented by gray bands.

(A)

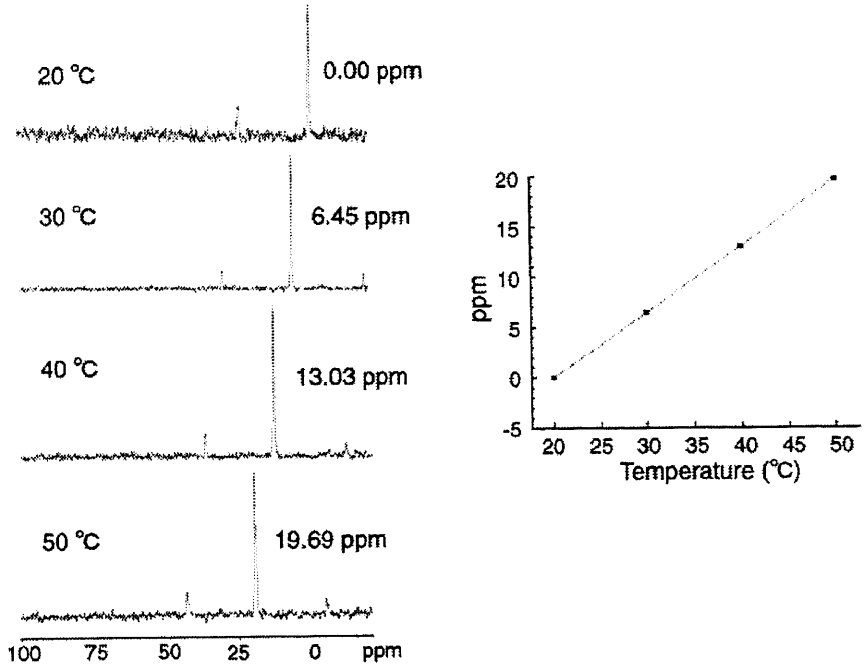

(B)

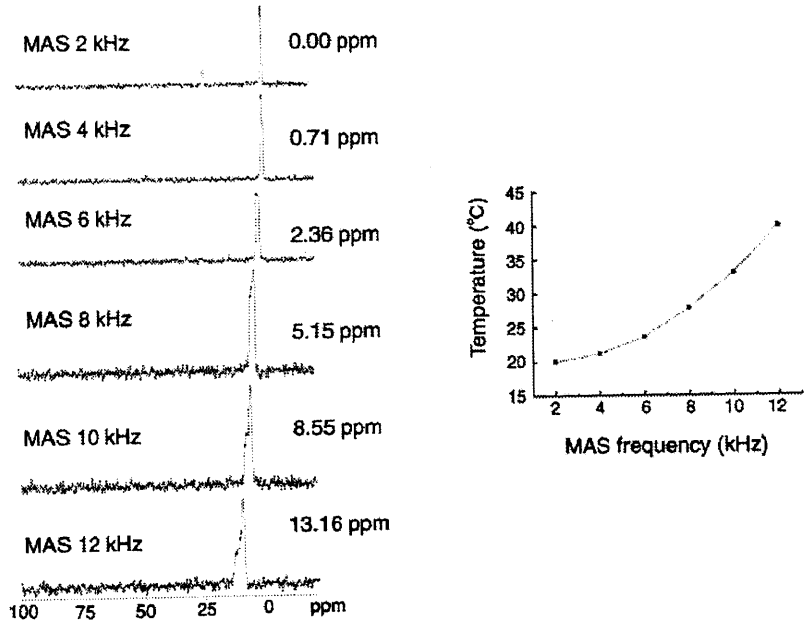

Figure 2. ^{207}Pb NMR spectra of $PbNO_3$ at various temperatures (A) and at various MAS frequencies (B). Plots of (A) ^{207}Pb chemical shifts variation versus temperatures with MAS frequency at 2.0 kHz through the measurements and (B) temperature variation versus magic angle spinning frequencies.

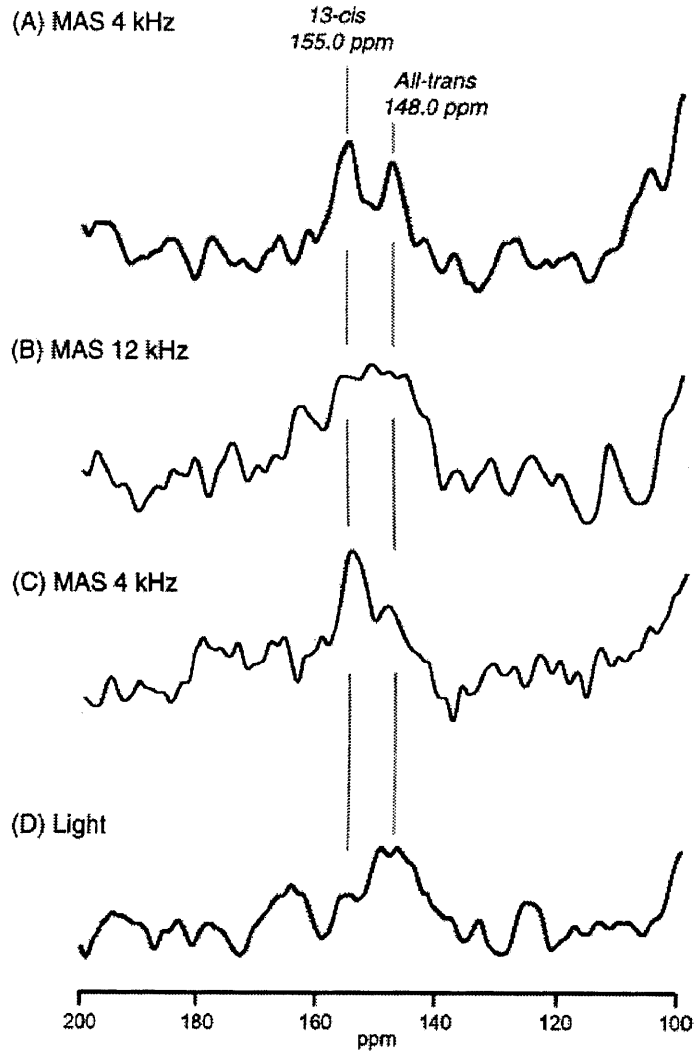

Figure 3. ^{15}N CP-MAS NMR spectra of [ζ-^{15}N]Lys of Schiff base in bR at MAS frequency of 4 and 12 kHz, respectively ((A) and (B)). After spinning sample at 12 kHz, CP-MAS NMR spectrum was observed at 4 kHz (C). *In situ* light-irradiation spectrum of bR (D).

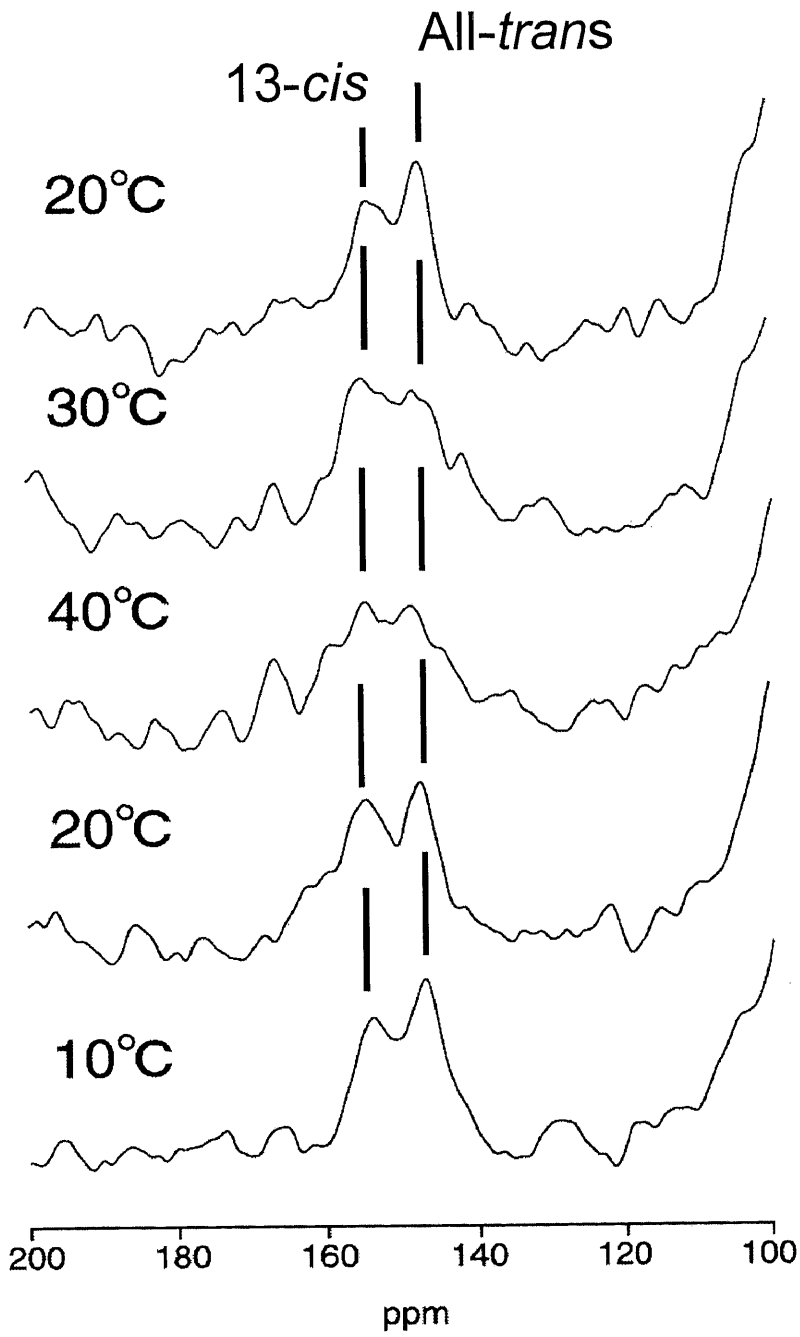

Figure 4. ^{15}N CP-MAS NMR spectra of [ζ-^{15}N]Lys of Schiff base in bR at various temperature and MAS 4 kHz.

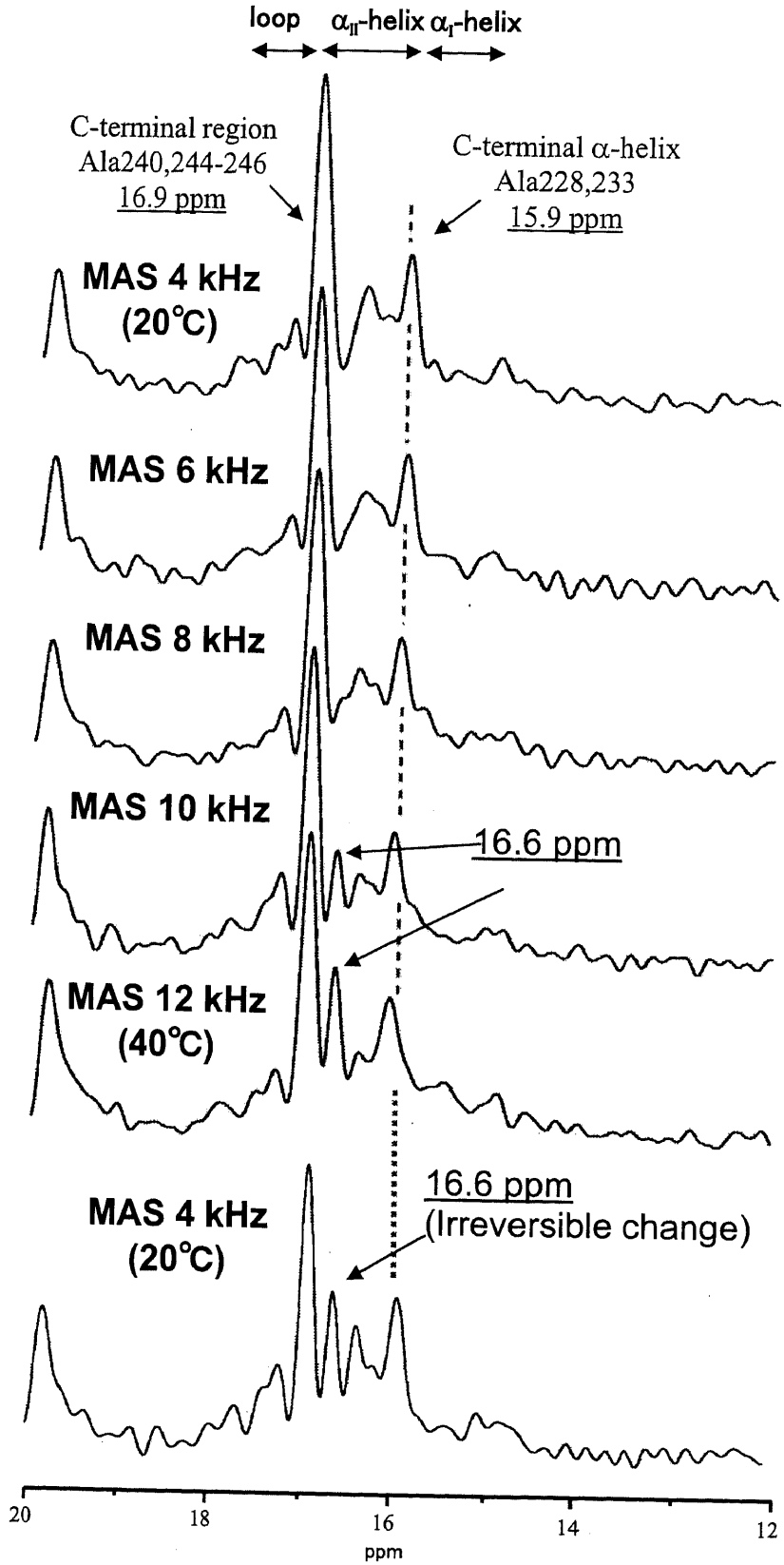

Figure 5. ^{13}C DD-MAS NMR spectra of [3-^{13}C]Ala-bR at various MAS frequencies up to 12 kHz. After spinning sample at 12 kHz, ^{13}C DD-MAS NMR spectrum was recorded at 4 kHz.

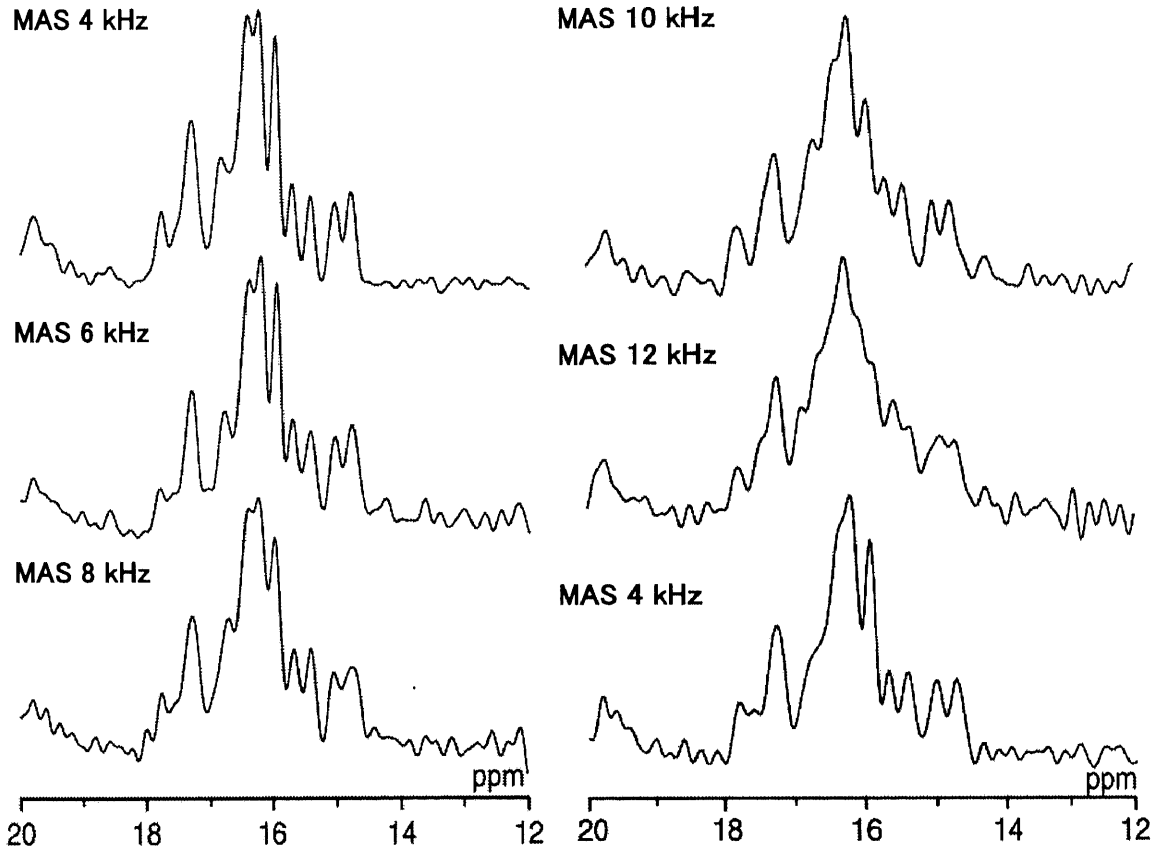

Figure 6. ^{13}C CP-MAS NMR spectra of [3-^{13}C]Ala-bR at various MAS frequencies up to 12 kHz. After spinning sample at 12 kHz, ^{13}C CP-MAS NMR spectrum was recorded at 4 kHz.

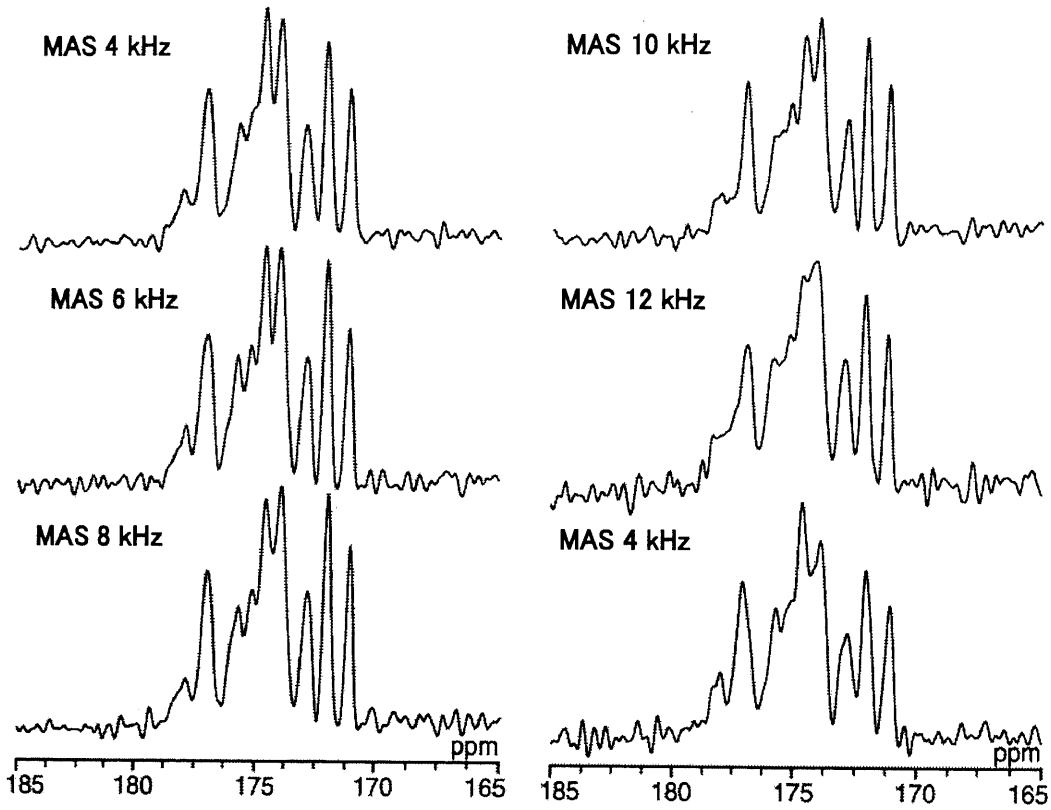

Figure 7. ^{13}C CP-MAS NMR spectra of [1-^{13}C]Val-bR at various MAS frequencies up to 12 kHz. After spinning sample at 12 kHz, ^{13}C CP-MAS NMR spectrum was recorded at 4 kHz.

Chapter 3

Two different backbone conformations at Tyr185 in bacteriorhodopsin corresponding to two retinal configurations

Abstract

Backbone conformations near tyrosine in bacteriorhodopsin (bR) corresponding to all-*trans* and 13-*cis* retinal configurations in the dark, light and pressure adapted states were investigated for Tyr-X peptide bonds by using double amino acid labeling with [1-^{13}C],[^{15}N]X-bR by means of rotational echo double resonance (REDOR) technique. The NMR signals obtained from the difference spectra between REDOR and full echo experiments allowed selectively detect on a tyrosine signals for Tyr185-Pro186, Tyr26-Phe27, and Tyr64-Gly65. Two ^{13}C NMR peaks were observed for REDOR-filtered spectrum of Tyr185 in the dark at ambient temperature. These two signals are attributed to the bR with all-*trans* and 13-*cis* retinals. REDOR-filtered spectra for Tyr26 and 64 show singlet lines because they are located far from the retinal. All-*trans* peak intensity was increased in the light adapted state, while the 13-*cis* state increased for pressure-adapted state. These results indicate that REDOR-filtered experiments provide us with valuable information of protein-retinal interaction.

Bacteriorhodopsin (bR), from *Halobacterium salinarum*, is a 26 kDa membrane protein that consists of seven transmembrane helices with a retinal covalently linked to Lys216 through protonated Schiff base. BR absorbs light to cause retinal photoisomerization from all-*trans* to 13-*cis*, 15-*anti* state followed by sequential proton-transfer reactions (**1**). The retinal configuration in the dark-adapted bR coexists as all-*trans* and 13-*cis*, 15-*syn* states with the isomeric ratio close to 1 (**2**). When illuminated (560 nm), the population of the all-*trans* state is increased. This all-*trans* populated state is called a light adapted state. The population of 13-*cis*, 15-*syn* state can be increased when pressure is increased (**3, 4**). Here, we refer to the 13-*cis* populated state as a pressure adapted state. X-ray diffraction study shows that primary amino acid residues, Arg82, Asp85, Tyr185, Asp212, and water molecules, W401, W402, W406, are located in the vicinity of the Schiff base region of retinal (**5**). It has been revealed that helix F, including Pro186 in the hinge region, moves outward by a tilt motion to open the proton channel at the cytoplasmic side in the M intermediate. Tyr residues in bR are known to be important for the photocycle and regulate color tuning; in particular, Tyr57, 83, and 185 are located in the vicinity of retinal (**6**). When these Tyr residues are replaced by other residues, the proton release rate is markedly delayed (**7**). This clearly indicates that tyrosine plays an important role in proton pump activity.

Rotational echo double resonance (REDOR) filtered experiments (**8**) in solid state NMR are a powerful method to observe a NMR peak of a specific nuclear pair with strong dipolar

interaction by using doubly isotopic labeling of a unique consecutive amino acid sequence in a protein. Namely, the NMR peak obtained from the difference spectrum between REDOR and full echo spectra show the signal of a labeled nucleus in a particular amino acid that is directly forming a peptide bond to the other labeled nucleus (**8**). Moreover, conformation dependent ^{13}C isotropic chemical shifts of [1-^{13}C]Tyr have been used to determine secondary structure in the vicinity of Tyr residues (**9**). In this paper, we use a REDOR filter to allow selective observation of Tyr-X peptide bonds in bR and characterize the backbone conformation of bR with respect to retinal-protein interactions. We also observed the Tyr signals corresponding to the dark, light, and pressure adapted states of bR. Here, *in situ* continuous photo-illumination was made by an optical fiber from outside the magnet through a tightly sealed piece of cap made of optical fiber glued to the rotor. Pressure on the samples was naturally applied by the centrifugal force induced by the MAS frequency. Since the centrifugal force is proportional to the square of rotor radius and the square of rotor frequency, pressure at inner wall of this rotor with 5 mm o.d. can be estimated to be 12 bar for the rotor frequency of 4 kHz.

The doubly isotopically labeled samples, a) [1-^{13}C]Tyr/[^{15}N]Phe-bR, b) [1-^{13}C]Tyr/[^{15}N]Gly-bR, and c) [1-^{13}C]Tyr/[^{15}N]Pro-bR, were prepared from *H. sarinarum* in the TS medium with [1-^{13}C]Tyr and [^{15}N]X, where X is Phe, Gly or Pro. Tyr185-Pro186 is located in the vicinity of retinal and a helix kink point in the photocycle. Tyr64-Gly65 is located at the membrane surface on the extracellular side and Tyr26-Phe27 in helix A at the cytoplasmic side (Figure 1). These samples were prepared in 5mM HEPES, 10 mM NaCl (pH7.0) as excess humidity membrane pellets (**10**). ^{13}C REDOR-filtered experiments were performed on a Chemagnetics CMX-400 Infinity FT-NMR spectrometer at the MAS spinning frequency of 4 kHz.

Figure 2 shows REDOR filtered ^{13}C NMR spectra of [1-^{13}C]Tyr/[^{15}N]X-bR. It is interesting to note that the REDOR- filtered spectrum of [1-^{13}C]Tyr/[^{15}N]Pro-bR obviously showed two peaks at 173.4 and 177.7 ppm corresponding to the [1-^{13}C] Tyr185 with an intensity ratio of 1:1 (Figure 2C). This finding is attributed to the presence of two retinal configurations in the dark adapted state. In fact, Tyr185 closely lies in the vicinity of retinal (**2, 6**). By contrast, the spectra of Tyr26 (Figure 2A) and Tyr64 (Figure 2B) of bR showed a single peak at 174.0 and 175.2 ppm, respectively. Tyr26 and Tyr64 are considered to be not sensitive to retinal configurations because they are located far from the retinal as shown in Figure 1. These spectra indicated that not only retinal configurations but also bR backbone conformations coexist in two states corresponding to the all-*trans* and 13-*cis*, 15-*syn* retinal configurations.

Notably, for the two peaks of Tyr185, the isotropic ^{13}CO chemical shift values are considerably different. The peak at 177.7 ppm is attributed to the all-*trans* retinal configuration,

according to ^{13}C REDOR-filtered experiments in the light adapted state (**8**). This unusually high chemical shift value of 177.7 ppm (176.7 ppm for α-helix in Tyr) (**9**) indicates α-helix structure with steric hindrance from all-*trans* retinal or with hydrogen bond such as bifurcated one (**9**). On the other hand, the peak at 173.4 ppm is influenced by the 13-*cis* retinal configuration and the shift value indicates a non α-helical structure or a highly distorted α-helix (**9**). The Schiff base region forms a pentagon cluster with strong hydrogen bond networks between Asp85, Asp212, and three water molecules (**5, 6**). Tyr185 forms a hydrogen bond with Asp212, but Y185F mutant may not perturb the pentagon cluster as disclosed by FTIR difference absorbance data (**5**). As a result of REDOR-filtered experiments, the backbone conformation near Tyr185 may change pronouncedly although the same pentagon hydrogen bond networks are retained (Figure 3).

REDOR-filtered ^{13}C NMR resonance of Tyr26 appeared as a single peak at 174.0 ppm. This value may indicate a dynamic α-helical conformation with 13-*cis* retinal. An increase in CO...HN hydrogen bond length causes an upfield shift of the isotropic ^{13}C chemical shift value. It is, therefore, considered that Tyr26 CO...Lys30HN length is slightly elongated and the region near Tyr26 has formed a disordered structure or dynamic α-helix (**10, 11**). The chemical shifts of Tyr64 indicated α-helical structure, although Tyr64 is located in the region of the extracellular membrane surface.

When the REDOR difference spectrum under MAS condition was taken with a long accumulation time of 60 hrs, the signal at 173.4 ppm for Tyr185 increased markedly (Figure 2D). This observation can be attributed to the pressure induced isomerization of retinal from all-*trans* to 13-*cis*, 15-*syn* state (**3**). This pressure induced isomerization has been observed by analyzing the photoisomer of retinal by chromatography (**3**) and NMR, (**4**) although pressure induced isomerization occurs at much lower pressure than the reported pressure in this experiment. It is noted that the protein rather than just retinal also changes conformation after the change of retinal configuration by pressure.

Figure 2E shows the difference spectrum between the dark and light adapted states using *in situ* photo-illumination experiments. Photo illumination can change the retinal isomer from 13-*cis* to all-*trans* configuration which subsequently induces the change of backbone conformation in bR. Line broadening was observed at 177.7 ppm, which can be attributed to the short lifetime of the all-*trans* state because this species can be transferred to the other excited states during photo illumination. It is also possible to cause broadening by the distribution of slightly different configurations of all-*trans* retinal and Tyr.

In conclusion, backbone conformations of Tyr185 in bR were strongly perturbed by the retinal configurations as disclosed from REDOR-filtered experiments (Figure 3). Consequently,

two different conformations of bR coexist near Tyr185 corresponding to the all-*trans* and 13-*cis* configuration of retinal. The populations of the two conformations of bR changes to all-*trans* populated state for the light adapted state, while the 13-*cis* populated state is dominant for the pressure adapted state. This local change of protein conformation was disclosed to be generated by photo isomerization of the retinal by means of the photo-illumination experiments. In contrast, only single conformations for Tyr26 and Tyr64 appeared. It is, therefore, revealed that the change of retinal configuration may induce a significant local change of backbone conformation in bR that is relevant to the regulation of light driven proton pathway.

Reference

1. J.K. Lanyi, B. Schobert. *Biochemistry* 2004 **43** 3-8.
2. (a) A. Maeda, T. Iwasa, T. Yoshizawa. *J. Biochem.* 1977 **82** 1599-1604. (b) H.-W. Trissl, W. Gartner. *Biochemistry* 1987 **26** 751-758. (c)H. J. De Groot, G. S. Harbison, J. Herzfeld, R. G. Griffin. *Biochemistry* 1989 **28** 3346-3353.
3. (a) M. Tsuda, T. G. Ebrey. *Biophys. J.* 1980 **30** 149-158. (b) K. Bryl, K. Yoshihara. *Eur. Biophys. J.* 2002 **31** 539-548.
4. I. Kawamura, Y. Degawa, S. Yamaguchi, K. Nishimura, S. Tuzi, H. Saitô, A. Naito. *Photochem. Photobiol.* 2007 In press.
5. M. Shibata, T. Tanimoto, H. Kandori. *J. Am. Chem. Soc.* 2003 **125** 13312-13313.
6. H. Luecke, B. Schobert, H.-T. Richter, J. P. Cartailler, J. K. Lanyi. *J. Mol. Biol.* 1999 **291** 899-911.
7. (a) F. Garczarek, L. S. Brown, J. K. Lanyi, K. Gerwert. *Proc. Natl. Acad. Sci. U.S.A.* 2005 **102** 3633-3638. (b) F. Delange, C. H. W. Klaassen, S. E. Wallace-Williams, P. H. M. Bovee-geuyrts, X. M. Liu, J. W. deGrip, K. Rothschild. *J. Biol. Chem.* 1998 **273** 23735-23739.
8. (a) T. Gullion, J. Schaefer. *Adv. Magn. Reson.* 1989 **13** 57-83. (b) J. C. Lansing, J. G. Hu, M. Belenky, R. G. Griffin, J. Herzfeld. *Biochemistry* 2003 **42** 3586-3593.
9. (a) H. Saitô, *Magn. Reson. Chem.* 1986 **24** 835-852. . (b) H. R. Kricheldorf, T. K. Haupt, D. Muller. *Magn. Reson. Chem.* 1986 **24** 41-52. (c) H. Saitô, S. Tuzi, M. Tanio, A. Naito. *Annu. Rep. NMR spectrosco.* 2002 **47** 39-108. (d) H. Saitô, J. Mikami, S. Yamaguchi, M. Tanio, A. Kira, T. Arakawa, K. Yamamoto, S. Tuzi. *Magn. Reson. Chem.* 2004 **42** 218-230.
10. H. Saitô, S. Tuzi, S. Yamaguchi, M. Tanio, A. Naito. *Biochim. Biophys. Acta* 2000 **1460** 39-48.
11. Y. Wei, D.-K. Lee, A. Ramamoorthy. *J. Am. Chem. Soc.* 2001 **123** 6118-6126.

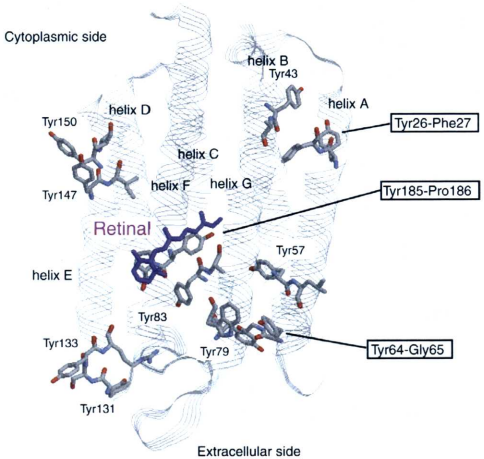

Figure 1. There are 11 Tyr residues in bR and Tyr-X peptide bond is unique in the sequence except when X is Ala. The three pairs of Tyr-X peptide bonds in bR for the REDOR filter experiments: Tyr26-Phe27, Tyr64-Gly65, and Tyr185-Pro186. Tyr185 lies close to retinal. (PDB code; 1C3W[6])

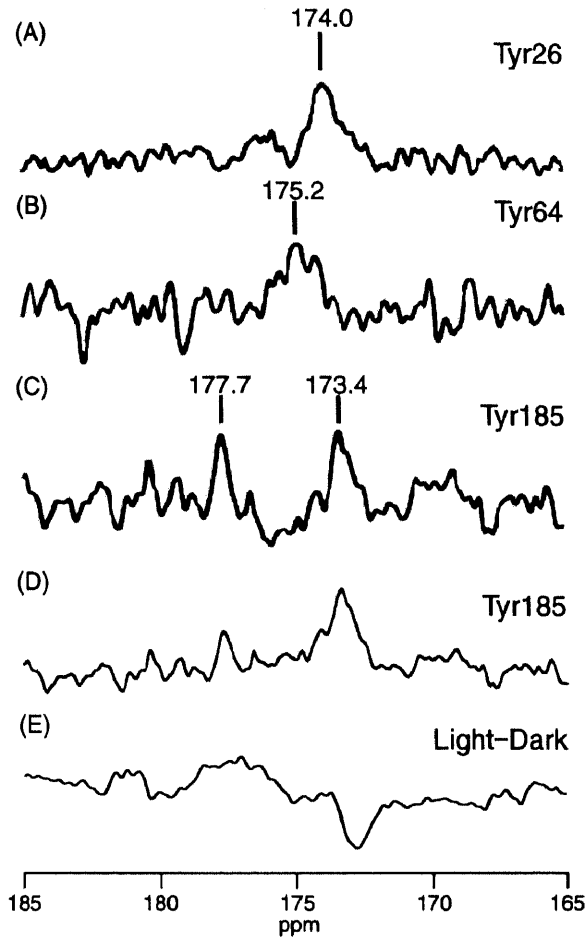

Figure 2. ^{13}C REDOR filtered spectra of: A) [1-^{13}C]Tyr/[^{15}N]Phe-bR, Tyr26: B) [1-^{13}C]Tyr/[^{15}N]Gly-bR, Tyr64: C) [1-^{13}C]Tyr/[^{15}N]Pro-bR, Tyr185; and D) [1-^{13}C]Tyr/[^{15}N]Pro-bR with pressure following longer accumulation (60 h), Tyr185 (13-*cis* retinal rich). The peak obtained from difference spectra between full echo and REDOR experiments can distinguish unique isotropic signal of directly bonded ^{13}C-^{15}N from others using short NcTr = 2 ms. E) ^{13}C CP-MAS difference NMR spectra between light and dark at ambient temperature. The ^{13}C chemical shifts are referenced to that of TMS as 0 ppm.

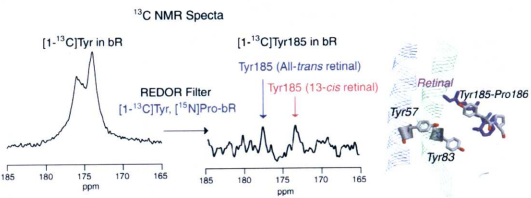

Figure 3. Backbone conformations near tyrosine in bacteriorhodopsin (bR) corresponding to all-*trans* and 13-*cis* retinal configurations in the dark, light and pressure adapted states were investigated for Tyr-X peptide bonds by using double amino acid labeling with [1-^{13}C],[^{15}N]X-bR by means of rotational echo double resonance (REDOR) technique.

Chapter 4

Dynamic aspects at BC loop in bacteriorhodopsin as studiedby relaxation time measurements and the removal of retinal

Abstract

In this study, dynamic modes of extracellular loops in bacteriorhodopsin (bR) have been determined by measuring the relaxation times of resolved signals from Val-Pro consecutive sequences. These signals were reassigned by REDOR (Rotational Echo Double Resonance) filter measurements, in order to assign [1-^{13}C]Val / [^{15}N] Pro signal to the specific sites. The resonance at 172.0 ppm was determined to Val69 by considering significantly dephasing effect. Spin-lattice relaxation times (T_1), spin-spin relaxation times (T_2), cross relaxation times (T_{NH}) and ^{1}H spin-lattice relaxation times in the rotating flame (^{1}H $T_{1\rho}$) on ^{15}N nucleus were measured in [^{15}N]Pro-bR. It turned out that Val69-Pro70 in the extracellular side has rigid β-sheet with large amplitude motions as revealed from ^{13}C and ^{15}N conformation dependent shifts and T_1, T_2 and T_{NH}. In addition, the BC loop conformation mostly disordered in bacterio-opsin as removal of retinal. Therefore, the motion of BC loop sufficiently correlates with the dynamics of retinal binding site.

Introduction

Bacteriorhodopsin (bR) is an intact membrane protein in purple membrane (PM) of *Halobacterium salinarum* and contains retinal covalently linked to Lys216 through a protonated Schiff base (**1**). BR consists of seven transmembrane α-helices and shows a function as a light-driven proton pump from extracellular side to cytoplasmic side. BR forms the specific component of PM containing BR molecules in 2D arrays and 3D structure of BR has been revealed by cryo-electron microscope or X-ray diffraction (**2, 3**). Strongly hydrogen-bonded water molecules with Asp85 to Asp212 in the vicinity of retinal play an important role in the proton transfer of bR (**4**).

Fully hydrated bR in PM or reconstituted in lipid bilayer shows a variety of local motions in the order of 10^2-10^8 Hz, which correlate with the proton pump (**5-7**). Dynamic aspects of bR are well-investigated by site-directed ^{13}C solid state NMR (**8-10**). In particularly, well-resolved, fully visible ^{13}C NMR signals are available from [3-^{13}C]Ala-bR in PM, owing to restricted motional frequencies in the transmembrane α-helices to order of 10^2 Hz (**11,12**). Further, we have revealed local dynamics caused by removal of retinal, site-directed mutagenesis, the variation of environmental factors such as pH, temperature, metal ions, etc (**13-15**). We have observed that cytoplasmic surface dynamics of [3-^{13}C]Ala-bR are altered by site-directed mutations of A160G, E166G, A168G and R227Q, and cation binding. Thus, cytoplasmic surface

regions of the C-terminal α-helix and cytoplasmic loops formed proton binding cluster and became joint motions (**15**).

REDOR (Rotational Echo DOuble Resonance) filter experiment by solid-state NMR is a powerful method to select NMR peak of specific peptide bond in membrane protein by using a consecutive amino acid sequence (**16-18**). REDOR, for determining the interatomic distances, can discriminate recoupling heteronuclear dipolar interactions under the MAS condition by synchronizing a π pulse with the rotor period (**19-21**). It turned out that accurate interatomic distances (±0.1 Å) provides for determination of 3D structure of peptides and proteins to yield (**22, 23**). The peak obtained from difference spectra between Full echo and REDOR experiments can distinguish unique isotropic signal of direct bond ^{13}C-^{15}N pair from others at short NcTr to give refined assignments of Val-Pro sequences in bR.

The aim of this study is to probe the dynamic modes of extracellular loop, BC and FG loop, in bR. Here, we have recorded REDOR dephasing effect on ^{13}C and ^{15}N NMR spectra of [1-^{13}C]Val- and [^{15}N]Pro-labeled bR to determine the NMR signals for Val-Pro consecutive sequence in bR. Using accurate assignments of Val-Pro sequences, we characterized dynamics of these peaks in view of various relaxation parameters at BC loop, FG loop and helix B to reveal respective dynamic mode. In addition, we observed ^{15}N NMR spectrum of [^{15}N]Pro-labeled bacterio-opsin (bO) to examine the interaction of retinal with extracellular side.

Materials and Methods

Halobacterium salinarum S9 was grown in temporary synthetic medium including [1-^{13}C]Val and [^{15}N]Pro to yield [1-^{13}C]Val-, [^{15}N]Pro- doubly labeled bR in purple membrane. The doubly isotopically labeled samples contain direct ^{13}C-^{15}N peptide bonds as three consecutive amino acid sequence of Val49-Pro50, Val69-Pro70 and Val199-Pro200. Purple membrane was isolated by the standard method as described (**24**) and suspended in 5 mM HEPES buffer containing 0.02 % NaN_3 and 10 mM NaCl at pH 7. The sample was concentrated by centrifugation and placed in 5.0 mm o.d. zirconia pencil-type rotor for fast magic angle spinning (MAS). Sample rotors were tightly shielded by Teflon caps and glued to the rotor by rapid Alardyte to prevent dehydration of pelleted samples. Similarly, the sample of [2-^{13}C]Val-labeled bR was prepared. ^{13}C and ^{15}N high-resolution solid-state NMR spectra in this study were recorded on Chemagnetics CMX-400 infinity FT-NMR Spectrometer at 100.1 MHz carbon and 40.3 MHz frequencies, Cross Polarization-Magic Angle Spinning (CP-MAS), single pulse excitation with Dipolar Decoupling-Magic Angle Spinning (DD-MAS) and REDOR experiments. A double resonance MAS probe for relaxation times measurements and triple

resonance MAS probe for REDOR experiments were used respectively. The peak obtained from difference spectra between REDOR and Full echo experiments shows the unique signal of consecutive amino acids sequences at short NcTr. The spinning frequencies were set to 4 kHz. ^{13}C chemical shifts and ^{15}N chemical shifts were externally referred to 176.03 ppm and 11.59 ppm for the carbonyl carbon and amine nitrogen of glycine from TMS and NH_4NO_3.

A double resonance MAS probe was also used for the ^{13}C and ^{15}N relaxation measurements of [1-^{13}C]Val-, [^{15}N]Pro-labeled bR. ^{13}C and ^{15}N spin-lattice relaxation times T_1 were corrected by cross polarization magnetization with inversion using 90° pulse during mixing time τ at 4.0 kHz spinning (**25,26**). Cross-polarization times (T_{CH} and T_{NH}) and proton spin-lattice relaxation times in the rotating frame (^1H $T_{1\rho}$) were measured by measuring the peak intensities with cross-polarization dynamics as a function of contact times.

Results and Discussion

Reassignment of Val69 by REDOR

The peak obtained from difference spectra between Full echo and REDOR experiments can distinguish unique isotropic signal of directly bonded ^{13}C-^{15}N pair from others at short NcTr (**15-21**). In Figure 1, we successfully detected two ^{13}C NMR peaks at 171.1 and 172.1 ppm as a ratio of signal intensity to 1:2 (higher field peak : lower field peak) deduced from Val-Pro consecutive amino acid sequences of Val49-Pro50, Val69-Pro70 and Val199-Pro200 in [1-^{13}C]Val-, [^{15}N]Pro-labeled bR *at ambient temperature* by REDOR filter experiment. In the previous study by Petkova et al. (**18**), ^{13}C NMR peaks of Val-Pro sequence positions were also clearly observed as a ratio of signal intensity to 1:2 although those peaks were not accurately assigned. ^{13}C NMR signals at 172.1 and 171.1 ppm have been assigned to Val49 and Val199 by site-directed mutation (**27, 28**) respectively. The signal at 172.1 ppm was able to decide to Val69 by combining present REDOR result with above effective site-directed mutation studies (**27, 28**). The displacements of isotropic chemical shift of Val49 and Val199 are distinctly differ from ^{13}C conformation dependent chemical shifts of α-helix at 174.9 ppm (**9, 10, 29, 30**). This finding may indicate that additional upfield displacements of these peaks by 1-2 ppm, to which carbonyl carbon of Val49 and Val199 directly bonded to the amide nitrogen of Pro residue (**31**). The peak of Val69 may resonate at 172.1 ppm with non-shift by proline effect although Val69 in B-C loop directly bonded to Pro70. In the ^{13}C CP-MAS NMR spectrum of [2-^{13}C]Val-labeled bR, the signals contained mainly two components of transmembrane α-helix region and β-sheet, was distinctly observed at 64.6 and 56.4 ppm (show Figure 2). The peak at 56.4 ppm deduced from β-sheet form by ^{13}C conformation- dependent chemical shifts of β-sheet at 58.4 ppm (**29,30**).

These findings indicated that structure in the vicinity of Val69 in bR formed β-sheet conformation.

Assignments of Pro50, Pro70 and Pro200 by REDOR experiments

In the ^{15}N CP-MAS NMR spectrum (Figure 3), five narrow signals were obviously recorded between 110 and 125 ppm. It is noted that obtained most resolved NMR spectrum in [^{15}N]Pro-bR is not overlapped with the background signal and to form 2D arrays in PM. By REDOR experiments, the resonance at 111.3, 114.0 and 122.0 ppm showed significantly dephasing effect, indicating that these Pro residues belong to Val-Pro sequence in bR at ambient temperature (Figure 4). The ^{15}N isotropic chemical shift of the α-helix form appears at higher field than that of β-sheet form. Thus, the displacements of ^{15}N isotropic chemical shifts are also largely related to the conformation (**32,33**). Moreover, ^{13}C-^{15}N correlations of above-mentioned three components showed that pairs of ^{13}C carbonyl carbon and ^{15}N amide chemical shifts are 171.1-114.0, 172.1-111.3 and 172.1-122.0 ppm (the ^{13}C and ^{15}N chemical shifts values are based on that we measured by using Gly 176.03 ppm from TMS and ^{15}N Gly 11.59 ppm) (**18**). Therefore, we found that three ^{15}N NMR signals at 111.3, 114.0 and 122.0 ppm in ^{15}N NMR CP-MAS spectrum of [^{15}N]Pro-labeled bR are uniquely assigned to Pro50, Pro200 and Pro70, respectively.

Local motions from ^{13}C and ^{15}N relaxation times measurements

Using above assignments, we determined various ^{13}C nuclear relaxation parameters, ^{13}C T_1, ^{13}C T_2, T_{CH} and ^1H $T_{1\rho}$ in [1-^{13}C]Val-, [^{15}N]Pro-bR, especially, about three signals at higher field. These results summarized in Table 1. T_1 value of Val199 (171.1 ppm) in the CP-MAS experiments is shorter by one order of magnitude than other signals. In addition, T_2 value of Val199 is distinctly longer and T_{CH} value of Val199 is not inferiority as the strength of dipole-interaction compared with that of Val49, 69 at 172.1 ppm. These results indicate that Val199 and F-G loop in the vicinity of Val199 show fast anisotropic fluctuations (~10^8 Hz; Zeeman frequency) and not sensitive to the proton decoupling frequency (10^4 Hz) in wild-type bR. Such dynamics in F-G loop on bR drastically changes the fluctuations in the order of 10^4-10^5 Hz for single and multiple mutants of E194Q, E204Q and E194Q/E204Q (**28, 34**). Therefore, fast fluctuations in the order of 10^8 Hz on F-G loop involving in proton release groups E194 and E204, also correlate with proton transfer to extracellular side. T_1 and T_2 values at 172.1 ppm may contain components of slow motion (10^2 Hz) although this peak has been superimposed on Val49 and Val69 at least.

We summarized the results of ^{15}N relaxation time measurements in Table 2. ^{15}N NMR peaks of Pro50 and Pro70 were clearly resolved at 111.4 and 122.4 ppm with other peaks and easily characterized for these relaxation times. But ^{15}N NMR peak of Pro200 is not characterized on the relaxation parameters because that is non-resolved and poorly cross polarization. ^{15}N T_1 values of Pro50 (111.4 ppm) and Pro70 (122.4 ppm) were longer than other peaks and ^{15}N T_2 values were not sensitive to the motion at 10^4 Hz. Therefore, these fluctuational frequencies of Pro50 (helix B) and Pro70 (BC loop) were in the fluctuation order of 10^2-10^3 Hz and formed β-sheet. Thus, it is of interest to note that T_{NH} value of Pro70 was 1.12 ms and distinctly longer than those of other four peaks. These findings indicate that B-C loop in the vicinity of Pro70 takes large amplitude motions to average dipolar interaction. In fact, T_{CH} value at 172.1 ppm corresponding to Val69 was also long, in which Val69 largely dominate in 172.1 ppm in view of the dynamic state. Therefore, it is emphasized that local structure in the vicinity of Val69-Pro70 in BC loop forms rigid β-sheet and takes large amplitude motions.

Drastic changes of BC loop on ^{15}N CP-MAS NMR spectrum of [^{15}N]Pro-labeled bO

Figure 5 shows the ^{15}N CP-MAS NMR spectrum of [^{15}N]Pro-bO with reference to that of [^{15}N]Pro-bR (Figure 2). It is noted that the ^{15}N NMR spectrum of [^{15}N]Pro-bO was significantly changed both Pro50 in helix B and Pro70 in BC loop when it removed retinal from bR. In particular, the peak at 122.4 ppm detected in bR was completely suppressed in CP-MAS spectrum of bO. Previously, this change has been detected from ^{13}C NMR peak of [1-^{13}C]Val-labeled bO. These results indicated that bO induced itself inhomogeneous conformation of BC loop formed β-sheet to modify hydrogen bond network from retinal to extracellular surface, and BC loop becomes long distance interactions with retinal. β-sheet in bR is correlated to its thermal stability by cleaved bond 71-72 position (**35**).

Conclusions

In order to characterize the dynamic features of Val-Pro consecutive positions of Val49-Pro50, Val69-Pro70 and Val199-Pro200 in bR as viewed on various relaxation parameters, REDOR filter experiments refined to NMR signal assignments of [1-^{13}C]Val-[^{15}N]Pro-doubly labeled bR. In spite of the presence of superimposed ^{13}C NMR signal from Val49 and Val69, we revealed the dynamic aspects in Val-Pro positions by ^{13}C and ^{15}N various relaxation times. BC loop in bR formed rigid β-sheet and showed large amplitude motions. This dynamic structure of BC loop in bR was disordered in the bacterio-opsin bO.

References

1. J. K. Lanyi.

Mechanism of ion transport across membranes. Bacteriorhodopsin as a prototype for proton pumps

J. Biol. Chem. 1997 **272** 31209-31212.

2. N. Grigorieff, T. A. Ceska, K. H. Dowing, J. M. Baldwin, R. Henderson

Electron-crystallographic refinement of the structure of bacteriorhodopsin.

J. Mol. Biol. 1996 **259** 393-421.

3. H. Luecke, B. Schobert, H. T. Richter, J. P. Cartailler, J. K. Lanyi

Structure of bacteriorhodopsin at 1.55 Å resolution.

J. Mol. Biol. 1999 **291** 899-911.

4. M. Shibata and H. Kandori

FTIR studies of internal water molecules in the Schiff base region of bacteriorhodopsin

Biochemistry 2005 **44** 7406-7413.

5. A. Kira, M. Tanio, S. Tuzi, H. Saitô.

Significance of low-frequency local fluctuation motions in the transmembrane B and C alpha-helices of bacteriorhodopsin, to facilitate efficient proton uptake from the cytoplasmic surface, as revealed by site-directed solid-state ^{13}C NMR.

Eur. Biophys. J. 2004 **33** 580-588.

6. M. Kamihira and A. Watts

Functionally Relevant Coupled Dynamic Profile of Bacteriorhodopsin and Lipids in Purple Membranes

Biochemistry 2006 **45** 4304-4313.

7. K. Yamamoto, S. Tuzi, H. Saitô, I. Kawamura, A. Naito

Conformation and dynamics changes of bacteriorhodopsin and its D85N mutant in the absence of 2D crystalline lattice as revealed by site-directed ^{13}C NMR

Biochem. Biophys. Acta 2006 **1758** 181-189.

8. H. Saitô, S. Tuzi and A. Naito

Empirical versus Nonempirical Evaluation of Secondary Structure of Fibrous and Membrane Proteins by Solid-state NMR: A Practical Approach

Annu. Rep. NMR Spectrosco. 1998 **36** 79-121.

9. H. Saitô, S. Tuzi, S. Yamaguchi M. Tanio, A. Naito

Conformation and backbone dynamics of bacteriorhodopsin revealed by ^{13}C-NMR

Biochem. Biophys. Acta. 2000 **1460** 39-48.

10. H. Saitô, S. Tuzi, M. Tanio, A. Naito.

Dynamics Aspects of Membrane Proteins and Membrane-Associated Peptides as Revealed by ^{13}C NMR: Lessons from Bacteriorhodopsin as an Intact Protein

Annu. Rep. NMR Spectrosco. 2002 **47** 39-108.

11. S. Tuzi, A. Naito, H. Saitô

Temperature-dependent conformational change of bacteriorhodopsin as studied by solid state ^{13}C NMR

Eur. J. Biochem. 1996 **239** 294-301.

12. H. Saitô.

Dynamics pictures of membrane proteins in two-dimensional crystal, lipid bilayer and detergent as revealed by site-directed solid-state ^{13}C NMR

Chem. Phys. Lipids 2004 **132** 101-112.

13. S. Yamaguchi, S. Tuzi, M. Tanio, A. Naito, J. K. Lanyi, R. Needleman, H. Saitô.

Irreversible Conformational Change of Bacterio-opsin Induced by Binding of Retinal during Its Reconstitution to Bacteriorhodopsin, as Studied by ^{13}C NMR.

J. Biochem. 2000 **127** 861-869.

14. S. Yamaguchi, K. Yonebayashi, H. Konishi, S. Tuzi, A. Naito, J. K. Lanyi, R. Needleman, H. Saitô.

Cytoplasmic surface structure of bacteriorhodopsin consisting of interhelical loops and C-terminal α-helix, modified by a variety of environmental factors as studied by ^{13}C-NMR.

Eur. J. Biochem. 2001 **268** 2218-2228.

15. K. Yonebayashi, S. Yamaguchi, S. Tuzi, H. Saitô.

Cytoplasmic surface structures of bacteriorhodopsin modified by site-directed mutations and cation binding as revealed by ^{13}C NMR.

Eur. Biophys. J. 2003 **32** 1-11.

16. A. J. Mason, G. J. Turner, C. Glaubitz

Conformational heterogeneity of transmembrane residues after the Schiff base reprotonation of bacteriorhodopsin: ^{15}N CPMAS NMR of D85N/T170C membranes.

FEBS J. 2005 **272** 2152-2164.

17. J. C. Lansing, J. G. Hu, M. Belenky, R. G. Griffin, J. Herzfeld.

Solid-state NMR investigation of the buried X-proline peptide bonds of bacteriorhodopsin

Biochemistry 2003 **42** 3586-3593.

18. A. T. Petkova, M. Baldus, M. Belenky, M. Hong, R. G. Griffin, J. Herzfeld.

Backbone and side chain assignment strategies for multiply labeled membrane peptides and proteins in the solid state.

J. Magn. Reson. 2003 **160** 1-12.

19. T. Gullion, J. Schaefer

Rotational-echo double-resonance NMR.

J. Magn. Reson. 1989 **81** 196–200.

20. T. Gullion, J. Schaefer

Detection of weak heteronuclear dipolar coupling by rotational-echo double resonance

Adv. Magn. Reson. 1989 **13** 57-83.

21. K. Nishimura and A. Naito

REDOR in Multiple Spin System

Handbook of Modern Magnetic Resonance, (Kluwer Academic) 2006 ***in press.***

22. A. Naito, K. Nishimura, S. Kimura, S. Tuzi, M. Aida, N. Yasuoka and H. Saitô

Determination of the Three-Dimensional Structure of a New Crystalline Form of N-Acetyl-Pro-Gly-Phe as Revealed by ^{13}C REDOR, X-Ray Diffraction, and Molecular Dynamics Calculation

J. Phys. Chem. 1996 **100** 14995-15004.

23. K. Nishimura, A. Naito, S. Tuzi, H. Saitô

Determination of the Three-Dimensional Structure of Crystalline Leu-Enkephalin Dihydrate Based on Six Sets of Accurately Determined Interatomic Distances from ^{13}C-REDOR NMR and the Conformation-Dependent ^{13}C Chemical Shifts

J. Phys. Chem. B 1998 **102** 7476-7483.

24. D. Oesterhelt and W. Stoeckenius.

Isolation of the cell membrane of Halobacterium halobium and its fractionation into red and purple membrane.

Methods Enzymol. 1974 **31** 667-678.

25. D. A. Torchia.

The measurement of proton-enhanced carbon-^{13}C T_1 values by a method which suppress artifacts.

J. Magn. Reson. 1978 **30** 613-616.

26. K. Akasaka, S. Ganapathy, C. A. McDowell, and A. Naito.

Spin-spin and spin-lattice contributions to the rotating frame relaxation of ^{13}C in L-alanine

J. Chem. Phys. 1983 **78** 3567-3571.

27.S. Tuzi, S. Yamaguchi, M. Tanio, H. Konishi, S. Inoue, A. Naito, R. Needleman, J. K. Lanyi, H. Saitô.

Location of a cation-binding site in the loop between helices F and G of bacteriorhodopsin as studied by ^{13}C NMR.

Biophys. J. 1999 **76** 1523-1531.

28. M. Tanio, S. Inoue, K. Yokota, T. Seki, S. Tuzi, R. Needleman, J. K. Lanyi, A. Naito, H. Saitô.

Long-distance effects of site-directed mutations on backbone conformation in bacteriorhodopsin from solid state NMR of [1-^{13}C]Val-labeled proteins.

Biophys. J. 1999 **77** 431-442.

29. H. Saitô.

Conformation-dependent ^{13}C chemical shifts: a new means of conformational characterization as obtained by high-resolution solid-state NMR.

Magn. Reson. Chem. 1986 **24** 835-852.

30. H. Saitô, and I. Ando.

High-resolution solid-state NMR studies of synthetic and biological macromolecules.

Annu. Rep. NMR spectrosco. 1989 **21** 209-290.

31. D. S. Wishart, C. G. Bigam, A. Holm, R. S. Hodges, B. D. Sykes.

^{1}H, ^{13}C, and ^{15}N random coil NMR chemical shifts of the common amino acids. 1. Investigations of nearest-neighbor effects.

J. Biomol. NMR 1995 **5** 67–81.

32. A. Shoji, T. Ozaki, T. Fujito, K. Deguchi and I. Ando.

High-resolution ^{15}N NMR study of solid homopolypeptides by the cross-polarization-magic angle spinning method: conformation-dependent ^{15}N chemical shifts characteristic of the α-helix and β-sheet forms

Macromolecules 1987 **20** 2441-2445.

33. A. Shoji, T. Ozaki, T. Fujito, T. Deguchi, S. Ando, I. Ando.

^{15}N chemical shift tensors and conformation of solid polypeptides containing ^{15}N-labeled L-alanine residues by ^{15}N NMR, 2:secondary structure reflected in sigma22

J. Am. Chem. Soc. 1990 **112** 4693-4697

34. H. Saito, S. Yamaguchi, K. Ogawa, S. Tuzi, M. Marquez, C. Sanz, E. Padros.

Glutamic acid residues of bacteriorhodopsin at the extracellular surface as determinants for conformation and dynamics as revealed by site-directed solid-state ^{13}C NMR.

Biophys. J. 2004 **86** 1673-81.

35. A. I. Azuaga, F. Sepulcve, E. Padros and P. L. Mateo.

Scanning Calorimetry and Fourier-Transform infrared studies into the thermal stability of cleaved bacteriorhodopsin systems.

Biochemistry 1996 **35** 16328-16335.

Table 1. ^{13}C T_1, ^{13}C T_2, T_{CH} and ^1H $T_{1\rho}$ values for three resolved ^{13}C NMR peaks of [1-^{13}C]Val-bR.

δ_{iso} ppm (residue)	^{13}C T_1 [s]	^{13}C T_2 [ms]	T_{CH} [ms]	^1H $T_{1\rho}$ [ms]
171.1 ppm (Val199)	6.5 ± 0.9	12.2 ± 1.7	0.46 ± 0.03	6.1 ± 0.5
172.1 ppm (Val49, 69)	24.9 ± 4.2	8.9 ± 1.6	0.74 ± 0.13	3.8 ± 0.7
172.9 ppm (Val34)	13.5 ± 0.9	5.1 ± 0.2	0.20 ± 0.05	15.1 ± 6.4

Table 2. ^{15}N T_1, ^{15}N T_2, T_{NH} and ^1H $T_{1\rho}$ values for five resolved ^{15}N NMR peaks of [^{15}N]Pro-bR.

δ_{iso} ppm (residue)	^{15}N T_1 [s]	^{15}N T_2 [ms]	T_{NH} [ms]	^1H $T_{1\rho}$ [ms]
111.4 ppm (Pro50)	46.3 ± 4.1	17.0 ± 2.2	0.67 ± 0.03	13.5 ± 1.1
114.5 ppm	25.6 ± 6.3	11.8 ± 2.2	0.63 ± 0.17	11.4 ± 4.9
116.4 ppm	20.5 ± 1.0	10.0 ± 0.6	0.72 ± 0.17	7.9 ± 2.3
117.9 ppm	10.8 ± 0.5	21.8 ± 1.6	0.76 ± 0.17	3.9 ± 0.8
122.4 ppm(Pro70)	40.2 ± 7.5	15.6 ± 1.9	1.12 ± 0.21	17.0 ± 8.8

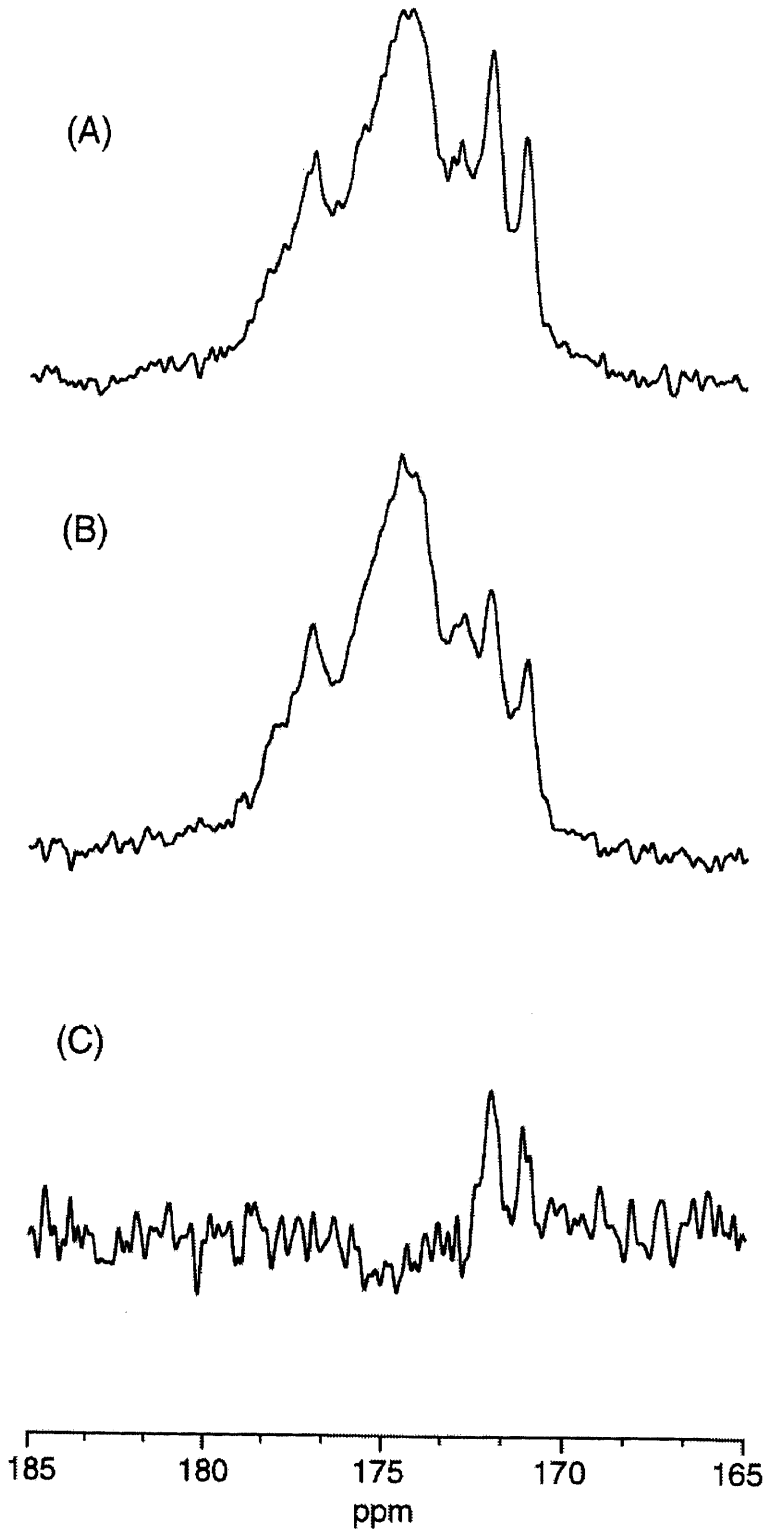

Figure 1. ^{13}C REDOR dephasing effects on NMR signals of [1-^{13}C]Val-, [^{15}N]Pro-labeled bR.

(A) Full echo (B)REDOR (C)The peak obtained from difference spectra between full echo and REDOR experiments.

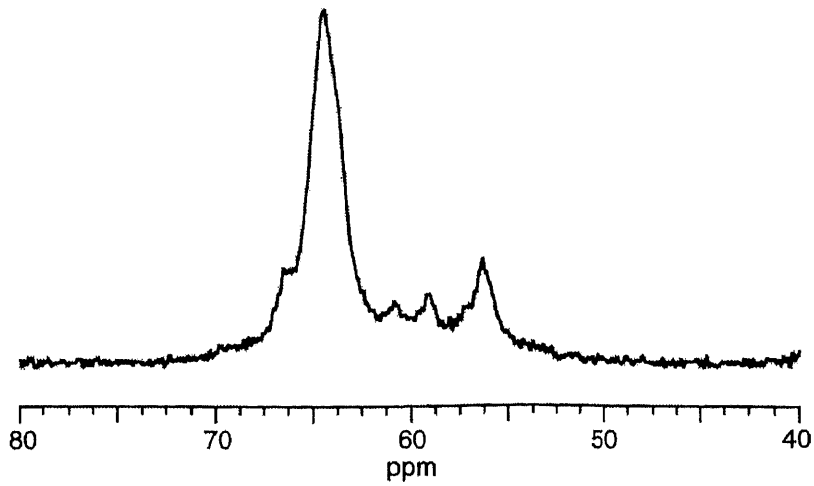

Figure 2. ^{13}C CP-MAS NMR signals of [2-^{13}C]Val-labeled bR. The peak at 56.4 ppm deduced from β-sheet form by ^{13}C conformation dependent chemical shifts of β-sheet at 58.4 ppm.

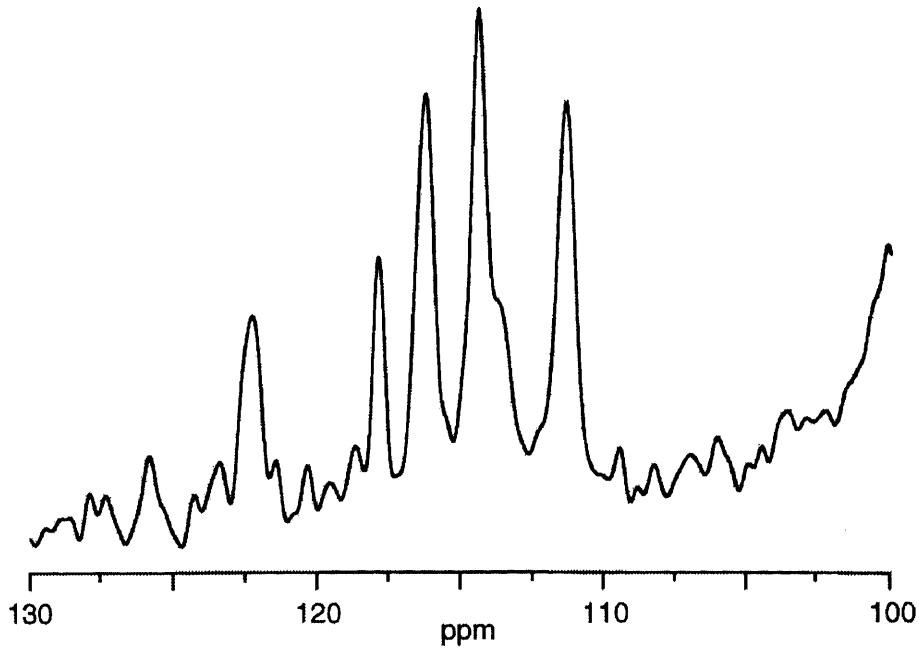

Figure 3. ^{15}N CP-MAS NMR signals of [^{15}N]Pro-labeled bR.

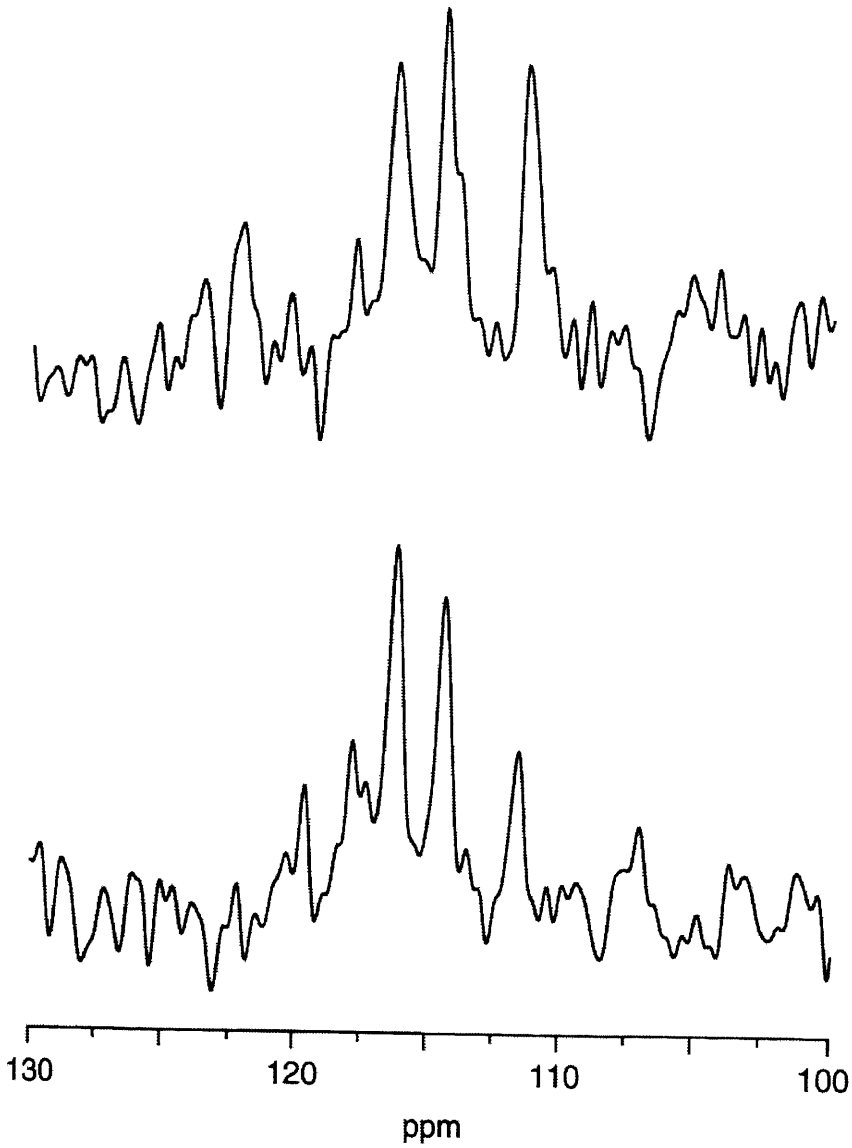

Figure 4. ^{15}N REDOR dephasing effects on NMR signals of [1-^{13}C]Val-, [^{15}N]Pro-labeled bR. (A) Full echo (B)REDOR

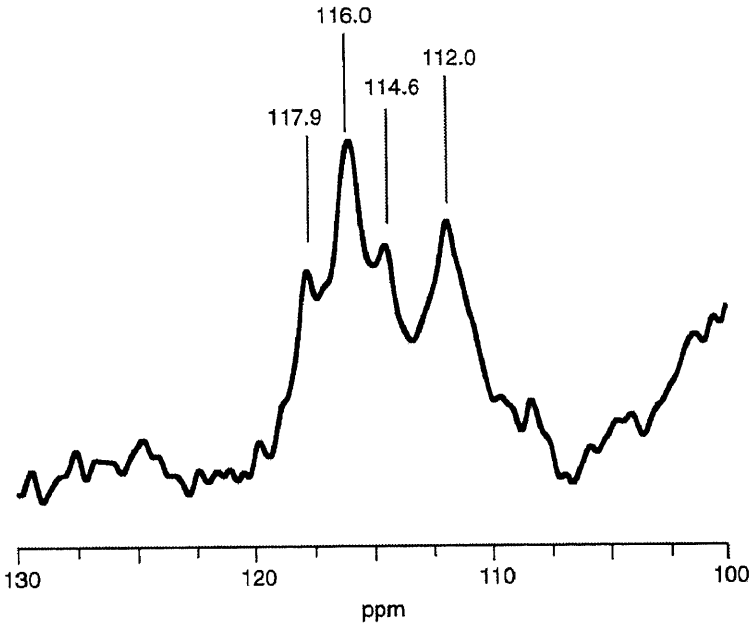

Figure 5. ^{15}N CP-MAS NMR signals of [^{15}N]Pro-labeled bO.

Chapter 5

Dynamics changes in the C-terminal α-helical region of *pharaonis* phoborhodopsin (sensory rhodopsin II) or D75N mutant and cytoplasmic α-helix in cognate transducer *p*HtrII in the complex formation leading to signal transduction as revealed by site-directed solid state ^{13}C NMR

ABSTRACT

Pharaonis phoborhodopsin (*p*pR or sensory rhodopsin II) is a negative phototaxis receptor through complex formation with its cognate transducer (*p*HtrII) from *Natronomonas pharaonis*, leading to the photo-induced signal transduction. We examined ^{13}C CP- and DD-MAS NMR spectra of [3-^{13}C]Ala-labeled *p*pR, *p*pR(1-220) and D75N mutant (an presumed activated state) complexed with *p*HtrII, in order to reveal accompanied dynamics changes and particularly a possible role of a C-terminal α-helical region protruding from the cytoplasmic surface in the signal transduction processes. The C-terminal α-helical region protruding from the cytoplasmic side consists of two region, more static stem (Ala221) and flexible tip (Ala228, 234, 236 and 238) regions, corresponding to the NMR peaks of [3-^{13}C]Ala *p*pR at 15.9 and 16.7-16.9 ppm, respectively. The latter tip portion of the C-terminal α-helix turns out to be participated also in the complex formation, in addition to the transmembrane α-helices, to result in motions with lowered frequency as judged from the suppressed peaks. In contrast, such spectral changes were not anymore present when *p*pR changes to D75N in the *p*HtrII complex. In fact, dynamics changes were induced to accelerate fluctuations in the C-terminal α-helix of *p*pR during the process of photo-activation of *p*pR-*p*HtrII complex (to D75N-*p*HtrII) as observed by solid state ^{13}C NMR. In contrast, it turned out that fluctuation frequency of the cytoplasmic α-helices of the transducer ([1-^{13}C]*p*HtrII) complexed with D75N as an activated from was lowered by one order of magnitude. It appears that this is caused by a switching of pairs in the helix-helix interactions in the cytoplasmic C-terminal α-helices of *p*HtrII from *p*pR to *p*HtrII itself, concomitant with the loosened interactions in the transmembrane and C-terminal α-helices of *p*pR caused by the disrupted salt-bridges. This finding gains insight into a signal relay pathway in the initial step of phototaxis receptor and its cognate transducer protein.

INTRODUCTION

Halobacteria contain a family of four retinal proteins. These proteins are heptahelical transmembrane proteins with a retinal via Lys in helix G and functionally classified into two distinct classes: bacteriorhodopsin (bR) (**1**) and halorhodopsin (hR) (**2**) are light-driven ion pumps to transport proton and chloride, respectively and sensory rhodopsin (sR) (**3**) and phoborhodopsin (pR, also called sensory rhodopsin II, sRII) (**4,5**) are positive and negative phototaxis receptors, respectively, by complex-formation with their respective cognate transducer proteins (**6**).

In particular, *pharaonis* phoborhodopsin (*p*pR) from *Natronomonas pharaonis* is a negative phototaxis receptor and forms a complex with its cognate transducer (*p*HtrII). The

resulting conformational changes of *p*pR induced by blue light including the wavelength at 498 nm transmit a signal to its cognate transducer *p*HtrII (**7,8**). The stoichiometry of *p*pR-*p*HtrII complex has been determined to be 1:1 in which *p*HtrII dimer is sandwiched between two *p*pR molecules in the cell membranes (**9,10**). Recently, the *p*pR-*p*HtrII interactions have been extensively examined using X-ray diffraction, EPR, FTIR spectroscopy, isothermal titration calorimetry (ITC), etc. X-ray diffraction and EPR studies showed that the F helix in *p*pR tilt towards *p*HtrII (**11, 12**) and hydrogen bonds between *p*pR and *p*HtrII in the binding surfaces are formed between $Y199^{ppR}$-$N74^{pHtrII}$, and $T189^{ppR}$-$E43^{pHtrII}$ and -$S62^{pHtrII}$ in the transmembrane region and extracellular side, respectively (**13,14**). Tyr199 is realized as a very important residue for a complex formation of *p*pR with its cognate *p*HtrII, because it is conserved even in sensory rhodopsin II (**15-17**). FTIR experiments revealed that residues Thr204 and Tyr174 in the retinal pocket form hydrogen bonds at the binding surface of *p*pR-*p*HtrII, and Thr204 in *p*pR helix G interacts with *p*HtrII (**18**).

ITC measurements revealed that, the dissociation constants (K_d) of *p*pR-*p*HtrII complex changes to higher affinity and consequently proton pump activity was inhibited by increasing the length of *p*HtrII in the cytoplasmic side (**19, 20**). It was also revealed that the EF loop residue Ser154 in *p*pR is in close proximity to residue 91-95 of membrane proximal region in *p*HtrII using fluorescent probes (**21**). These experimental findings indicate that not only *p*pR-*p*HtrII interactions in the transmembrane region but also those in the cytoplasmic side play an important role in signal relay. A "*linker switch model*" for photo-signal transduction from *p*pR to *p*HtrII in detergent solution proposed that movement of F helix in *p*pR induces structural changes in the linker region (G83-Q149) of *p*HtrII leading to dissociation from *p*pR (**22**). Molecular detail of switching mechanism, however, has not yet been characterized.

D73N mutant of sRII from *H. salinarum* (corresponding to D75N mutant of *p*pR in *N.pharaonis*) produces repellent signals by forming complex with transducer HtrII from *H.salinarum* even in the dark. In a similar manner, disruption of salt-bridge in D75N mutant of *p*pR would induce the receptor activation in the dark because Asp75 of *p*pR in *N. pharaonis* is a counter ion of the protonated Schiff base via Lys205 (**23**). This is analogous also to D85N of bR mutant in which the counter anion of Schiff base at Asp85 is neutralized (**24**). In fact, D75N mutant complexed with *p*HtrII changes the protein conformation in the transmembrane region including $Y199^{ppR}$-$N74^{pHtrII}$ (**25**).

Solid-state ^{13}C NMR approach has proved to be a very convenient and useful means, to examine underlying such conformation and dynamics changes in membrane environment (**26-28**). In fact, we have analyzed conformation and dynamics of [3-^{13}C]Ala- and [1-^{13}C]Val-labeled *p*pR or *p*HtrII(1-159) with reference to the ^{13}C NMR data based on our

previous works by ^{13}C NMR (**29, 30**). Structures of the C-terminal regions as well as the cytoplasmic surface of *p*pR in lipid bilayer was characterized based on solid state ^{13}C NMR measurements of selectively ^{13}C amino-acid- residues- labeled bR (**31-34**). Further, ^{13}C NMR spectra for [3-^{13}C]Ala, [1-^{13}C]Val or [1-^{13}C]Pro-labeled D85N mutant in bR (corresponding to D75N of *N.pharaonis*) have been recorded (**35, 36**). Accordingly, it turned out that fluctuation motions with the frequency range from 10^4 to 10^5 Hz are induced at the cytoplasmic loops and ends of transmembrane B, C, F, G helices during the M-like state of D85N at ambient temperature.

In the present study, we aimed to clarify the local changes of conformation and dynamics in the C-terminal α-helix portions of *p*pR in egg PC bilayer as well as that of the complex with *p*HtrII(1-159) utilizing C-terminal truncated *p*pR(1-220) with reference to the ^{13}C conformation-dependent chemical shifts of Ala C_β and Val C=O signals (**28, 37, 38**). Further, we analyzed how conformation and dynamics of the C-terminal and transmembrane portion in *p*pR and *p*HtrII are modified when D75N (an activated state) was replaced by *p*pR. Finally we will show the conformation and dynamics changes of the transducer (*p*HtrII) by forming complex with *p*pR and D75N.

Materials and Methods

[3-^{13}C]Ala-,[1-^{13}C]Val-D75N and *p*pR(1-220) (C-terminal region in *p*pR is truncated) with His-Tag (6 × His) at the C-terminus (Figure 1) were expressed in *Escherichia coli* BL21(DE3) strain in M9 medium containing [3-^{13}C] L-Ala and [1-^{13}C] L-Val (CIL, Andover, MA) by addition of 1 mM IPTG and 10 μM all-*trans* retinal. These proteins were solubilized using n-dodecyl-β-D-maltoside (DM) and purified with a Ni-NTA column (QIAGEN) as described previously (**39, 40**). ^{13}C-labeled *p*HtrII(1-159) was prepared by a similar method as mentioned above. Purified proteins were incorporated into a lipid film of egg PC (*p*pR: egg PC molar ratio of 1:50), followed by gently stirring at 4℃ for overnight. DM was removed using Bio-Beads to incorporate the proteins into the egg PC bilayers. Reconstituted dispersions were concentrated by centrifugation and suspended in 5 mM HEPES and 10 mM NaCl buffer solution (pH 7). The pelleted mixture with *p*pR: *p*HtrII molar ratio of 1:1 in egg PC bilayer was placed in 5.0 mm o.d. zirconia pencil-type rotor for magic angle spinning (MAS) experiments.

High-resolution solid-state ^{13}C NMR spectra were recorded on Chemagnetics CMX-400 infinity FT-NMR spectrometer at the resonance frequency of 100.16 MHz for carbon nuclei. Cross polarization-magic angle spinning (CP-MAS) and single pulse excitation, and dipolar decoupling-magic angle spinning (DD-MAS) experiments were performed. A doubly tuned MAS probe equipped with 5.0 mm o.d. rotor assembly was used. The spinning frequency was

set to 4 kHz and the duration of 90° pulse for observed nucleus was 5.5 μs. In CP-MAS experiments, the contact and repetition times were set to 1 ms and 4 s, respectively. At ambient temperature, it was shown that reconstituted *p*pR in egg PC bilayer undergoes fluctuational motions with the frequencies spanning from 10^4 to 10^8 Hz, depending on the location in *p*pR (**29**). These wide dynamic ranges were distinguished by observing the signals corresponding to the motional region with the frequency range of 10^6-10^8 Hz by DD-MAS from the rigid region with the frequency range lower than 10^6 Hz by CP-MAS experiment. The incoherent random molecular fluctuations with the frequencies of 10^4 and 10^5 Hz were identified by the presence of suppressed or broadened peaks by interference of fluctuation frequencies by magic angle spinning and proton decoupling, respectively (**41, 42**). ^{13}C chemical shifts were externally referred to 176.03 ppm for the carbonyl carbon of glycine from TMS.

RESULTS

Assignments of the ^{13}C NMR signals to two types of C-terminal α-helices in *p*pR

Figure 2 compares the ^{13}C CP-MAS (*left*) and DD-MAS (*right*) NMR spectra of [3-^{13}C] Ala-*p*pR (A, B) in egg PC bilayer with those of [3-^{13}C]Ala-*p*pR (1-220) (C, D) at ambient temperature, in order to assign Ala C_β ^{13}C NMR signals from the portion of the C-terminal region of *p*pR(221-239). The ^{13}C NMR peaks at 14.1 ppm can be assigned to those of the methyl carbons from egg PC. The obviously suppressed peaks at 15.8 and 16.7-16.9 ppm in the ^{13}C CP-MAS and DD-MAS NMR of the truncated *p*pR (1-220) (Figure 2 C and D, the arrowed peaks) are readily ascribed to the C-terminal region of *p*pR (221-239) as compared with those of wild-type *p*pR (Figure 2A and B, gray peaks). They are resonated at the peak-position of α_{II}-helix as indicated at the top of the spectra. This is because Ala C_β ^{13}C NMR peaks exhibit dynamics-dependent ^{13}C chemical shifts, besides the ordinary conformation-dependent displacement of peaks (**28**). Namely, Ala C_β ^{13}C chemical shits of the α–helical portions in membrane proteins undergoing low-frequency fluctuation motions could be resonated at the lower field peak-positions than those of the static α-helical $(Ala)_n$ in the solid state (α_I-helix) (**28, 43**). This peak-position can be expressed also as α_{II}-helix utilizing the definition of Krimm and Dwivedi based on IR measurements (**43**).

The former peak at 15.8 ppm was unequivocally assigned to Ala 221 of the stem region of the C-terminal α-helix with reference to the conformation-dependent displacement of peaks and also the peak-position of the C-terminal α-helix portion of bR taking similar environment (Ala 228 and 323) (**32-34**). The remaining ^{13}C NMR peaks at 16.7-16.9 ppm (lower field gray peaks)

could be then ascribed to those of Ala 228, 234, 236 and 238 in the C-terminal α-helical tip region, exhibiting the dynamics-dependent ^{13}C shift because of low-frequency fluctuation motion. The lowest-field peak position at 16.9 ppm, however, cannot be distinguished from that of random coil form (**28, 31, 44**). The existence of the α–helix can be supported by the fact that this peak at 16.9 ppm is clearly visible by the CP-MAS NMR (Figure 2A) owing to the presence of residues undergoing anisotropic fluctuation rather than ordinary random coil form undergoing isotropic fluctuation motions. In some instances, it was identified that Ala84 signal of bR is superimposed upon the peak-position of random coil (**45**), although most of the peaks resonating at the peak-positions of the α_I and α_{II}-peaks of *p*pR in egg PC bilayer were ascribed to the transmembrane α-helices (**29**). It is, therefore, concluded that the C-terminal portion of *p*pR consists of the two types of α-helices, static stem (Ala 221) and flexible tip (Ala 228, 234, 236 and 238) portions, depending upon the extent of fluctuation frequencies as viewed from the different dynamic-environment as illustrated in Figure 1. The former α-helix stem portion is visible but the latter tip portion is not by X-ray diffraction study on *p*pR complexed with *p*HtrII (1-114) (**13**). The latter α-helix may be ascribed to disordered peaks by X-ray diffraction study, although they could be predicted by Chou-Fasman diagram (**46**).

To assign the carbonyl ^{13}C NMR signals from the portion of [1-^{13}C]Val-*p*pR(221-239), the ^{13}C CP-MAS (Figure 3 left) and DD-MAS (Figure 3 right) NMR spectra of [1-^{13}C] Val-*p*pR (Figure 3A and B) (**29**) were compared with those of [1-^{13}C]Val-*p*pR (1-220) (Figure 3C and D) recorded in egg PC bilayer at ambient temperature. The ^{13}C NMR signals of [1-^{13}C]Val-*p*pR located at the peak-position of the α-helix was previously assigned to the transmembrane α-helices (**28**). Because the peak at 173.6 ppm of [1-^{13}C]Val-*p*pR (1-220) by ^{13}C DD-MAS method was clearly suppressed as compared with that of [1-^{13}C]Val-*p*pR, this peak was assigned to Val230 and 237 from the tip region of the C-terminal α-helix (Figure 1). It should be noted that this peak was overlapped with the carbonyl components of egg PC bilayer. Since the peaks of egg PC were also suppressed, it is interesting to note that dynamics of carbonyl regions of lipid is influenced when *p*pR has truncated C-terminal region (221-239).

^{13}C NMR spectra of [3-^{13}C]Ala-labeled D75N and *p*pR complexed with *p*HtrII (1-159)

Figure 4 shows the ^{13}C CP-MAS (left) and DD-MAS (right) NMR spectra of [3-^{13}C]Ala- *p*pR- (C, D) and D75N-*p*HtrII(1-159) (E, F) complexes with reference to those of [3-^{13}C]Ala-labeled *p*pR (A, B). It is noted that the ^{13}C NMR spectra of [3-^{13}C]Ala-*p*pR were significantly changed

both at the C-terminal α-helix and the transmembrane α-helices when it formed complex with *p*HtrII(1-159) (see Figure 4 A-D). In particular, the ^{13}C DD-MAS NMR signals from the more flexible tip portion of the C-terminal α-helix at 16.7-16.9 ppm (Figure 4B) are largely suppressed in the complex formation (Figure 4D), due to dynamics change with the fluctuation frequency in the order from 10^8 Hz to 10^5 Hz in the tip portion which could be interfered with the proton decoupling frequency as summarized in Table 1, together with the data from our previous works (**29, 30**). At the same time, the intense five signals of the transmembrane α-helices are well resolved for the [3-^{13}C]Ala-*p*pR-*p*HtrII (1-159) complex, as recorded by the ^{13}C CP-MAS NMR (Figure 4C). This may be attributed to a conformational rearrangement of the transmembrane α-helices of *p*pR by forming complex with *p*HtrII. This complex was shown to be stabilized by interhelical hydrogen bonds between $Y199^{ppR}$-$N74^{pHtrII}$, and $T189^{ppR}$-$E43^{pHtrII}$ and -$S62^{pHtrII}$ and van der Waals contacts of helices F and G with TM2 helix (**13, 16, 47**). In addition, the ^{13}C NMR signals from the loop region at 17.2 and 17.4 ppm are clearly made visible for the *p*pR-*p*HtrII (1-159) complex, as recorded by the ^{13}C DD-MAS NMR (Figure 4D), although ^{13}C NMR signals from such loop regions are usually suppressed for *p*pR (**29**) and bR (**48-50**) in a monomeric state.

The disruption of the interhelical salt-bridge between helix C and G in *p*pR by changing to an activated state (D75N) may cause a change of the structures and molecular motions (**23**). Consistent with this expectation, the ^{13}C NMR signals of the transmembrane α-helices from [3-^{13}C]Ala-D75N complexed with *p*HtrII are not any more well-resolved as recorded by ^{13}C CP-MAS NMR spectrum, as a result of weakened TM helix-helix interaction (Figure 4E), in view of the expectation in the structure and molecular motions (**23**). As a result, the presence of the peaks from the rather flexible tip of the C-terminal α-helix of D75N-*p*HtrII complex are evident in the ^{13}C DD-MAS NMR spectrum (Figure 4F) in which ^{13}C NMR signals from 16.7-16.9 ppm in the more flexible tip portion are not any more suppressed in the complex formation. This finding indicates that the C-terminal tip α-helix becomes more flexible by changing the receptor part from *p*pR to D75N in the complex state.

Figure 5 shows the ^{13}C CP-MAS (*left*) and DD-MAS (*right*) NMR spectra of [1-^{13}C]Val-*p*pR (Figure 5A and B), *p*pR-*p*HtrII(1-159) (Figure 5C and D) and [1-^{13}C]Val-D75N-*p*HtrII(1-159) (Figure 5E and F), respectively. The reason why we record ^{13}C NMR spectra of [1-^{13}C]Val-labeled *p*pR and D75N is that the protein dynamics with fluctuation frequency in the order of 10^4 Hz is preferentially available from the suppressed peaks caused by interference with frequency of magic angle spinning, if any (**42**). Indeed, the ^{13}C DD-MAS NMR spectra (Figure 5 B and D) of [1-^{13}C]Val-*p*pR and *p*pR-*p*HtrII(1-159) showed that the signal intensity of the C-terminal tip region at 173.6 ppm (Val230 and 237, and lipid carbonyl

carbons) was significantly suppressed when it formed complex with *p*HtrII(1-159). This is obviously due to the dynamics change with fluctuation frequency of this region in the order from 10^6 to 10^4-10^5 Hz which could be interfered with the frequencies of magic angle spinning and proton decoupling as summarized in Table 1. The signal suppression was also noticed in CP-MAS NMR, although its absolute change in the peak intensity is much the less than that in DD-MAS. On the contrary, the ^{13}C DD-MAS NMR spectra (Figure 5 D and F) show that the signal intensity of the C-terminal tip region of D75N at 173.7 ppm (Val230, 237) was not completely suppressed when [1-^{13}C]Val-D75N was complexed with *p*HtrII (Figure 5D and F). Further, the ^{13}C CP-MAS NMR peaks of [1-^{13}C]Val-D75N-*p*HtrII(1-159) were substantially broadened due to the presence of induced fluctuation motions with frequency in the order of 10^4 Hz in the transmembrane α-helices caused by the absence of salt-bridge between the Schiff base and its neutralized counter ion, in contrast to those of *p*pR-*p*HtrII(1-157) (Figure 5 C and E). These findings about [1-^{13}C]Val-*p*pR and D75N mutant are consistent with the dynamics change available from the ^{13}C NMR study on [3-^{13}C]Ala-*p*pR in the C-terminal α-helical tip region and transmembrane helices during the course of the complex formation of *p*HtrII with *p*pR and D75N . This kind of dynamics change might be caused by the presence of the intermolecular association of D75N with *p*HtrII (1-159) through interaction between the α-helices protruding from the membrane surface.

[3-^{13}C]Ala-*p*HtrII (1-159) complexed with D75N or *p*pR

Further, we recorded the ^{13}C CP-MAS (Figure 6 *left*) and DD-MAS (Figure 6 *right*) NMR spectra of [3-^{13}C]Ala *p*HtrII (1-159) complexed with D75N mutant as a model for photo-activated receptor *p*pR (Figure 6 E and F) with reference to those of uncomplexed [3-^{13}C]Ala-*p*HtrII(1-159) (Figure 6 A and B) and complex with wild type *p*pR (Figure 6 C and D) (**30**). The estimated fluctuation frequencies for the cytoplasmic and transmembrane α-helices in the [3-^{13}C]Ala-*p*HtraII-*p*pR complex was already estimated in the order of $> 10^6$ and 10^4 Hz, respectively (**30**). The obviously suppressed ^{13}C DD-MAS and CP-MAS NMR signals of [3-^{13}C]Ala *p*HtrII (1-159)-D75N complex both at the cytoplasmic and transmembrane α-helices from are also noteworthy with reference to ^{13}C NMR signals of *p*HtrII (1-159)-*p*pR complex and also to the peak-intensity of the asterisked lipid methyl carbon signal at 14.1 ppm. Naturally, the transmembrane α-helices (TM 1 and 2) of *p*HtrII (1-159) complexed with D75N was made more flexible (with the fluctuation frequency ~10^5 Hz) than that of the complex with *p*pR (10^4 Hz) due to the above-mentioned, weakened intermolecular hydrogen bonds and van der Waals contacts of the transmembrane α-helices caused by the disrupted salt-bridges. On the contrary, it

is noteworthy that the cytoplasmic α-helical portions of *p*HtrII (1-159) are made more rigid in the complex with D75N (estimated as 10^5 Hz), owing to formation of the helix-helix interaction between the α-helices in the protruded cytoplasmic side, as compared with the complex with *p*pR (10^6 Hz), as schematically illustrated in Figure 7.

DISCUSSION

Dynamic states of *p*pR, D75N and *p*HtrII

Here, we noted that the accompanied spectral changes due to the complex formations of *p*pR or D75N with *p*HtrII (1-159) are quite different as viewed from the ^{13}C NMR spectra of [3-^{13}C]Ala-labeled *p*pR, D75N and *p*HtrII (1-159): significant spectral changes are noted for [3-^{13}C]Ala-labeled *p*pR complexed with *p*HtrII (1-159) both from the spectral resolution of the transmembrane α-helices arising from the conformational rearrangement (Figure 4C) and dynamics change of the more flexible tip portion of the C-terminal α-helix with fluctuation frequency from 10^8 to 10^5 Hz as viewed from the intensity changes (Figure 4D). The latter frequency is readily available from the interference of the underlying fluctuation frequency with frequency of the proton decoupling. Indeed, this "restrained" C-terminal α-helix may be stabilized by a helix-helix interaction between the C-terminal α-helix of *p*pR and cytoplasmic α-helix of *p*HtrII at the cytoplasmic surface. Such spectral changes, however, were less significant in the case of [3-^{13}C]Ala-D75N-*p*HtrII (1-159) complex (Figures 4E and F), although the presence of surprisingly stabilized helix-helix interaction was clearly seen as a reduced fluctuation frequency from the ^{13}C NMR spectra of [3-^{13}C]Ala-*p*HtrII-D75N complex as shown in Figures 6E and F. This is obviously caused by a switching of pairs in the helix-helix interactions in the cytoplasmic C-terminal α-helix of *p*HtrII from *p*pR to *p*HtrII itself, initiated by the loosened interactions between *p*HtrII and D75N by the disrupted salt-bridges.

For the *correct* interpretation of the dynamics changes arising from the selectively suppressed or enhanced peak-intensities, it is essential to have a prior knowledge as to the dynamic stage of a certain portion of membrane proteins under consideration which could be widely modified by a manner of sample preparations, temperature, hydration, etc. as summarized in Table 1, based on our previous site-directed ^{13}C NMR studies of bR, *p*pR and *p*HtrII (**29, 30, 49-51**). In short, fluctuation frequency of the transmembrane α-helices in bR from two-dimensional crystal in purple membrane at ambient temperature is in the order of 10^2 Hz. On the contrary, membrane protein present as monomeric species as in reconstituted bR, its D85N mutant, or *p*pR in lipid bilayers is more flexible in the absence of specific protein-protein

contact and their fluctuation frequency is increased to the order of 10^4-10^5 Hz, as summarized in Table 1. In the monomer of proteins reconstituted in egg PC bilayer, ^{13}C NMR signals from the loop regions are accordingly suppressed, because there are fluctuation motions with frequencies in the order of 10^4 or10^5 Hz which could be interfered with either frequency of MAS or proton decoupling, to result in failure in the peak-narrowing by the CP-MAS or DD-MAS experiments (**28, 41,42, 49, 50**). Nevertheless, it is interesting to note that the recovery of such signals from the loop region in the [3-^{13}C]Ala-*p*pR complexed with *p*HtrII (Figure 4D) is caused by an escape from such interference due to reduced fluctuation frequency which is not any more close to the proton decoupling frequency as a result of modified helix-helix interaction in the complex.

Therefore, it should be taken into account that the suppressed ^{13}C NMR signals of certain [3-^{13}C]Ala-labeled proteins peak could be interpreted in terms of the presence of either decreased or increased fluctuation frequency, depending upon the initial state with fluctuation motion higher or lower than the boundary state of 10^4-10^5 Hz. In other word, the presence of the suppressed peaks could be interpreted in terms of stabilized or dissociated complex depending upon the above-mentioned initial state.

Role of the C-terminal and transmembrane α-helix of *p*pR and D75N in the complex formation with *p*HtrII (1-159)

The suppressed signals during the course of the complex formation in Figures 1-4 are attributed to the reduced fluctuation-frequency in the cytoplasmic α-helix from 10^8 Hz in the free state to ~10^4 or 10^5 Hz in the complexed state, depending upon the type of interference of fluctuation frequency either with frequency of the magic angle spinning or proton decoupling and can be utilized as very convenient means to evaluate a parameter to characterize undergoing local protein dynamics (Table 1). It should be pointed out that this sort of interaction can not be detectable by solution NMR, even if examined in the micelle solution, because the local motion with the frequency range of 10^4-10^5 Hz cannot be characterized under the rapid motion of the micelle particles used in the solution NMR (**22**). Further, caution was made about a possibility that solubilization of membrane protein can result in impaired structure and/or function of the molecules under investigation (**52**). The present solid state NMR experiments indicate that even the tip region of the C-terminal α-helix of *p*pR in the cytoplasmic surface is participated also in the complex formation with *p*HtrII(1-159) through a helix-helix interaction with the C-terminal α-helix of *p*pR (see Figure 7 A). The X-ray diffraction studies on *p*pR and *p*pR-*p*HtrII(1-114) complex reveals that the binding with transducer slightly changes the secondary structure of

*p*pR (**13, 14, 53**). In fact, the observed CP-MAS NMR spectral changes in the transmembrane α-helices of *p*pR between uncomplexed and *p*pR-*p*HtrII (1-159) complex forms are consistent with the proposed conformational rearrangement by X-ray diffraction: hydrogen bonds of $Y199^{ppR}$-$N74^{pHtrII}$, and $T189^{ppR}$-$E43^{pHtrII}$ and $S62^{pHtrII}$ are formed on the binding surface of *p*pR-*p*HtrII complex. Nevertheless, region of helix G in *p*pR-*p*HtrII(1-114) expands to His223 according to crystallographic structure. In this NMR data, it is found that interaction between the C-terminal tip region in *p*pR and *p*HtrII(1-159) is made available by means of association of the α-helical region protruding from the membrane surface. In other word, the C-terminal α-helix of *p*pR plays an important role for an additional stabilization for the 2:2 complex through mutual interaction between the cytoplasmic α-helix (*p*HtrII) (1-159) and C-terminal α-helix (*p*pR) (Figure 7A).

These findings suggest a possibility that the C-terminal α-helix plays an important role for stabilization of the *p*pR complex with *p*HtrII. This is consistent with the results that K_d of the truncated *p*HtrII (101) is increased by almost two orders (10 μM) as compared with that of *p*HtrII (114) and *p*HtrII (157) (**20**). K_d of *p*HtrII (157) is small by 1.5 fold even if *p*HtrII (1-159) is compared with *p*HtrII(114). Therefore, the C-terminal α-helical position of *p*HtrII (102-113) plays an important role for the interactions with *p*pR. Moreover, proton pump activity of *p*pR is lost by binding with *p*HtrII (114) and *p*HtrII (157), although it remains by binding with *p*HtrII (101) (**9, 19, 20, and 54**). It is, therefore, suggested that the complex formation of the C-terminal α-helical regions of *p*pR with *p*HtrII(>114) is related to a proton pump activity and signal relay initially to *p*HtrII and then to CheA and CheW proteins.

Structure and dynamics of D75N-*p*HtrII(1-159) complex as an activated state

In the DD-MAS NMR spectra, the peak intensities of the tip region of the C-terminal α-helix from [3-^{13}C]Ala- and [1-^{13}C]Val- D75N complex with *p*HtrII(1-159) as an activated state at 16.7-16.9 ppm (Ala228, 234, 236, 238) and 173.5 ppm (Val230, 237), respectively, are recovered as viewed from the intensity of the uncomplexed *p*pR as compared with those of *p*pR-*p*HtrII(1-159) as a grand state (see Figure 4). Subsequently, the disruption of the interhelical salt-bridge (helix C-G) at an activated state may cause increased fluctuation to lead instability of the complex to weaken the above-mentioned hydrogen bonds in the binding surface between D75N and *p*HtrII (Figure 7A and B) Accordingly, the interaction of the tip region of the C-terminal α-helix in *p*pR complex with the cytoplasmic α-helix of *p*HtrII(1-159) is significantly weakened when *p*pR is replaced by D75N in the complex with *p*HtrII(1-159) as schematically depicted in Figure 7B. Dissociation constants (K_d) of the M-intermediate of the

wild-type *p*pR-*p*HtrII (1-159) is 15 μM, that is larger by almost 100 folds than that of wild-type *p*pR-*p*HtrII(1-159) in the dark (**9**). In the same experiment, K_d of D75N-*p*HtrII (1-159) (an activated state) turned out to be almost similar to the values of *p*pR-*p*HtrII(1-159) in the dark (**16**). However, it is important to point out that this local conformational change in the cytoplasmic side in *p*pR-*p*HtrII is related to a signal relay. In fact, the significant change in the peak intensity and spectral pattern in the ^{13}C CP-MAS and DD-MAS NMR spectra of D75N-*p*HtrII (1-159) indicate the existence of locally dynamics change to be compared with those of the uncomplexed *p*pR and *p*pR-*p*HtrII(1-159). In the case of bR, solid state ^{13}C NMR of [3-^{13}C]Ala-, [1-^{13}C]Val-D85N mutant (M-like intermediate in bR), the peaks of Ala51, 53, 215 in the vicinity of the retinal binding pocket, Ala160 in EF loop, and the other parts were suppressed even in 2D crystalline preparation (**35, 36**). Therefore, global change is conformation and dynamics of the protein backbone to the flexible state by deprotonating Schiff base (**31, 35**). It is therefore suggested that consequent change of the C-terminal α-helical tip region in *p*pR may be involved in production of repellent signal for blue light to the signal cascade system.

In the DD-MAS spectra of uncomplexed *p*HtrII (1-159) and *p*pR-*p*HtrII (1-159) complex, high frequency components (>10^5 Hz) of [3-^{13}C]Ala-labeled *p*HtrII in the cytoplasmic side are recorded (**30**). When *p*pR was changed to D75N, the signal intensities of *p*HtrII complex with *p*pR were significantly decreased. Therefore, dynamics of *p*HtrII in the complex with D75N in the cytoplasmic side largely decreased because *p*HtrII helix interacts with each other (Figure 7B). While, spectral pattern of [3-^{13}C]Ala-labeled *p*HtrII (1-159) complexed with D75N remains unchanged indicating that the structures do not change prominently. On the other hand, the transmembrane part of *p*HtrII is made flexible as a result of the disrupted salt-bridges and consequent change of the interfacial hydrogen bonds as shown in CP-MAS spectra. This finding is consistent with the less flexible nature of the cytoplasmic side of Tsr as bacterial chemotaxis receptor on active state (**55**). In this present experiments, however, we have not yet determined the ^{13}C NMR signals of the particular position of the C-terminus of *p*HtrII (1-159), and which part of *p*HtrII (1-159) interacts with the C-terminal region. It is likely that the C-terminal α-helix in *p*pR may interact with region of *p*HtrII (>114) according to the data of Hippler-Mreyen et al. and Sudo et al. (**20,22**).

CONCLUSION

We found that the C-terminal residues of *p*pR, protruding from the cytoplasmic surface, consist of the C-terminal α-helix stem and tip regions, based on comparative study on the ^{13}C NMR spectra of *p*pR with those of *p*pR(1-220) and the conformation-dependent as well as

dynamic-dependent ^{13}C chemical shifts. It turned out that the latter tip region in *p*pR is also in direct interaction with *p*HtrII(1-159), in addition to the mutual helix-helix interaction stabilized by the salt-bridge between the transmembrane α–helices. This sort of interaction, however, was destabilized in D75N complex with *p*HtrII(1-159) as disclosed from ^{13}C DD-MAS NMR data. Consequently, a switching of pairs in the helix-helix interaction occurs from *p*HtrII-*p*pR to *p*HtrII itself when *p*pR is converted to an activated state (D75N). It is evident that these conformational and dynamical changes of *p*pR and *p*HtrII are related to transmit a signal to *p*HtrII. It is evident that these conformational and dynamical changes of *p*pR and *p*HtrII are related to transmit a signal to *p*HtrII. Spudich et al. observed that D73N mutant of sRII was constitutively active from negative phototaxis of *H. salinarum*, which verified Spudich's hypothesis (**56**). D73N mutant of sRII corresponds to D75N mutant in *p*pR employed in this investigation. Hence, the present study shows that the disruption of the salt-bridge between C- and G-helix causes the rigidness of transducer in the cytoplasmic side and these processes may trigger the phototaxis. We, however, must keep it in mind that this may not be only a trigger but there may exist other signals from the sensor to the changes in the intracellular interaction between *p*pR and *p*HtrII may be necessary as is shown by Yang et al. and Sudo et al.

REFERENCES

1. J. K. Lanyi. Mechanism of Ion Transport across Membranes. *J. Biol. Chem.* 1997 **272** 31209-31212.

2. G. Varo.
Analogies between halorhodopsin and bacteriorhodopsin.
Biochim. Biophys. Acta. 2000 **1460** 220-22.

3. R. A. Bogomolni and J. L. Spudich. Identification of a third rhodopsin-like pigment in phototactic *Halobacteirum halobium.*
Proc. Natl. Acad. Sci. USA 1982 **79** 6250-6254.

4. T. Takahashi, H. Tomioka, N. Kamo, and Y. Kobatake.
A photosystem other than PS370 also mediates the negative phototaxis of *Halobacterium halobium. FEMS Microbiol. Lett.* 1985 **28** 161-164.

5. T. Takahashi, B. Yan, P. Mazur, F. Derguini, K. Nakanishi, and J. L. Spudich.
Color regulation in the Archaebacterial phototaxis receptor phoborhodopsin (sensory rhodopsin II). *Biochemistry* 1990 **29** 8467-8474.

6. J. L. Spudich, C. S. Yang, K. H. Jung, and E. N. Spudich.
Retinylidene proteins: structures and functions from archaeal to humans.
Annu. Rev. Cell Dev. Biol. 2000 **16** 365-392.

7. R. Seidel, B. Scharf, M. Gautel, K. Kleine, D. Oesterhelt and M. Engelhard.
The primary structure of sensory rhodopsin II: A member of an additional retinal protein subgroup is coexpressed with its transducer, the halobacterial transducer of rhodopsin II.
Proc. Natl. Acad. Sci. USA 1995 **92** 3036-3040.

8. N. Kamo, K. Shimono, M. Iwamoto and Y. Sudo.
Photochemistry and photoinduced proton-transfer by *pharaonis* phoborhodopsin.
Biochemistry (Moscow). 2001 **66** 1277-1282.

9. Y. Sudo, M. Iwamoto, K. Shimono, and N. Kamo.
Pharaonis phoborhodopsin binds to its cognate truncated transducer even in the presence of a detergent with a 1:1 stoichiometry.
Photochem. Photobiol. 2001 **74** 489-494.

10. Y. Sudo, M. Iwamoto, K. Shimono, N. Kamo.
Association between a photo-intermediate of a M-lacking mutant D75N of *pharaonis* phoborhodopsin and its cognate transducer.
Photochem. Photobiol. B 2002 **67** 171-176.

11. A.-A. Wegner, J. P. Klare, M. Engelhard, H.-J. Steinhoff.
Structural insights into the early steps of receptor-transducer signal transfer in archaeal

phototaxis.

EMBO J. 2001 **20** 5312-5319.

12. J. P. Klare, E. Bordignon, M. Engelhard, and H. J. Steinhoff.

Sensory rhodopsin II and bacteriorhodopsin: Light activated helix F movement.

Photochem. Photobiol. Sci. 2004 **3** 543-547.

13. V. I. Gordeliy, J. Labahn, R. Moukhametzianov, R. Efemon, J. Granzin, R. Schlesinger, G. Buldt, T. Savopol, J. P. Klare and M. Engelhard.

Molecular basis of transmembrane signaling by sensory rhodopsin II-transducer complex.

Nature 2002 **419** 484-487.

14. R. Moukhametzianov, J. P. Klare, R. Efremov, C. Baeken, A. Goppner, J. Labahn, M. Engelhard, G. Buldt and V. I. Gordeliy.

Development of the signal in sensory rhodopsin and its transfer to the cognate transducer.

Nature 2006 **440** 115-119.

15. K. Ihara, T. Umemura, I. Katagiri, T .Kitajima-Ihara, Y. Sugiyama, Y. Kimura and Y. Mukohata Evolution of the archaeal rhodopsins: evolution rate changes by gene duplication and functional differentiation.

J. Mol.Biol. 1999 **285** 163-174.

16. Y. Sudo, M. Iwamoto, K. Shimono, N. Kamo.

Tyr-199 and charged residues of *pharaonis* Phoborhodopsin are important for the interaction with its transducer. *Biophys. J.* 2002 **83** 427-432.

17. Y. Sudo, M. Yamabi, S. Kato, C. Hasegawa, M. Iwamoto, K. Shimono and N. Kamo.

Importance of specific hydrogen bonds of archaeal rhodopsins for the binding to the transducer protein.

J. Mol. Biol. 2006 **357** 1274-1282.

18. Y. Sudo, Y. Furutani, K. Shimono, N. Kamo and H. Kandori.

Hydrogen bonding alteration of Thr-204 in the complex between *pharaonis* phoborhodopsin and its transducer protein.

Biochemistry 2003 **42** 14166-14172.

19. M. Iwamoto, C. Hasegawa, Y. Sudo, K. Shimono, T. Araiso, and N. Kamo.

Proton release and uptake of *pharaonis* phoborhodopsin (sensory rhodopsin II) reconstituted into phospholipids.

Biochemistry 2004 **43** 3195-3203.

20. S. Hippler-Mreyen, J. P. Klare, A. A. Wegener, R. Seidel, C. Herrmann, G.. Schmies, G.. Nagel, E. Bamberg and M. Engelhard.

Probing the sensory rhodopsin II binding domain of its cognate transducer by calorimetry

and electrophysiology.
J. Mol. Biol. 2003 **330** 1203-1213.

21. C. S. Yang, O. Sineshchekov, E. N. Spudich and J. L. Spudich.
The cytoplasmic membrane-proximal domain of the HtrII transducer interacts with the E-F loop of photoactivated *Natronomonas pharaonis* sensory rhodopsin II.
J. Biol. Chem. 2004 **279** 42970-42976.

22. Y. Sudo, H. Okuda, M. Yamabi, Y. Fukuzaki, M. Mishima, N. Kamo, and C. Kojima
Linker region of a halobacterial transducer protein interacts directly with its sensor retinal protein. *Biochemistry* 2005 **44** 6144-6152.

23. E. N. Spudich, W. Zhang, M. Alam, and J. L. Spudich.
Constitutive signaling by the phototaxis receptor sensory rhodopsin II from disruption of its protonated Schiff base-Asp-73 internal helical salt bridge.
Proc. Natl. Acad. Sci. USA 1997 **94** 4960-4965.

24. L. S. Brown, H. Kamikubo, L. Zimanyi, M. Kataoka, F. Tokunaga, P. Verdegem, J. Lugtenburg, J. K. Lanyi.
A local electrostatic change is the cause of the large-scale protein conformation shift in bacteriorhodopsin.
Proc. Natl. Acad. Sci. USA 1997 **94** 5040-5044.

25. V. B. Bergo, E. N. Spudich, K. J. Rothschild and J. L. Spudich
Photoactivation perturbs the membrane-embedded contacts between sensory rhodopsin II and its transducer.
J. Biol. Chem. 2005 **280** 28365-28369.

26. A. Watts, S. K. Straus, S. L. Grage, M. Kamihira, Y. H. Lam and X. Zhao.
In Methods in Molecular Biology: Techniques in Protein NMR
Humana Press 2004 **278** 403-473.

27. S. J. Opella and F. M. Marassi
Structure determination of membrane proteins by NMR spectroscopy.
Chem. Rev. 2004 **104** 3587-3606.

28. H. Saitô, S. Tuzi, M. Tanio and A. Naito.
Dynamic aspects of membrane proteins and membrane-associated Peptides as revealed by ^{13}C NMR: Lessons from bacteriorhodopsin as an *intact* protein.
Annu.Rep.NMR Spectrosco. 2002 **47** 39-108.

29. T. Arakawa, K. Shimono, S. Yamaguchi, S. Tuzi, Y. Sudo, N. Kamo, and H. Saitô.
Dynamic structure of *pharaonis* phoborhodopsin (sensory rhodopsin II) and complex with a cognate truncated transducer as revealed by site-directed ^{13}C solid-state NMR.

FEBS Letter 2003 **536** 237-240.

30. S. Yamaguchi, K. Shimono, Y. Sudo, S. Tuzi, A. Naito, N. Kamo, H. Saitô.
Conformation and dynamics of the [3-^{13}C]Ala-,[1-^{13}C]Val-labeled truncated *pharaonis* transducer, *p*HtrII(1-159) as revealed by site-directed ^{13}C Solid-state NMR: changes due to association with phoborhodopsin (sensory rhodopsin II).
Biophys. J. 2004 **86** 3131-3140.

31. H. Saitô,
Dynamic pictures of membrane proteins in two-dimensional crystal, lipid bilayer and detergent as revealed by site-directed solid-state ^{13}C NMR.
Chem. Phys. Lipids 2004 **132** 101-112.

32. S. Yamaguchi, S. Tuzi, T. Seki, M. Tanio, R. Needleman, J. K. Lanyi, A. Naito, and H. Saitô.
Stability of the C-terminal-helical domain of bacteriorhodopsin that protruded from the membrane surface, as studied by high-resolution solid-state ^{13}C NMR.
J. Biochem. (Tokyo). 1998 **123** 78-86.

33. S. Yamaguchi, K. Yonebayashi, H. Konishi, S. Tuzi, A. Naito, J. K. Lanyi, R. Needleman, H. Saitô.
Cytoplasmic surface structure of bacteriorhodopsin consisting of interhelical loops and C-terminal α-helix, modified by a variety of environmental factors as studied by ^{13}C NMR.
Eur. J. Biochem. 2001 **268** 1-12.

34. K. Yonebayashi, S. Yamaguchi, S. Tuzi, H. Saitô.
Cytoplasmic surface structures of bacteriorhodopsin modified by site-directed mutaions and cation binding as revealed by ^{13}C NMR.
Eur. Biophys. J. 2003 **32** 1-11.

35. Y. Kawase, M. Tanio, A. Kira, S. Yamaguchi, S. Tuzi, A. Natio, M. Kataoka, J. K. Lanyi, R. Needleman, H. Saitô.
Alteration of conformation and dynamics of bacteriorhodopsin induced by protonation of Asp 85 and deprotonation of Schiff base as studied by ^{13}C NMR.
Biochemistry 2000 **39** 14472-14480.

36. A. Kira, M. Tanio, S. Tuzi and H. Saitô.
Significance of low frequency local fluctuation motions in the transmembrane B and C α-helices of bacteriorhodopsin, to facilitate efficient proton uptake from the cytoplasmic surface, as revealed by site-directed solid-state ^{13}C NMR.
Eur. Biophys. J. 2004 **33** 580-588.

37. H. Saitô
Conformation-dependent ^{13}C chemical shifts: a new means of conformational

characterization as obtained by high-resolution solid-state NMR.
Magn. Reson. Chem. 1986 **24** 835-852.

38. H. Saitô and I. Ando.
High-resolution solid-state NMR studies of synthetic and biological macromolecules.
Annu. Rep. NMR spectrosco. 1989 **21** 209-290.

39. K. Shimono, M. Iwamoto, M. Sumi and N. Kamo.
Functional expression of *pharaonis* phoborhodopsin in *Escherichia coli.*
FEBS Letters 1997 **420** 54-56

40. H. Kandori, K. Shimono, Y. Sudo, M. Iwamoto, Y. Shichida and N. Kamo.
Structural changes of *pharaonis* phoborhodopsin upon photoisomerization of the retinal chromophore: infrared spectral composition with bacteriorhodopsin.
Biochemistry 2001 **40** 9238-9246.

41. W. P. Rothwell and J. S. Waugh.
Transverse relaxation of dipolar coupled spin systems under rf irradiation: detection motions in solid. *J. Chem. Phys.* 1981 **75** 2721-2732.

42. D. W. Suwelack, W. P. Rothwell, and J. S.Waugh.
Slow molecular motion detected in the NMR spectra of rotating solids.
J. Chem. Phys. 1980 **73** 2559-2569

43. S. Krimm and A. M. Dwivedi.
Infrared spectrum of the purple membrane: clue to a proton conduction mechanism?
Science. 1982 **216** 407-408.

44. H. Saitô, S. Tuzi, S.Yamaguchi, M. Tanio, and A. Naito.
Conformation and backbone dynamics of bacteriorhodopsin revealed by ^{13}C NMR.
Biochim. Biophys. Acta 2000 **1460** 39-48.

45. S. Yamaguchi, S. Tuzi, M. Tanio, A. Naito, J. K. Lanyi, R. Needleman and H. Saito.
Irreversible conformational change of bacterio-opsin induced by binding of retinal during its reconstitution to bacteriorhodopsin, as studied by ^{13}C NMR.
J. Biochem. (Tokyo) 2000 **127** 861-869.

46. P. Y. Chou and G. D. Fasman.
Conformational parameters for amino acids in helical, β-sheet, and random coil regions calculated from proteins.
Biochemistry 1974 **13** 222-245

47. Y. Sudo, M. Yamabi, M. Iwamoto, K. Shimono and N. Kamo.
Interaction of *Natronobacterium pharaonis* Phoborhodopsin (Sensory Rhodopsin II) with its Cognate Transducer Probed by Increase in the Thermal Stability.

Photochem. Photobiol. 2003 **78** 511-516.

48. H. Saitô, K. Yamamoto, S. Tuzi, and S. Yamaguchi.
Backbone dynamics of membrane proteins in lipid bilayers: the effect of two dimensional array formation as revealed by site-directed solid-state ^{13}C NMR studies on [3-^{13}C]Ala- and [1-^{13}C] Val-labeled bacteriorhodopsin.
Biochim. Biophys. Acta. 2003 **1616** 127-136.

49. H. Saitô, T. Tsuchida, K. Ogawa, T. Arakawa, S. Yamaguchi and S. Tuzi.
Residue-specific millisecond to microsecond fluctuations in bacteriorhodopsin induced by disrupted or disorganized two-dimensional crystalline lattice, through modified lipid-helix and helix-helix interactions, as revealed by ^{13}C NMR. *Biochim. Biophys. Acta.* 2002 **1565** 97-106.

50. Yamamoto, K., S. Tuzi, H. Saitô, I. Kawamura and A. Naito.
Conformation and dynamics changes of bacteriorhodopsin and its D85N mutant in the absence of 2D crystalline lattice as revealed by site-directed ^{13}C NMR.
Biochim. Biophys. Acta. 2006 **1758** 181-189.

51. S. Yamaguchi, S. Tuzi, K. Yonebayashi, A. Naito, R. Needleman, J. K. Lanyi and H. Saitô.
Surface dynamics of bacteriorhodopsin as revealed by ^{13}C NMR studies on [1-^{13}C]Ala-labeled proteins: Detection of millisecond or microsecond motions in interhelical loops and C-terminal α-helix.
J. Biochem (Tokyo). 2001 **129** 373-382.

52. J. P. Klare, E. Bordignon, M. Doebber, J. Fitter, J. Kriegsmann, I. Chizhov, H.-J. Steinhoff and M. Engelhard.
Effects of solubilization on the structure and function of the sensory rhodopsin II/transducer complex. *J. Mol. Biol.* 2006 **356** 1207-1221.

53. H. Luecke, B. Schobert, J. K.Lanyi, E. N. Spudich, and J. L. Spudich.
Crystal structure of sensory rhodopsin II at 2.4 Angstroms: insight into color tuning and transducer interaction.
Science 2001 **293** 1499-1503.

54. G.. Schmies, B. Lüttenberg, I. Chizhov, M. Engelhard, A. Becker, and E. Bamberg.
Sensory Rhodopsin II from the Haloalkaliphilic *Natronobacterium pharaonis*: Light-Activated Proton Transfer Reactions.
Biophys. J. 2000 **78** 967-976.

55. S. H. Kim, W. Wang, and K. K. Kim.
Dynamic and clustering model of bacterial chemotaxis receptors: Structural basis of signaling and high sensitivity.

Proc. Natl. Acad. Sci. USA. 2002 **99** 11611-11615.

56. J. L. Spudich and J. K. Lanyi.

Shuttling between two conformations: The common mechanism for sensory transduction and ion-transport.

Curr. Opinion in Cell Biol. 1996 **8** 452-457.

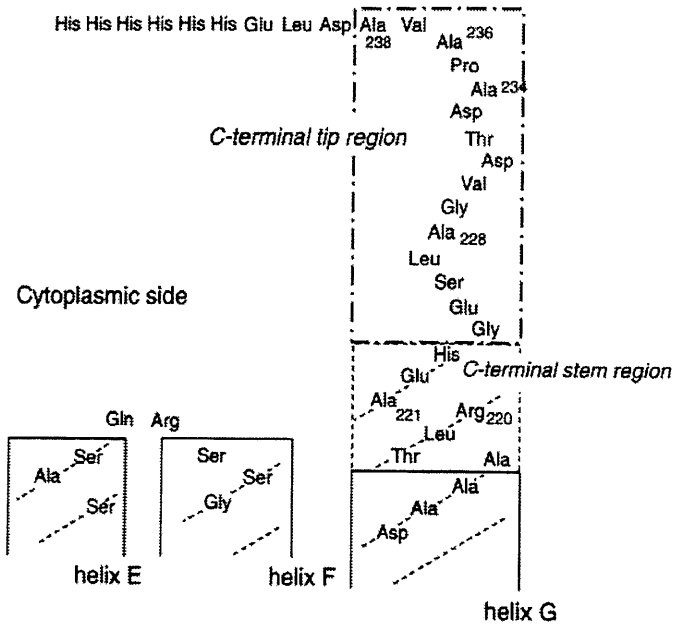

Figure 1. A schematic representation of the helices E, F, G and C-terminal region in *p*pR on the cytoplasmic side, based on the crystallographic structures reported by Luecke et al. (53) (*p*pR: PDB code 1JGJ) and Gordeliy et al. (13) (*p*pR-*p*HtrII(1-114): PDB code 1H2S). The dotted line box is helix G region of *p*pR-*p*HtrII(1-114) and the solid line box is helix G region of *p*pR alone from X-ray diffraction data.

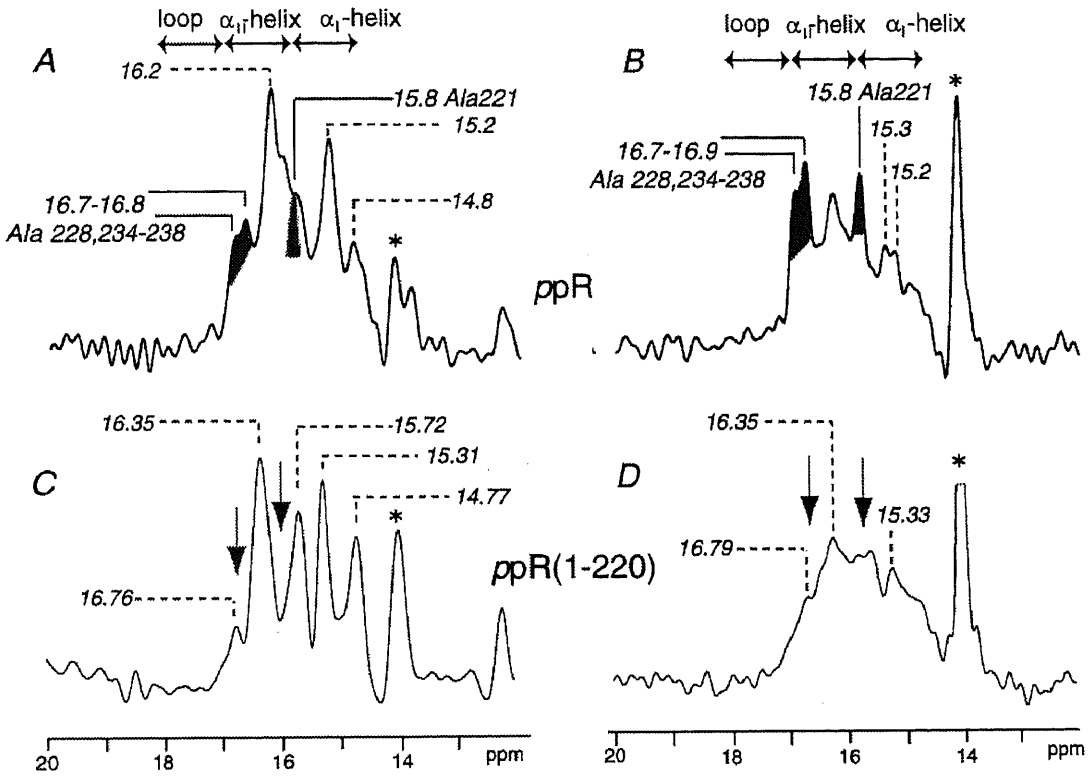

Figure 2. ^{13}C CP-MAS (left) and DD-MAS (right) NMR spectra of [3-^{13}C]Ala-*pp*R alone (A, B) and truncated *pp*R(1-220) (C, D) reconstituted in egg PC bilayer, respectively. ^{13}C NMR signals from the C-terminal region in *pp*R are shown in the gray (A and B) and arrows (C and D). The resonance peak at 14.1 ppm is ascribed to the methyl carbon peak of egg PC as shown by the asterisk.

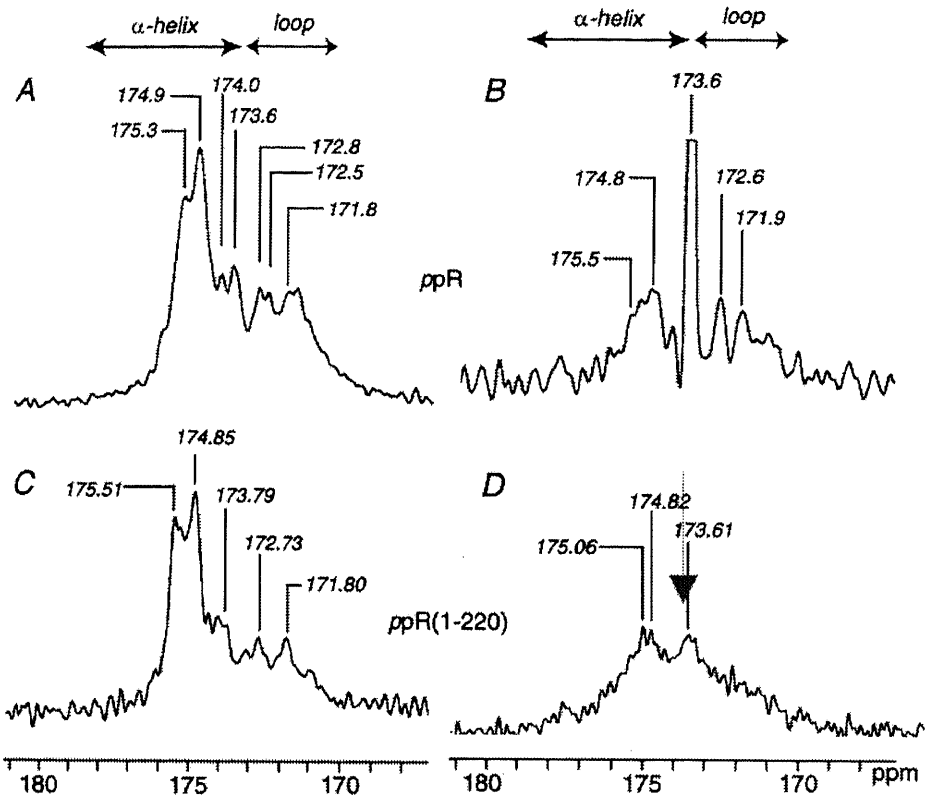

Figure 3. ^{13}C CP-MAS (left) and DD-MAS (right) NMR spectra of [1-^{13}C]Val-*pp*R (A, B) and truncated *pp*R(1-220) (C, D) reconstituted in egg PC bilayer, respectively. ^{13}C NMR signals from the C-terminal region in *pp*R are shown in the gray (A and B) and arrows (C and D). The resonance peak at 14.1 ppm is ascribed to the methyl carbon peak of egg PC as shown by the asterisk.

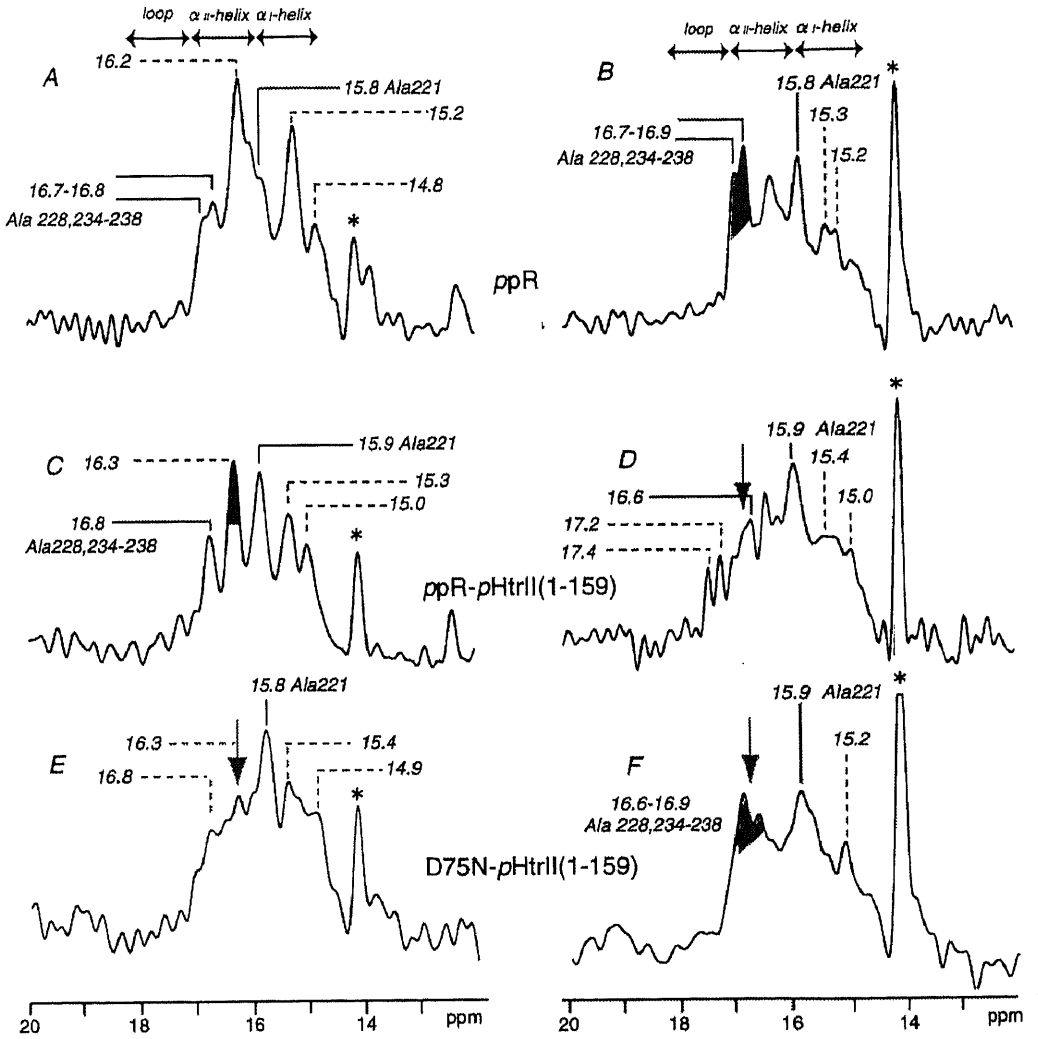

Figure 4. ^{13}C CP-MAS (*left*) and DD-MAS (*right*) NMR spectra of uncomplexed [3-^{13}C] Ala-labeled *p*pR (A, B), *p*pR-*p*HtrII (1-159) (C, D) and D75N-*p*HtrII (1-159) (E,F) reconstituted in egg PC bilayer, respectively. ^{13}C NMR signals from the C-terminal region of *p*pR, *p*pR to *p*pR-*p*HtrII(1-159) and D75N-*p*HtrII (1-159) are shown in the gray (B,F) and arrows (D,F). The resonance peak at 14.1 ppm is the methyl peak of egg PC as shown as asterisk.

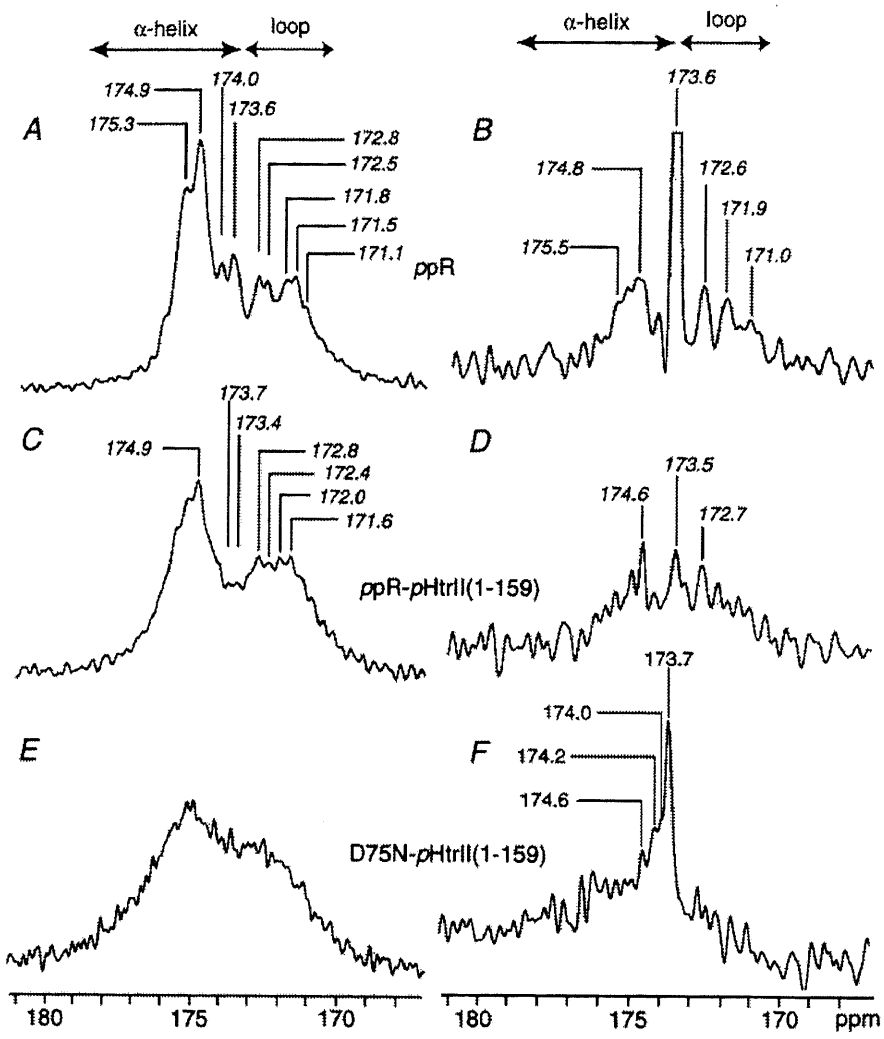

Figure 5. ^{13}C CP-MAS (*left*) and DD-MAS (*right*) NMR spectra of uncomplexed [1-^{13}C] Val-labeled *p*pR (A, B), *p*pR-*p*HtrII (1-159) (C, D) and D75N-*p*HtrII(1-159) (E,F) reconstituted in egg PC bilayer, respectively.

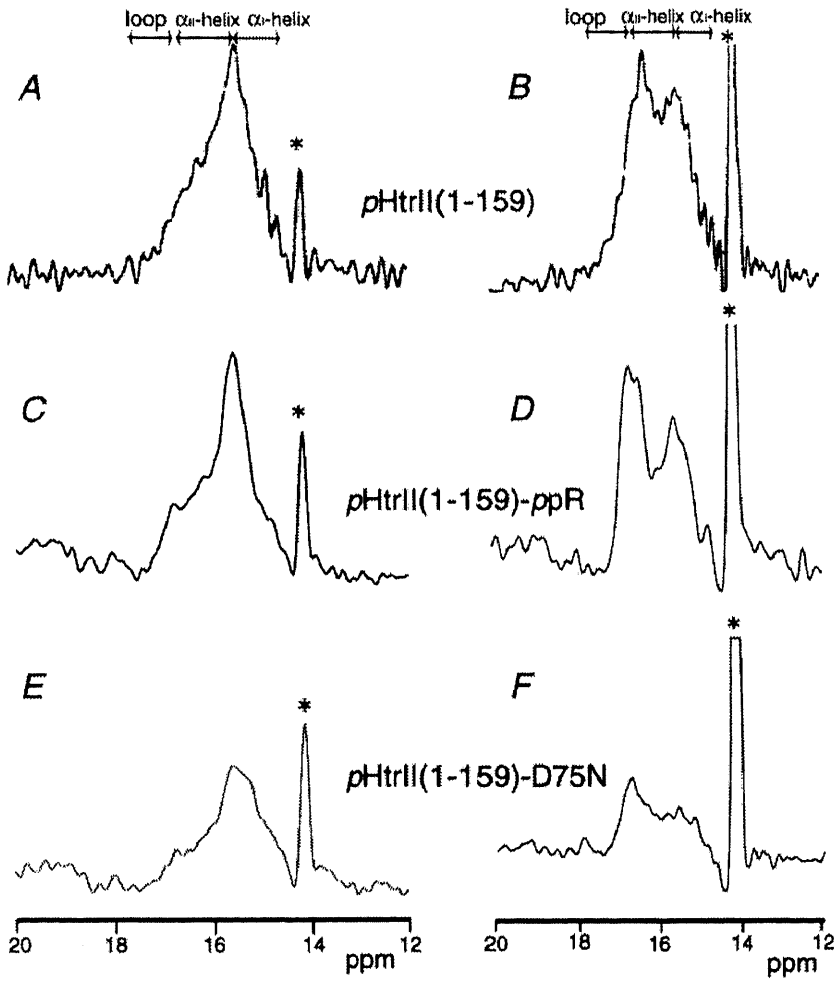

Figure 6. ^{13}C CP-MAS (*left*) and DD-MAS (*right*) NMR spectra of uncomplexed [3-^{13}C]Ala-labeled *p*HtrII (1-159) (A,B), *p*HtrII (1-159)-*pp*R complex (C,D) and *p*HtrII(1-159)-D75N complex (E, F), respectively, in reconstituted in egg PC bilayer.

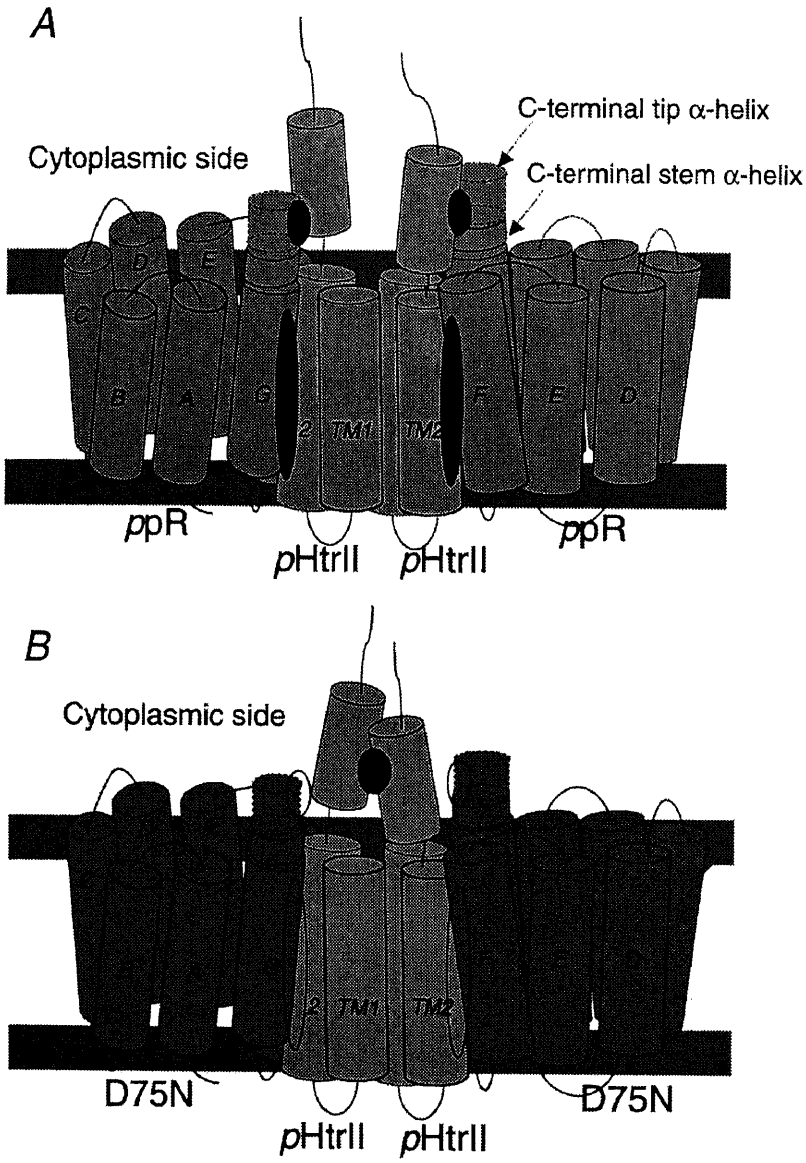

Figure 7. Schematic representation of the manner of interaction of the C-terminal α-helical tip region in *p*pR (A) and D75N (B) with the transmembrane and cytoplasmic α-helices of *p*HtrII(1-159). The helix-helix interactions between the cytoplasmic α-helices are also presented. Elliptical gray areas and open areas show the enhanced and weakened interaction parts, respectively.

Chapter 6

Participation of the surface structure of *pharaonis* phoborhodopsin, *p*pR and its A149S and A149V mutants, consisting of the C-terminal α-helix and EF loop, in the complex-formation with the cognate transducer *p*HtrII, as revealed by site-directed ^{13}C solid-state NMR

ABSTRACT

We have recorded ^{13}C solid state NMR spectra of [3-^{13}C]Ala-labeled *pharaonis* phoborhodopsin *p*pR, and its mutants, A149S and A149V, complexed with the cognate transducer *p*HtrII (1-159), to gain insight into a possible role of their cytoplasmic surface structure including the C-terminal α-helix and E-F loop for stabilization of the 2:2 complex, by both cross-polarization magic angle spinning (CP-MAS) and dipolar decoupled-magic angle spinning (DD-MAS) NMR techniques. We found that ^{13}C CP-MAS NMR spectra of [3-^{13}C]Ala-*p*pR, A149S, and A149V complexed with the transducer *p*HtrII are very similar, reflecting their conformation and dynamics changes caused by mutual interactions through the transmembrane α-helical surfaces. In contrast, their DD-MAS NMR spectral features are quite different between [3-^{13}C]Ala-A149S and A149V in the complexes with *p*HtrII: ^{13}C DD-MAS NMR spectrum of [3-^{13}C]Ala-A149S complex is rather similar to that of the uncomplexed form, while the corresponding spectral feature of A149V complex is similar to that of *p*pR complex in the C-terminal tip region. This is because more flexible surface structure detected by the DD-MAS NMR spectra are more directly influenced by the dynamics changes than the CP-MAS NMR. It turned out, therefore, that an altered surface structure of A149S resulted in destabilized complex as viewed from the ^{13}C NMR spectrum of the surface areas, probably because of modified conformation at the corner of the helix E in addition to the change of hydropathy. It is, therefore, concluded that the surface structure of *p*pR including the C-terminal α-helix and the E-F loops is directly involved in the stabilization of the complex through conformational stability of the helix E.

INTRODUCTION

The archaeal sensory rhodopsins, SRI and SRII, are sensors for positive and negative phototaxis, respectively, on binding with the cognate transducer proteins (**1**). *Pharaonis* phoborhodopsin (*p*pR) is a negative phototaxis receptor, and forms a complex with *pharaonis* halobacterial transducer II protein (*p*HtrII). The stoichiometry of the *p*pR-*p*HtrII complex has been estimated to be 2:2 in cell membrane. When blue light is irradiated, this complex activates the phosphorylation cascade in the cytoplasmic side and regulates the switch of flagella motor (**2-5**).

The *p*pR-*p*HtrII interactions have been well investigated by using x-ray diffraction (XRD), FTIR spectroscopy, etc: it was shown that the $Y199^{ppR}$-$N74^{pHtrII}$, and $T189^{ppR}$-$E43^{pHtrII}$ and

-S62^{pHtrII} hydrogen bonds are formed between the binding surfaces of *p*pR and *p*HtrII in the transmembrane and extracellular region (**6-10**). In particular, Tyr199 conserved even in sensory rhodopsin II is a very important residue when *p*pR forms a complex with its cognate *p*HtrII (**11, 12**). In addition, FTIR results strongly indicated that Thr204-Tyr174 forms a hydrogen bond between the retinal pocket and binding surface of *p*pR-*p*HtrII, and Tyr199 and Thr204 in helix G play an important role for the interaction with *p*HtrII (**13-15**). On the other hand, the *p*pR-*p*HtrII interactions in the cytoplasmic regions are very important to take part in a signal relay, because the E-F loop in *p*pR turned out to interact with membrane proximal region in *p*HtrII as viewed from fluorescent probes (**16**). Further, *p*HtrII(1-114) in the cytoplasmic side is tightly bound with *p*pR inhibiting the proton release, although this activity depends on the length of *p*HtrII (**17**). It is also reported that the introduction of mutation into membrane proximal region in HtrI activates the proton release in SRI in spite of HtrI binding with SRI (**18**).

Fully hydrated membrane proteins are not always rigid solid at ambient temperature but rather flexible, exhibiting a variety of local motions as revealed by site-directed ^{13}C NMR, which are well related with their biological functions (**19-22**). Site-specific assignments of individual ^{13}C NMR peaks recorded by MAS NMR are essential to locate such portions, as demonstrated for the previous ^{13}C NMR studies on [3-^{13}C]Ala-, [1-^{13}C]Val- and [1-^{13}C]Trp-labeled bacteriorhodopsin (bR) from purple membrane (**23-25**). To this end, a variety of approaches such as cleavage of the C-terminal residues, site-directed mutation, and line-broadenings due to Mn^{2+} ion-induced transverse relaxation process were utilized. As a result, the organization of the cytoplasmic surface structures, including the C-terminal α-helix and the E-F loop as a function of metal ions, pH, temperature, etc., plays an essential role for the stabilization of the three-dimensional structure of bR at ambient temperature (**26-29**). It is demonstrated here that the ^{13}C NMR signals of the C-terminal α-helical region were also recently identified for [3-^{13}C]Ala- and [1-^{13}C]Val-labeled *p*pR and D75N mutant in the presence or absence of *p*HtrII(1-159) in egg PC bilayers (**30-32**) (see Figure 1 for the amino-acid sequence of *p*pR).

In this paper, we examined the conformation and dynamics of [3-^{13}C]Ala-labeled *p*pR, A149S and A149V mutants of *p*pR with emphasis of a possible role of the E-F loop by means of ^{13}C solid-state NMR techniques with reference to those of bR previously examined (**26-28**), because Ala149 in *p*pR is highly preserved on the other archaeal retinal proteins (**11**). The isotropic ^{13}C CP-MAS NMR peak of Ala149 was initially assigned by comparing ^{13}C NMR peak of [3-^{13}C]Ala-labeled *p*pR with that of [3-^{13}C]Ala-labeled A149S and A149V. We further examined the corresponding spectral changes of ^{13}C DD-MAS NMR for [3-^{13}C]Ala-labeled

A149S and A149V complexed with *p*HtrII(1-159). It turned out that mutation of *p*pR at Ala149 resulted in dynamical changes of the *p*pR-*p*HtrII(1-159) complex as far as membrane surface is concerned. It is therefore suggested that residues in the E-F loop regulate dynamics of membrane surface residues in *p*pR by binding with *p*HtrII.

MATERIALS AND METHODS

[3-^{13}C]Ala-,[1-^{13}C]Val-labeled A149S and A149V of *p*pR with His-Tag (6 × His) at the C-terminal were expressed in *Escherichia coli* BL21(DE3) strain in M9 medium containing [3-^{13}C] L-Alanine and [1-^{13}C] L-Valine (CIL, Andover, MA) by induction with 1 mM IPTG and 10 μM all-*trans* retinal. These proteins were solubilized by using *n*-dodecyl-β-D-maltoside (DM) and purified with a Ni-NTA column (QIAGEN, Hilden, Germany) as described previously (**32,33**). The truncated transducer, *p*HtrII(1-159), was prepared by using the above method. Purified proteins in DM micelles were incorporated into a lipid film of egg PC (*p*pR: egg PC molar ratio of 1:50), followed by gently stirring at 4℃ for overnight. DM was removed using Bio-Beads (Bio-Rad, Hercules, CA) to yield egg PC bilayers. Reconstituted suspensions were concentrated by centrifugation and suspended in 5 mM HEPES, 10 mM NaCl buffer solution (pH 7). The pelleted mixture of the complex with *p*pR: *p*HtrII ratio of 1:1 in egg PC bilayers was placed in 5.0 mm o.d. zirconia pencil-type rotor for magic angle spinning (MAS) experiments.

High-resolution ^{13}C solid-state NMR spectra were recorded on a Chemagnetics CMX-400 infinity FT-NMR spectrometer at 100.16 MHz for the carbon resonance frequency. Both cross polarization-magic angle spinning (CP-MAS) and single pulse excitation with dipolar decoupling-magic angle spinning (DD-MAS) were used to record ^{13}C NMR spectra. Mostly, 5000 transients were accumulated and 30 Hz of Gaussian broadening function was applied at the center point of 0.40 prior to Fourier transformation. A doubly tuned MAS probe equipped with a 5.0 mm o.d. rotor was used. The spinning frequency was set to 4 kHz and the duration of 90° pulse for the observed ^{13}C nucleus was 5.5 μs. In CP-MAS experiments, two pulses phase modulation (TPPM) proton decoupling (**34**) was used, and the contact and repetition times were 1 ms and 4 s, respectively. At ambient temperature, fully hydrated *p*pR undergoes fluctuation motions with frequency range from 10^2 to 10^8 Hz depending on its location (**30**). These wide dynamic ranges allowed us to distinctly observe motional components with the frequency range of 10^6-10^8 Hz by DD-MAS and rigid components with the frequency range of 10^2-10^6 Hz by CP-MAS methods. When the frequency of incoherent random molecular fluctuations in the region with the order of 10^4-10^5 Hz could be interfered with frequency of magic angle spinning or proton decoupling frequency, and hence observed ^{13}C NMR signal in such region could be

broadened or suppressed as a low efficiency of peak narrowing (**35, 36**). ^{13}C chemical shifts were externally referred to 176.03 ppm for the carbonyl carbon of glycine from TMS.

RESULTS

Transmembrane α-helical portion of wild type *p*pR and mutants at Ala149

Figure 2 illustrates the ^{13}C CP-MAS NMR spectra of [3-^{13}C]Ala-*p*pR (A) (**30**), A149S (B) and A149V (C) reconstituted in egg PC bilayers at ambient temperature. The ^{13}C NMR peak at 14.1 ppm was assigned to that of the methyl carbon from egg PC (**30**). The assignment of the upper field shoulder peak at 14.1 ppm of *p*pR in egg PC is not clear at present, although this peak arises definitely from the portion of lipids and not present in the ^{13}C NMR spectra of the mutants. It should be noted that many of the ^{13}C NMR peaks of [3-^{13}C]Ala-bR were resonated at the peak-position of the α_{II}-helix at 15.9-16.9 ppm which is resonated at lower field portion of the conformation-dependent ^{13}C chemical shift of α-helical Ala C_β, in the presence of dynamics-dependent ^{13}C chemical shifts for α-helix (**19,27**), rather than the plausibly distorted torsion angles as proposed by Krimm and Dwivedi based on IR spectra (**37**). It is noteworthy that the peak-intensity at 15.9 ppm from the ^{13}C CP-MAS NMR spectra of [3-^{13}C]Ala-A149S and A149V proteins is significantly reduced with reference to that of [3-^{13}C]Ala-*p*pR owing to the absence of the ^{13}C signals in these mutants (see Figures 2 (A)-(D)). In fact, this is consistent with the difference spectrum between [3-^{13}C]Ala-*p*pR and [3-^{13}C]Ala-A149V (see Figure 2(D)). The reduced peak area is 0.06 relative to whole area between 14.5 and 16.9 ppm. This value is twice as large as that of 0.03 as estimated from the number of labeled Ala residues in *p*pR, namely 1/31. This is because a part of Ala C_β does not appear in the ^{13}C CP-MAS NMR spectrum. Therefore, the ^{13}C NMR peak at 15.9 ppm can be uniquely assigned to Ala149 which is involved in the α-helix portion with reference to the conformation-dependent ^{13}C chemical shifts of the α-helix (**19, 27, 38**). In particular, Ala149 is located in the α_{II}-helix portion near at the E-F loop in the cytoplasmic side, as judged from the conformation-dependent ^{13}C chemical shifts (**19, 27, 38**) (Figure 1).

Figure 3 shows the ^{13}C CP-MAS NMR spectra of [3-^{13}C]Ala-labeled *p*pR (A) (**30**), A149S (B), and A149V (C) which are complexed with *p*HtrII(1-159) in egg PC bilayers. As compared with the spectral patterns in the absence of the transducer (Figure 2A), the five (or six) well-resolved signals were observed for *p*pR and mutants at Ala 149, when they are complexed with *p*HtrII(1-159) (Figure 3). It should be pointed out that the contribution of peaks in the region between 14.5 and 16.9 ppm, from residues of natural abundance in *p*pR-*p*HtrII

complex appeared to be very low. This is because 28Ala C_β (from *p*HtrII), 23Ile $C_{\gamma 2}$ (from *p*pR and *p*HtrII), and 11Met C_ε (from *p*pR and *p*HtrII) are possibly resonated at this region (**39**) in the vicinity of Ala C_β but the relative peak intensity from natural abundance is extremely low (less than 2%) compared with the ^{13}C-labeled peaks from 31Ala C_β of *p*pR. In fact, no such contribution was seen for similar preparations of [3-^{13}C]Ala-labeled bR (**40**). The observed spectral changes in the compex formation mainly from the transmembrane region are obviously explained in terms of the accompanied conformational and dynamics changes due to the presence of van der Waals contact and hydrogen bonds in the binding surface of the transmembrane α-helices between *p*pR and *p*HtrII, since the CP-MAS NMR spectra mainly reflect the changes in the transmembrane regions of the *p*pR-*p*HtrII(1-159) complex. Naturally, the peak-intensity at 15.8-15.9 ppm in the CP-MAS NMR is significantly reduced in the mutants, because no ^{13}C NMR signal from Ala 149 is present. The interaction of *p*HtrII with *p*pR increases the thermal stability of *p*pR with the formation of Y199^{ppR}-N74^{pHtrII} hydrogen bond in the transmembrane region (**14**). In fact, it is confirmed that Ala149 mutants interacted with *p*HtrII(1-159) increases the thermal stability (data not shown). These results indicate that the structure and dynamics of the transmembrane region are retained in these mutants in which Y199^{ppR}-N74^{pHtrII} hydrogen bond is conserved even in the Ala149 mutants (**5, 12, 13**).

Membrane surface residues of *p*pR and Ala149 mutants

It is noteworthy that the peak-intensities of the two kinds of ^{13}C NMR peaks for [3-^{13}C]Ala-labeled *p*pR and A149V, resonated at 16.7-16.9 and 15.8-15.9 ppm, are substantially suppressed when these two proteins are complexed with the cognate transducer *p*HtrII, as shown in Figures 4B and 4F with reference to Figures 4A and 4E, respectively. This sort of the spectral change turns out to be less pronounced for A149S mutant, however (Figures 4C and 4D). As to the assignment of the above-mentioned peaks, we previously demonstrated that the peaks at 16.7-16.9 and 15.8-15.9 ppm were ascribed to the more flexible tip (Ala228, 234, 236 and 238) and rather static stem (Ala221) regions of the C-terminal α-helix in the cytoplasmic side, respectively. This assignment is made possible on the basis of our recent comparative ^{13}C NMR study on intact *p*pR and truncated *p*pR (1-220) (Kawamura et al., Biochemistry, manuscript in preparation) and also in analogy with the data of the similar ^{13}C NMR studies on [3-^{13}C]Ala-labeled bR (**23, 25, 27**), as summarized in Table 1.

Obviously, such drastic intensity-changes by the complex-formation might be caused by an accompanied dynamics change at the flexible tip and (rather static) stem portions of the C-terminal α-helical region from the fluctuation frequency in the order from 10^8 Hz and 10^6 Hz

in the uncomplexed state to 10^5 Hz in the complexed state, respectively. This is a consequence of the peak-broadenings due to a failure of the proton decoupling, interfered with frequency of coherent proton decoupling and incoherent fluctuation frequency in the order of 10^5 Hz in the surface structure (**21, 27, 31, and 35**). Naturally, such a spectral change is more pronounced in the larger dynamics change in the flexible tip portion. It is further noted that the peaks in the loop region at 17.2 and 17.4 ppm, which cannot be usually observed in bR or *p*pR incorporated as a monomer in lipid bilayers, emerge in the 2:2 complex of *p*pR-*p*HtrII (1-159) as a result of an "escape" from such interference leading to the peak-suppression (Figure 4 (B)).

This finding strongly indicates that the cytoplasmic C-terminal α-helix in *p*pR and the cytoplasmic α-helix (TM2) in *p*HtrII, protruding from the membrane surface, are also participated in the stability of the complex-formation with *p*HtrII (1-159), besides the role of the above-mentioned transmembrane α-helices as revealed by the CP-MAS NMR experiments. In this connection, it appears that Ala149 or Val 149 for *p*pR and A149V mutant are stably located at the corner of the transmembrane α-helix E in the vicinity of the E-F loop, although its direct evidence as to the mutant is unavailable at moment but might play an important role for the stabilization of the complex with *p*HtrII(1-159) in the cytoplasmic side.

DISCUSSION

We found that the ^{13}C DD-MAS NMR peak-intensities of the C-terminal α-helix from [3-^{13}C]Ala-*p*pR and A149V are substantially reduced when they are complexed with the cognate transducer *p*HtrII(1-159) (Figures 4B and 4F), whereas those of [3-^{13}C]Ala-A149S are almost unchanged (Figure 4D). This is obviously caused by the characteristic dynamics change leading to reduced fluctuation frequency, in the surface structure including the C-terminal stem and tip portion of the α-helix and the E-F loop of *p*pR, which is interfered with the proton decoupling frequency (10^5 Hz). This finding suggests that mutual interaction between the two types of α-helices, the C-terminal α-helix of *p*pR and cytoplasmic α-helix of *p*HtrII (1-159) (TM2) is responsible for the stabilization of the complex as viewed from the surface structure. Indeed, we also demonstrated that the C-terminal α-helix of *p*pR is a very important site to be able to interact with the cytoplasmic α-helix of *p*HtrII (1-159) (Kawamura et al., Biochemistry, manuscript in preparation), although the surface structure of A149S mutant is not participated in the stabilization of the complex at the membrane surface. This means that the surface structure of the latter could be significantly modified to the extent that such a mutual interaction is geometrically unfavorable. Nevertheless, it should be pointed out that the *p*pR-*p*HtrII interaction in the transmembrane region remains unchanged among *p*pR, A149V and A149S as manifested

from the similar ^{13}C CP-MAS NMR spectra (Figure 2).

The three-dimensional structure of the *p*pR-*p*HtrII complex as viewed from the transmembrane region has been shown by x-ray diffraction study on crystalline sample (**8**) and EPR study on spin-labeled reconstituted preparation (**41**): the straight TM2 (C-terminal side) is oriented parallel to the helix G of the receptor, although the residues (115-159) in the cytoplasmic α-helix of the truncated transducer (1-114) used is absent in the former (**8**). Therefore, it appears that the transmembrane α-helix G of *p*pR is in direct contact with the TM2 α–helix of *p*HtrII(1-159) leading to stabilization of the surface structure. Therefore, it is likely that the E-F loop of *p*pR interacts with the membrane proximal region in *p*HtrII(1-159) (**14**) in an indirect manner, because its direct interaction with the transducer might be stereochemically unfavorable as viewed from the relative orientation of these moieties (**8,41**). It is probable, therefore, that the location of the hydrophobic Ala 149 (and also Val 149) at the corner of the helix E, linked to the hydrophilic E-F loop, is very important for the sake of maintaining the surface structure necessary for the mutual interaction between the receptor and transducer. Indeed, Ala149 (and Val 149) in *p*pR is well conserved for the other archaeal retinal proteins (**11**). On the contrary, the helical structure at the position 149 might be less stable for Ser 149 at this corner in A149S mutant, especially at the interface between the hydrophobic and hydrophilic environment. In fact, it is known that Ala, Val, and Ser residues are strong α-helix former, α-former and indifferent for α-helix, respectively (**42**). In addition to the change of stabilization in the corner of the helix E, the change of hydropathy among Ala149, Val149 and Ser149 may be responsible for surface dynamics (**43**). Therefore, the surface structure might be distorted to some extent from that of wild-type protein and is unfavorable for the stabilization of the complex as viewed from the cytoplasmic surface, although the strong hydrogen bond $Y199^{ppR}$-$N74^{pHtrII}$, and $T189^{ppR}$ -$E43^{pHtrII}$ and -$S62^{pHtrII}$ in transmembrane region are concerved in *p*pR and these two kinds of mutants (**5,9,12-15**). This is the reason why the influence by the mutations is rather limited to the area of cytoplasmic side.

In contrast, it is also interesting to note that a single-mutation in the E-F loop results in significantly modified surface and dynamics structures in bR which also include the C-terminal α-helix and the E-F loop, as manifested from the ^{13}C NMR spectra of A160G and A160V of bR mutants (corresponding to Ala149 in *p*pR) (**25, 29**) (Table 1), by taking into account of the well-known structural homology between *p*pR and bR. It is, therefore, suggested that dynamics of the membrane surface residues including the E-F loop in the cytoplasmic side in *p*pR are strongly correlated with the manner of mutual interaction with *p*HtrII and its resulting biological function in relation to signal relay.

Finally, it is pointed out that site-directed ^{13}C NMR approach is a very valuable means to

clarify a missing link between pictures by x-ray diffraction studies and biological studies: a potential role of the mutual interactions between the cytoplasmic α-helix in *p*pR and the cytoplasmic α-helix in the C-terminus (TM2) in the cytoplasmic surface.

CONCLUSION

It was revealed that dynamics of membrane surface residues in *p*pR complexed with *p*HtrII (1-159) were greatly changed among ppR, A149V and A149S mutants. Therefore, the surface structure near E-F loop of *p*pR plays dominant role to regulate membrane surface dynamics when *p*pR interacts with *p*HtrII(1-159) through direct interaction of the. C-terminal α-helix region in *p*pR interacts with the cytoplasmic α-helical region of *p*HtrII (1-159). These interactions may correlate with the signal relay mechanism.

REFERENCES

1. J. L. Spudich.
Variations on a molecular switch: transport and SENSORY signaling by archaeal rhodopsins.
Mol. Microbiol. 1998 **28** 1051-1058.

2. N. Kamo, K. Shimono, M. Iwamoto and Y. Sudo.
Photochemistry and photoinduced proton-transfer by *pharaonis* phoborhodopsin.
Biochemistry (Moscow) 2001 **66** 1277-1282.

3. C. S. Yang, and J. L. Spudich.
Light-induced structural changes occur in the transmembrane helices of the
Natronobacterium pharaonis HtrII transducer
Biochemistry 2001 **40** 14207-14214.

4. Y. Sudo, M. Iwamoto, K. Shimono and N. Kamo.
pharaonis Phoborhodopsin binds to its cognate truncated transducer even in the presence of a detergent with a 1:1 stoichiometry.
Photochem. Photobiol. 2001 **74** 489-494.

5. Y. Sudo, H. Kandori and N. Kamo
Molecular mechanism of protein-protein interaction of *pharaonis* phoborhodopsin/transducer and photo-signal transfer reaction by the complex.
Recent Res. Devel. Biophys. 2004 **3** 1-16.

6. A. A. Wegner, J. P. Klare, M. Engelhard and H. J. Steinhoff.
Structural insights into the early steps of receptor-transducer signal transfer in archaeal phototaxis, *EMBO J.* 2001 **20** 5312-5319.

7. H. Luecke, B. Schobert, J. K. Lanyi, E. N. Spudich and J. L. Spudich

Crystal structure of sensory rhodopsin II at 2.4 Angstroms: insight into color tuning and transducer interaction.
Science 2001 **293** 1499-1503.

8. V. I. Gordeliy, J. Labahn, R. Moukhametzianov, R. Efemov, J. Granzin, R. Schlesinger, G. Buldt, T. Savopol, A. Scheldig, J. P. Klare and M. Engelhard
Molecular basis of transmembrane signaling by sensory rhodopsin II-transducer complex.
Nature 2002 **419** 484-487.

9. R. Moukhametzianov, J. P. Klare, R. Efremov, C. Baeken, A. Goppner, J. Labahn, M. Engelhard, G. Bűldt and V. I. Gordeliy.
Development of the signal in sensory rhodopsin and its transfer to the cognate transducer.
Nature 2006 **440**115-119.

10. Y. Sudo, M. Iwamoto, K. Shimono and N. Kamo.
Tyr-199 and charged residues of *pharaonis* phoborhodopsin are important for the interaction with its transducer.
Biophys. J. 2002 **83** 427-432.

11. K. Ihara, T. Umemura, I. Katagiri, T .Kitajima-Ihara, Y. Sugiyama, Y. Kimura and Y. Mukohata Evolution of the archaeal rhodopsins: Evolution rate changes by gene duplication and functional differentiation.
J. Mol. Biol. 1999 **285** 163-174.

12. Y. Sudo, M. Yamabi, S. Kato, C. Hasegawa, M. Iwamoto, K. Shimono and N. Kamo.
Importance of specific hydrogen bonds of archaeal rhodopsins for the binding to the transducer protein. *J. Mol. Biol.* 2006 **357** 1274-1282.

13. Y. Sudo, Y. Furutani, K. Shimono, N. Kamo and H. Kandori.
Hydrogen bonding alteration of Thr-204 in the complex between *pharaonis* phoborhodopsin and its transducer protein.
Biochemistry 2003 **42** 14166-14172.

14. Y. Sudo, M. Yamabi, M. Iwamoto, K. Shimono and N. Kamo
Interaction of *Natronobacterium pharaonis* phoborhodopsin (sensory rhodopsin II) with its cognate transducer probed by increase in the thermal stability.
Photochem. Photobiol. 2003 **78** 511-516.

15.Y. Furutani, K. Kamada, Y. Sudo, K. Shimono, N. Kamo and H. Kandori
Structural changes of the complex between *pharaonis* phoborhodopsin and its cognate transducer upon formation of the M Photointermediate.
Biochemistry 2005 **44** 2909-2915.

16. C. S. Yang, O. Sineshchekov, E. N. Spudich and J. L. Spudich

The cytoplasmic membrane-proximal domain of the HtrII transducer interacts with the E-F loop of photoactivated *Natronomonas pharaonis* sensory rhodopsin II.
J. Biol. Chem. 2004 **279** 42970-42976.

17. S. Hippler-Mreyen, J. P. Klare, A. A. Wegener, R. Seidel, C. Herrmann, G.. Schmies, G.. Nagel, E. Bamberg and M. Engelhard
Probing the sensory rhodopsin II binding domain of its cognate transducer by calorimetry and electrophysiology,
J. Mol. Biol. 2003 **330** 1203-1213.

18. X. Chen and J. L. Spudich
Five residues in the HtrI transducer membrane-proximal domain close the cytoplasmic proton-conducting channel of sensory rhodopsin I
J. Biol. Chem. 2004 **279** 42964-42969.

19. H. Saitô, S. Tuzi, M. Tanio and A. Naito
Dynamic aspects of membrane proteins and membrane-associated peptides as revealed by ^{13}C NMR: Lessons from bacteriorhodopsin as an *Intact* protein.
Annu. Rep. NMR Spectrosc. 2002 **47** 39-108.

20. H. Saitô, I. Ando and A. Naito
Solid state NMR spectroscopy for biopolymers: principles and applications,
Springer 2006 The Netherland

21. H.Saitô, Y. Kawase, A. Kira, K. Yamamoto, M. Tanio, S. Yamaguchi, S. Tuzi and A.Naito
Surface and dynamic structures of bacteriorhodopsin in a 2D crystal, a distorted or disrupted lattice, as revealed by site-directed solid-state ^{13}C NMR.
Photchem. Photobiol. 2007 in press.

22. A.Watts.
Solid-state NMR approaches for studying the interaction of peptides and proteins with membranes. *Biochim. Biophys. Acta.* 1998 **1376**, 297-318.

23. H. Saitô, J. Mikami, S. Yamaguchi, M. Tanio, A. Kira, T. Arakawa, K. Yamamoto and S. Tuzi. Site-directed ^{13}C solid-state NMR studies on membrane proteins: strategy and goals toward revealing conformation and dynamics as illustrated for bacteriorhodopsin labeled with [1-^{13}C]amino acid residues.
Magn. Reson. Chem. 2004 **42** 218-230.

24. S. Tuzi, J. Hasegawa, R. Kawaminami, A. Naito and H. Saitô
Regio-selective detection of dynamic structure of transmembrane α-helices as revealed from ^{13}C NMR spectra of [3-^{13}C]Ala-labeled bacteriorhodopsin in the presence of Mn^{2+} ion.
Biophys. J. 2001 **81** 425-434.

25. S. Yamaguchi, K. Yonebayashi, H. Konishi, S. Tuzi, A. Naito, J. K. Lanyi, R. Needleman and H. Saitô
Cytoplasmic surface structure of bacteriorhodopsin consisting of interhelical loops and C-terminal α helix, modified by a variety of environmental factors as studied by ^{13}C NMR.
Eur. J. Biochem. 2001 **268** 2218-2228.

26. P. Barré, S. Yamaguchi, H. Saitô and D. Huster
Backbone dynamics of bacteriorhodopsin as studied by ^{13}C solid-state NMR spectroscopy.
Eur. Biophys. J. 2003 **32** 578-584.

27. H. Saitô, S. Tuzi, S. Yamaguchi, M. Tanio and A. Naito
Conformation and backbone dynamics of bacteriorhodopsin revealed by ^{13}C-NMR.
Biochem. Biophys. Acta. 2000 **1460** 39-48.

28. H. Saitô, S. Yamaguchi, K. Ogawa, S. Tuzi, M. Márquez, C. Sanz and E.Padrós
Glutamic acid residues of bacteriorhodopsin at the extracellular surface as determinants for conformation and dynamics as revealed by site-directed solid-state ^{13}C NMR.
Biophys. J. 2004 **86** 1673-1681.

29. K. Yonebayashi, S. Yamaguchi, S. Tuzi and H. Saitô.
Cytoplasmic surface structures of bacteriorhodopsin modified by site-directed mutations and cation binding as revealed by ^{13}C NMR.
Eur. Biophys. J. 2003 **32** 1-11.

30. T. Arakawa, K. Shimono, S. Yamaguchi, S. Tuzi, Y. Sudo, N. Kamo and H. Saitô
Dynamic structure of *pharaonis* phoborhodopsin (sensory rhodopsin II) and complex with a cognate truncated transducer as revealed by site-directed ^{13}C solid-state NMR.
FEBS Lett. 2003 **536** 237-240.

31. S. Yamaguchi, K. Shimono, Y. Sudo, S. Tuzi, A. Naito, N. Kamo and H. Saitô
Conformation and dynamics of the [3-^{13}C]Ala-,[1-^{13}C]Val-labeled truncated *pharaonis* transducer, *p*HtrII(1-159) as revealed by site-directed ^{13}C solid-state NMR: Changes due to association with phoborhodopsin (sensory rhodopsin II).
Biophys. J. 2004 **86** 3131-3140.

32. K. Shimono, M. Iwamoto, M. Sumi and N. Kamo
Functional expression of *pharaonis* phoborhodopsin in *Escherichia coli*
FEBS Letter 1997 **420** 54-56

33. H. Kandori, K. Shimono, Y. Sudo, M. Iwamoto, Y. Shichida and N. Kamo
Structural changes of *pharaonis* phoborhodopsin upon photoisomerization of the retinal chromophore: Infrared spectral composition with bacteriorhodopsin.
Biochemistry 2001 **40** 9238-9246.

34. A. W. Bennet, C. M. Rienstra, M. Augar, K. V. Lakshmi and R. G. Griffin
Heteronuclear decoupling in rotating solids.
J. Chem. Phys. 1995 **103** 6951-6958.

35. W. P. Rothwell and J. S. Waugh
Transverse relaxation of dipolar coupled spin systems under rf irradiation: detection motions in solid.
J. Chem. Phys. 1981 **75** 2721-2732.

36. A. Naito, A. Fukutani, M. Uitdehaag, S. Tuzi and H. Saitô
Backbone dynamics of polycrystalline peptides studied by measurements of ^{15}N NMR lineshapes and ^{13}C transverse relaxation times,
J. Mol. Struct. 1998 **441**, 231-241.

37. S. Krimm and A. M. Dwivedi
Infrared spectrum of the purple membrane: clue to a proton conduction mechanism?
Science 1982 **216** 407-408.

38. H. Saitô and I. Ando
High-resolution solid-state NMR studies of synthetic and biological macromolecules.
*Annu. Rep. NMR spectrosc.*1989 **21** 209-290.

39. O. W. Howarth, and D. M. J. Lilley
Carbon-13 NMR of peptides and proteins.
Prog. NMR Spectrosc. 1978 **12** 1-40.

40. S. Tuzi, S. Yamaguchi, A. Naito, R. Needleman, J. K. Lanyi and H. Saitô
Conformation and dynamics of [3-^{13}C]Ala-labeled bacteriorhodopsin and bacterioopsin, induced by interaction with retinal and its analogs, as studied by ^{13}C nuclear magnetic resonance.
Biochemistry 1996 **35** 7520-7527

41. A.-W. Wegener, J. P. Klare, M. Engelhard and H.-J. Steinhoff
Structural insights into the early steps of receptor-transducer signal transfer in archaeal phototaxis. *EMBO J.* 2001 **20** 5312-5319.

42. P. Y. Chou, and G. D. Fasman.
Conformational parameters for amino acids in helical, β-sheet, and random coil regions calculated from proteins.
Biochemistry 1974 **13** 222-245

43. J. Kyte and R. F. Doolittle
A simple method for displaying the hydropathic character of a protein.
J. Mol. Biol. 1982 **157** 105-132.

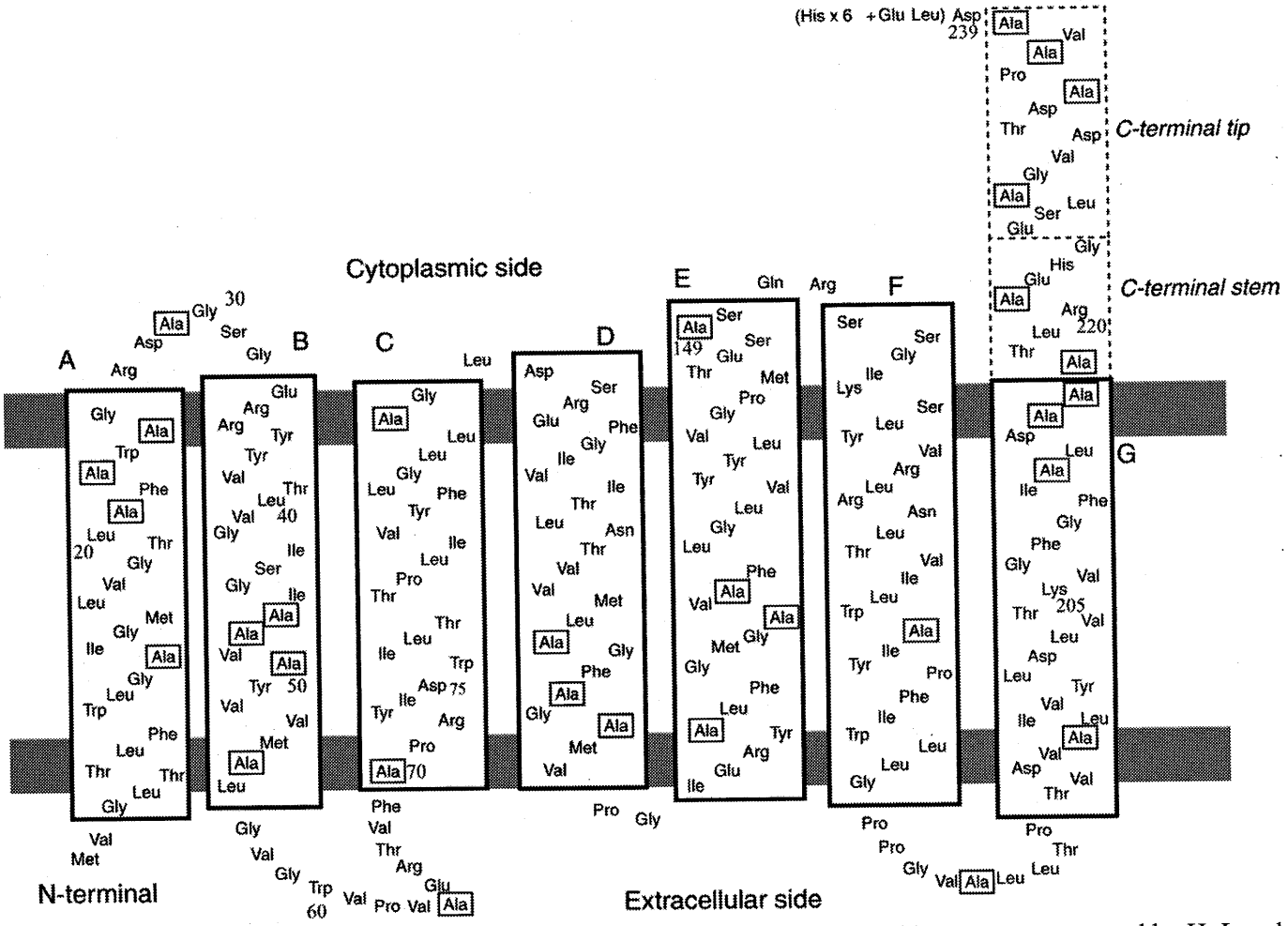

Figure 1: A schematic representation of the secondary structures in *p*pR based on crystallographic structures reported by H. Luecke et al. (*p*pR: PDB code 1JGJ) and V. I. Gordeliy et al. (*p*pR-*p*HtrII(1-114): PDB code 1H2S) The surface areas of the lipid bilayer are represented by gray bands. [3-^{13}C]Ala residues are marked with squares.

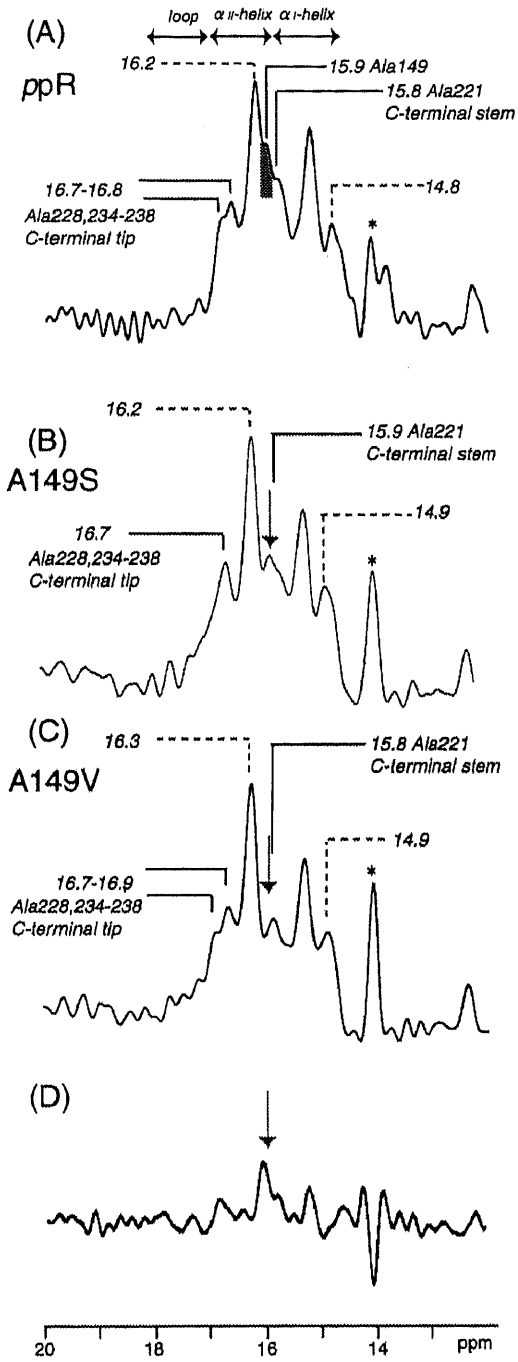

Figure 2. ^{13}C CP-MAS NMR spectra of uncomplexed [3-^{13}C]Ala-labeled *pp*R(A), A149S(B) and A149V(C) alone, reconstituted in egg PC bilayer. ^{13}C NMR signal at 15.9 ppm corresponding to Ala149 in *pp*R is shown in the gray (A) and arrows (B, C and D). The resonance peak at 14.1 ppm is ascribed to methyl carbon peak of egg PC as shown as asterisk. Difference spectrum between (A) and (C) is shown in (D).

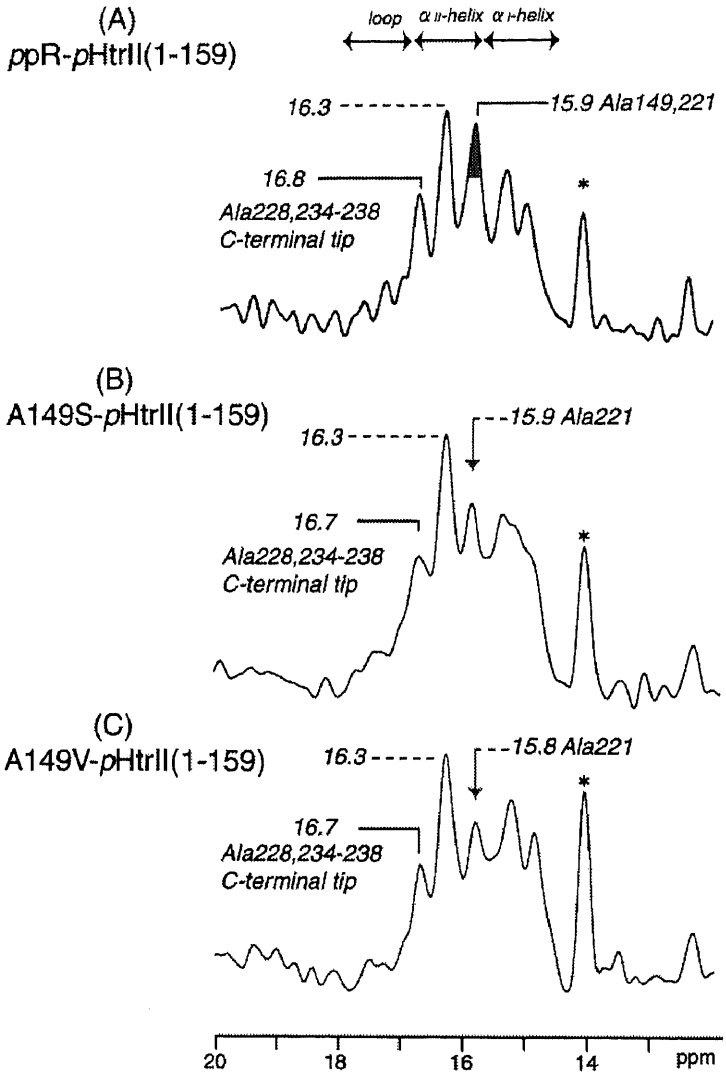

Figure 3. ^{13}C CP-MAS NMR spectra of [3-^{13}C]Ala-labeled *pp*R(A), A149S(B) and A149V(C) complexed with *p*HtrII(1-159), reconstituted in egg PC bilayer. ^{13}C NMR signal from Ala149 in the vicinity of E-F loop in *pp*R is shown in the gray (A) and arrows (B and C). The resonance peak at 14.1 ppm is the methyl carbon peak of egg PC as shown as asterisk.

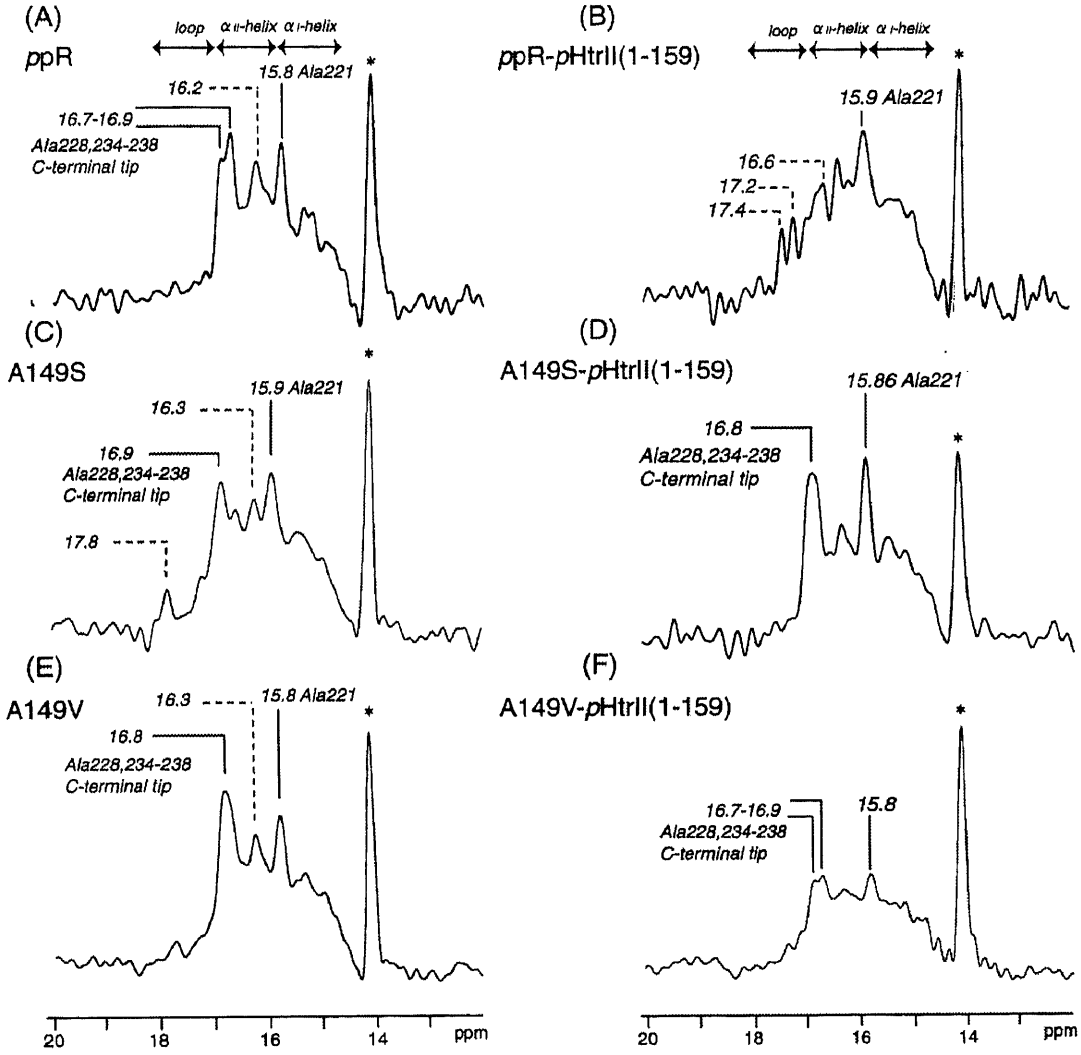

Figure 4. ^{13}C DD-MAS NMR spectra of uncomplexed [3-^{13}C]Ala-labeled *pp*R (A), A149S (C) and A149V (E) (left panel) and those complexed with *p*HtrII(1-159) (right panel). And those of *pp*R (B), A149S(D) and A149V(F) complexed with *p*HtrII(1-159) reconstituted in egg PC bilayer (right panel).

Chapter 7

Conclusions

The conformational and dynamical changes of the retinal-protein corresponding to the changes of retinal configurations were investigated by pressure effect of fast MAS, *In situ* photo-illumination under MAS condition, REDOR filter with isotope enrichments of [1-^{13}C]Tyr-[^{15}N]X-, [1-^{13}C]Val-[^{15}N]Pro-labeled protein and site-directed mutagenesis.

Chapter 2: Noticeable pressure effects on bR in purple membrane in the molecular level were observed at the first time in these experiments. Increased pressure (63 bar) by the fast MAS frequencies induced isomerization from the all-*trans* to 13-*cis* retinal. In addition, increased pressure induced dynamical change of site-directed residues in the vicinity of retinal. It turned out that the conformational change was caused by the pressure effect on the local site in the vicinity of retinal in bR.

Chapter 3: Backbone conformations of Tyr185 in bR were strongly perturbed by the retinal configurations as disclosed from REDOR-filtered experiments. Consequently, two different conformations of bR coexist near Tyr185 corresponding to the all-*trans* and 13-*cis* configurations of retinals. The populations of the two conformations of bR changes to all-*trans* populated state for the light adapted state, while the 13-*cis* populated state is dominant for the pressure adapted state. This local change of protein conformation was disclosed to be generated by photo isomerization of the retinal by means of the photo-illumination experiments. In contrast, only single conformations for Tyr26 and Tyr64 appeared. It is, therefore, revealed that the change of retinal configuration may induce a significant local change of backbone conformation in bR that is relevant to the regulation of light driven proton pathway.

Chapter 4: In order to characterize the dynamic features of Val-Pro consecutive positions of Val49-Pro50, Val69-Pro70 and Val199-Pro200 in bR using various relaxation parameters, REDOR filter experiments were performed to reassign NMR

signals of [1-^{13}C]Val-[^{15}N]Pro-doubly labeled bR. In spite of the presence of superimposed ^{13}C NMR signal from Val49 and Val69, we revealed the dynamic aspects in Val-Pro positions by observing ^{13}C and ^{15}N various relaxation times. BC loop in bR formed rigid β-sheet and showed large amplitude motions. This dynamic structure of BC loop in bR was disordered in bO.

Chapter 5: We found that the C-terminal residues of *p*pR, protruding from the cytoplasmic surface, consist of the C-terminal α-helix stem and tip regions, based on comparative study on the ^{13}C NMR spectra of *p*pR with those of *p*pR(1-220) and the conformation-dependent as well as dynamic-dependent ^{13}C chemical shifts. It turned out that the latter tip region in *p*pR is also in direct interaction with *p*HtrII(1-159), in addition to the mutual helix-helix interaction stabilized by the salt-bridge between the transmembrane α–helices. This sort of interaction, however, was destabilized in D75N complex with *p*HtrII(1-159) as disclosed from ^{13}C DD-MAS NMR data. Consequently, a switching of pairs in the helix-helix interaction occurs from *p*HtrII-*p*pR to *p*HtrII itself when *p*pR is converted to an activated state (D75N). It is evident that these conformational and dynamical changes of *p*pR and *p*HtrII are related to transmit a signal to *p*HtrII. It is evident that these conformational and dynamical changes of *p*pR and *p*HtrII are related to transmit a signal to *p*HtrII. Spudich et al. observed that D73N mutant of sRII was constitutively active from negative phototaxis of *H. salinarum*, which verified Spudich's hypothesis. D73N mutant of sRII corresponds to D75N mutant in *p*pR employed in this investigation. Hence, the present study shows that the disruption of the salt-bridge between C- and G-helix causes the rigidness of transducer in the cytoplasmic side and these processes may trigger the phototaxis. We, however, must keep it in mind that this may not be only a trigger but there may exist other signals from the sensor to the changes in the intracellular interaction between *p*pR and *p*HtrII may be necessary as is shown by Yang et al. and Sudo et al.

Chapter 6: It was revealed that dynamics of membrane surface residues in *p*pR complexed with *p*HtrII (1-159) were greatly changed among *p*pR, A149V and A149S mutants. Therefore, the surface structure near E-F loop of *p*pR plays dominant role to

regulate membrane surface dynamics when *p*pR interacts with *p*HtrII(1-159) through direct interaction of the C-terminal α-helix region in *p*pR interacts with the cytoplasmic α-helical region of *p*HtrII (1-159). These interactions may correlate with the signal relay mechanism.

In summary, local conformation and dynamics of retinal proteins in view of retinal-protein interactions were obtained in detail by high resolution solid-state NMR with various approach (fast MAS, *in situ* photo-illumination under MAS conditions, REDOR filter with isotope enrichments for consecutive amino acids sequence and site-directed mutations). As a result, dynamic structure of retinal proteins relevant to the functions was revealed and the proton pump and the signal relay pathway from interactions of the retinal-protein were able to be clarified.

Acknowledgements

Many grateful thanks are due to my supervisor Prof. Akira Naito who initiated the present work. I am very grateful for all his help, support, guidance and encouragements I received during the last five years.

I am very grateful to Prof. Hazime Saitô (Hiroshima University), Associate Prof. Satoru Tuzi (University of Hyogo) and Dr. Satoru Yamaguchi (University of Hyogo) for the useful discussions and the technical supports about bacteriorhodopsin (bR). I also thank to Associate Prof. Katsuyuki Nishimura (Institute for Molecular Science) for technical advice of solid-state NMR and encouragements.

I am indebted to Prof. Naoki Kamo, Yoichi Ikeda, Dr. Yuki Sudo, Dr. Kazumi Shimono, Dr. Masayuki Iwamoto, Chisa Hasegawa (Hokkaido University) for the useful discussions and the technical supports about *pharaonis* phoborhodopsin (*p*pR).

I am grateful to Yokohama National University for young grant of a "Research Aid Program for Ph. D. Candidates."

Special thanks to all of the members in Naito Laboratory for their encouragements and supports.

Izuru Kawamura